

AN ABSTRACT OF THE THESIS OF

ROBERT JOHN SCHUYLER for the DOCTOR OF PHILOSOPHY in
(Name) (degree)

BIOPHYSICS presented on Oct 18, 1971
(Major) (Date)

TITLE: MONOPHOTON DECAY TIME FLUOROMETRY. THEORY, DESIGN, AND
APPLICATION TO BIOCHEMICAL SYSTEMS.

Redacted for privacy

Abstract approved:

Irvin Isenberg

In the determination of binding heterogeneity and rotational diffusion relaxation times, fluorescence decay curves often take the form of sums of exponential decay times. An instrument is described which includes features permitting the collection of high precision time decay data, which may successfully be resolved into component decays.

The instrument incorporates several novel features that significantly improve the monophoton technique. A decay curve is built up by successively adding to the memory of a pulse height analyzer events, which represent the time between a brief excitation pulse and the detection of a single emitted photon from the sample. This decay curve represents the true probability of emission as a function of time only if the events measured are single photon events. By measuring the pulse height of the detected signals and rejecting all

events not characteristic of single photons, we are able to collect single photon data at a rate significantly higher than that required for avoiding multi-photon events by using signal attenuation.

The performance of the instrument is demonstrated by a number of tests. In all cases the experimental data are analyzed by a method of moments. We have successfully measured the decay time of NADH in water and obtained a value, $0.48 \pm .05$ nanoseconds, which is much shorter than the three nanosecond half width of our excitation pulse. Subnanosecond discrimination is demonstrated by the difference in the reproducible decay times of air equilibrated and deoxygenated solutions of anthracene in benzene, 3.65 and 4.00 nanoseconds respectively. We rigorously demonstrate the ability to resolve a double exponential decay curve by successively adding to the memory of the pulse height analyzer data from a solution of quinine and a solution of anthranilic acid. The data from each are analyzed and the results compared with a double exponential analysis of the summed decay curve. Finally we give the first example of the analysis of a single polarized component of emission yielding the zero point anisotropy, the excited state lifetime, and the rotational relaxation time of a dye protein complex. These values for an ANS-apomyoglobin complex are 0.33, 16.5 nanoseconds, and 28.4 nanoseconds respectively.

MONOPHOTON DECAY TIME FLUOROMETRY.
THEORY, DESIGN, AND APPLICATION
TO BIOCHEMICAL SYSTEMS

by

ROBERT JOHN SCHUYLER

A THESIS
submitted to
Oregon State University

in partial fulfillment of
the requirements for the
degree of

DOCTOR OF PHILOSOPHY

June 1972.

APPROVED:

Redacted for privacy

Professor of Biophysics

in charge of major

Redacted for privacy

Acting Chairman of Biochemistry/Biophysics Department

Redacted for privacy

Dean of Graduate School

Date thesis is presented

Oct 18, 1971

Typed by Linda Knuth for

Robert John Schuyler

ACKNOWLEDGEMENT

I express my sincere appreciation to Dr. Irvin Isenberg, my major professor, for his patience and guidance, without which this work would not have been completed.

Among the many others who were helpful in this work, I extend my thanks particularly to Spencer L. Baird, who constructed and tested sections of the instrument in the early stages of assembly, and Dr. Robert D. Dyson, who did the computer programming for the decay analyses.

I appreciate also the financial support of the United States Public Health Service in the form of a National Institutes of Health Predoctoral Fellowship.

To my wife whose understanding
and love made possible the com-
pletion of this work.

TABLE OF CONTENTS

| <u>Chapter</u> | <u>Page</u> |
|--|-------------|
| INTRODUCTION | 1 |
| I. THEORETICAL EXPRESSIONS FOR EXCITED STATE LIFETIMES | 3 |
| II. APPLICATIONS OF DECAY TIME FLUOROMETRY TO BIOCHEMICAL AND BIOPHYSICAL STUDIES | 9 |
| A. Environmental Effects on the Fluorescence Lifetime | 9 |
| B. Dynamic Polarization | 13 |
| C. Energy Transfer | 27 |
| III. MEASUREMENT OF TIME DECAY | 33 |
| IV. THE INSTRUMENT - DESIGN, CONSTRUCTION, AND FUNCTION | 44 |
| A. The Flash Lamp | 48 |
| B. The Sample Chamber | 56 |
| C. The Photomultiplier Tubes | 59 |
| D. Pulse Timing | 65 |
| E. The Linear Channel and Single Photon Window | 69 |
| F. Signal Routing and Timing | 71 |
| G. Radio Frequency Interference | 72 |
| V. ANALYSIS OF DATA | 75 |
| VI. TESTING AND PERFORMANCE | 81 |
| A. Single Photon Window | 81 |
| B. Short Lifetime Decay | 87 |
| C. Subnanosecond Resolution | 90 |
| D. Double Exponential Decay | 92 |
| E. Long Lifetime Decays - Analysis Without Convolution | 96 |
| F. Dynamic Polarization | 97 |

| | <u>Page</u> |
|--|-------------|
| REFERENCES | 105 |
| APPENDICES | |
| I. Commercial Suppliers | 122 |
| II. Polarizer Settings for Intensity Measurements | 126 |
| III. Derivation of the Poisson Distribution for a Photon Counting Experiment | 128 |
| IV. Operating Instructions and General Tuning Procedures for the Monophoton Fluorometer | 130 |

LIST OF TABLES

| <u>Table</u> | <u>Page</u> |
|---|-------------|
| I. Effect of Cutoff Point on Decay Analysis | 80 |
| II. Test of Double Exponential Decay | 93 |
| III. Decay Parameters versus Peak Count | 95 |
| IV. Fluorescence Lifetime, Intrinsic Anisotropy, and Rotational Relaxation Time of the Apomyoglobin - ANS Complex | 103 |

LIST OF FIGURES

| <u>Figure</u> | | <u>Page</u> |
|---------------|--|-------------|
| 1 | Geometry of a fluorescence polarization experiment. | 15 |
| 2 | Schematic of the monophoton technique. | 38 |
| 3 | Block diagram of the monophoton fluorometer. | 46 |
| 4 | Lamp design. | 51 |
| 5 | Lamp circuitry. | 53 |
| 6 | Relative spectral output of the nanosecond flash lamp. | 55 |
| 7 | Diagram of the sample chamber. | 57 |
| 8a | Photoelectron pulse height resolution of an RCA 8850 photomultiplier. | 61 |
| 8b | Same as 8a, with the electrostatic focus voltage in the photomultiplier slightly altered. | 61 |
| 9 | Photomultiplier shielding configuration. | 63 |
| 10 | Comparison of the photomultiplier anode pulse resulting from a single photoelectron emitted from the cathode with the same pulse after amplification and shaping in the Ortec 454 Timing Filter Amplifier. | 66 |
| 11 | Lamp pulse shape determined using leading edge and constant fraction triggering. | 68 |
| 12 | A decay curve of quinine distorted by pickup of radio frequency interference. | 73 |
| 13 | Demonstration of curve fitting with incorrect parameters. | 77 |
| 14 | Frequency of single and multiple photon events versus the fraction of events collected per lamp flash according to the Poisson distribution law. | 83 |

| <u>Figure</u> | | <u>Page</u> |
|---------------|--|-------------|
| 15 | Signal pulse height spectra at different collection efficiencies. | 84 |
| 16 | Decay curves of anthranilic acid in methanol. | 86 |
| 17 | Decay of NADH in aqueous solution. | 89 |
| 18 | Decay of deoxygenated anthracene in benzene. | 91 |
| 19 | Double exponential decay test. | 94 |
| 20 | Summed decays of pyrene in cyclohexane at two different oxygen concentrations. | 98 |
| 21 | Decay of the ANS-apomyoglobin complex. | 102 |

MONOPHOTON DECAY TIME FLUOROMETRY. THEORY,
DESIGN, AND APPLICATION TO BIOCHEMICAL SYSTEMS

INTRODUCTION

Fluorescence techniques have seen considerable use in physical biochemistry since their introduction by Weber in 1952. Information about the rotatory motions and sizes of proteins and nucleic acids has been provided by the use of fluorescence polarization and energy transfer studies. Dye binding and quantum yield measurements have been used as analytical tools and probes of macromolecular environment.

To date, most studies have used steady state fluorescence measurements. These often involve difficult technical problems when quantum yields are determined or when energy transfer is studied. The interpretation of steady state fluorescence polarization measurements requires severe assumptions. The technical difficulties and assumptions attending the use and interpretation of steady state studies introduces uncertainty in the results.

Some of these problems and assumptions may be avoided if dynamic measurements are used. Dynamic or lifetime measurements not only provide an additional parameter for the characterization of a fluorescent system, but may also be used independently to study the

system. With their use the determination of quantum yield is simplified, the experimental problems in the study of energy transfer are reduced, and, most importantly, many assumptions in depolarization studies are eliminated.

In view of the power of dynamic techniques, it may be somewhat surprising that they have been little used in biochemistry. This surprise is tempered, however, by the recognition that the use of dynamic fluorescence measurements in biochemistry involves the application of near state-of-the-art timing techniques to intrinsically complex macromolecular systems. In most earlier applications of time decay measurements only one parameter, the excited state lifetime, was extracted from the data. It has become clear, however, that in biochemical studies decay profiles are seldom simple exponential functions. In many cases the data take the form of sums of exponentials. The relative amplitudes and decay constants of the component exponentials yield more detailed information about the system under study but require much higher experimental precision. Until recently the precision needed was unobtainable because of time jitter and low data collection rates. The mathematical methods for resolution of multicomponent decays have also only recently been described.

Improvements in fast pulse technology and the availability of powerful analytical methods have now made it possible to extend the range of fluorescence studies on biochemical systems to include high resolution time decay measurements.

I. THEORETICAL EXPRESSIONS FOR EXCITED STATE LIFETIMES

The theory of fluorescence time decay began with Einstein's treatment of transition probabilities from excited electronic states (Einstein, 1917). He assumed the probability of spontaneous emission to take the form of a first order rate constant in analogy with the rate law for the decay of radioactive substances.

$$\frac{dN}{dt} = -NA \quad N = N_0 e^{-At} \quad (1)$$

where N is the number of molecules in the excited state at time t , N_0 is the number present at $t = 0$, and A is the rate constant. The excited state radiative lifetime or intrinsic lifetime is simply the reciprocal of A , the rate constant.

$$\tau_0 = \frac{1}{A} \quad (2)$$

In the absence of nonradiative transitions to the ground state, the physical meaning of the radiative lifetime is the time it takes for the number of excited states to decrease by a factor of $1/e$. In 1917 Einstein developed his famous relationship between the induced absorption and the spontaneous emission of dipole oscillators in a radiation field. This relation, which has served as the basis for all subsequent theoretical expressions for excited state lifetime, is, in modern terminology,

$$A = \frac{1}{\tau_0} = 8\pi h \nu^3 B, \quad (3)$$

where h is Plank's constant, $\bar{\nu}$ is the wave number, $1/\lambda$, of the transition, and B is the rate of induced absorption per unit radiation density. Tolman (1924) related B to the experimental absorption coefficient, and Perrin (1926) expressed the relationship in terms of experimental parameters for singlet-singlet transitions encountered in the absorption and fluorescence of organic molecules. Again updating the terminology, Perrin's relation is

$$A = \frac{1}{\tau_0} = 2.88 \times 10^{-9} \bar{\nu}^2 n^2 \int \epsilon(\bar{\nu}) d\bar{\nu}. \quad (4)$$

The integral of the molar extinction coefficient, $\epsilon(\bar{\nu})$, is taken over the lowest energy singlet absorption band. n is the refractive index of the medium. Lifetimes calculated using (4) are of the order 10^{-8} to 10^{-7} seconds. Because equation (4) is a crude approximation for work involving broad-band emission, Förster (1951, p. 158-159) somewhat generalized the result. In his work, the emission is permitted to be broad band, but there is still the restriction that the emission band be the mirror image of the absorption. The assumptions were further reduced by Strickler and Berg (1962), who derived an equation which assumes only a similar nuclear configuration in the ground and excited states. With allowances made for the optical dispersion of the solvent (Birks and Dyson, 1963), the result is

$$\frac{1}{\tau_0} = 2.88 \times 10^{-9} \frac{n_f^3}{n_a} \langle \bar{\nu}_f^{-3} \rangle_{ave}^{-1} \int \frac{\epsilon(\bar{\nu})}{\bar{\nu}} d\bar{\nu}, \quad (5)$$

where n_f and n_a are the mean refractive indices over the fluorescence and absorption bands respectively, and

$$\langle \bar{\nu}^{-3} \rangle_{\text{ave}}^{-1} = \frac{\int F(\bar{\nu}) d\bar{\nu}}{\int F(\bar{\nu}) \bar{\nu}^{-3} d\bar{\nu}}. \quad (6)$$

The integrals in (6) are over the emission band.

To discuss the applicability of equation (5), I now introduce the concept of quantum yield and its relationship to the radiative lifetime and the observed lifetime. Stern and Volmer (1919) presented a relationship between the fluorescence intensity, lifetime, and rates of non-radiative transitions for collisional quenching of gases. This result was generalized by Perrin (1926, 1929) to cover all causes of time independent non-radiative transitions. If we let k_r be the rate constant for radiative transitions, i.e.

$$k_r = \frac{1}{\tau_0}, \quad (7)$$

and k_1, k_2, k_3, \dots etc. be the first order rate constants for all other time independent processes of excited state deactivation, the total rate of deactivation will be

$$k_{\text{tot}} = k_r + k_1 + k_2 + \dots \quad (8)$$

The observed rate of decay is then

$$\frac{dN}{dt} = -N(k_{\text{tot}}) \quad N = N_0 e^{-k_{\text{tot}} t} \quad (9)$$

and

$$k_{\text{tot}} = \frac{1}{\tau} \quad (10)$$

The quantum yield is given by the ratio of excited molecules decaying with the emission of light to the total number leaving the excited state.

$$q = \frac{k_r}{k_r + k_1 + k_2 + \dots} = \frac{k_r}{k_{\text{tot}}} \quad (11)$$

We thus get the relation

$$\tau = q\tau_0 \quad (12)$$

The generality of this result will be discussed later.

If the relation is assumed valid, it is clear that lifetime and quantum yield measurements can be used to check equation (4). A number of workers have done this (Strickler and Berg, 1962; Birks and Dyson, 1963; Ware and Baldwin, 1964; Lami, et al., 1966; Birks and Munro, 1967). These authors point out that τ_0 values calculated from equation (4) and equation (12) are in good agreement except in cases where the assumptions in the derivation of (4) may not be met. Birks and Dyson (1963) point out that, although equation (5) is not based on mirror image symmetry between absorption and emission bands, it does assume a similar nuclear configuration in the ground and excited states. Such a similarity is often reflected in mirror image symmetry, and the greatest discrepancies between the experimental and theoretical results occur when the symmetry is poor. In the case of those aromatic hydrocarbons which exhibit long lifetimes, for example pyrene and naphthalene, the lowest lying singlet state is poorly allowed and is distorted in the absorption spectra of these compounds by the proximity of a more intense band. When this is true the

radiative lifetime cannot be accurately calculated. In some cases a weak singlet state may be completely masked by a stronger absorption band, as has been suggested for biphenyl (Berlman and Steingraber, 1965).

A full evaluation of equation (4) must await more complete and accurate lifetime and quantum yield measurements. For example, Birks and Dyson (1963) questioned the theory at one point, because it predicts (using experimental lifetime measurements) a value of 0.73 for the quantum yield of quinine in 0.1 N sulfuric acid, while for years quinine had been used as a quantum yield standard with a value of 0.55. The discrepancy was recently removed, however, when it was determined that the yield of quinine was $0.70 \pm .02$ (Scott, et al., 1970).

In cases where good mirror image symmetry between the absorption and emission spectra is observed, the use of equations (4) and (12) and the measurement of excited state lifetime may soon replace the laborious and uncertain steady state calculations of quantum yield.

There are some cases, though, where equation (12) does not apply. Among these are all time dependent deexcitation paths, which lead not only to a breakdown of equation (12) but also to non-exponential decays. Hevesi (1969) has shown that the diffusion controlled concentration and iodide quenching of viscous solutions of fluorescein and rhodamine B lead to non-proportionality between the relative intensities and lifetimes. Further demonstrations and discussion of this phenomenon is given in a paper by Ware and Novros (1966), and

in the review of Weller (1961). On the other hand, when quenching is caused by static complexes between the emitting species and quencher, that is by complexes which may be formed prior to excitation, the lifetime can remain constant with decreasing quantum yield. An extended discussion of fluorescence quenching and lifetime measurements may be found in the thesis of R. Spencer (1970).

In most biochemical applications the relationship given in equation (12) holds. The deactivation paths are mainly the time independent radiationless transition to the ground state and intersystem crossing to the triplet state followed by thermal degradation.

II. APPLICATIONS OF DECAY TIME FLUOROMETRY TO BIOCHEMICAL AND BIOPHYSICAL STUDIES

Decay time is an intensive parameter of a fluorescent system and its measurement gives a different kind of information from the extensive, steady state fluorometric techniques. A combination of dynamic and steady state measurements provides a far more detailed picture of the fluorescent system than either alone. Where steady state measurements are used to obtain intensive parameters, as in depolarization studies, the dynamic technique provides more detailed information and requires fewer assumptions. I will now examine some areas of the application of time decay techniques to biochemical and biophysical studies which exemplify these statements.

A. Environmental Effects on the Fluorescence Lifetime

It has long been known that the quantum yield of a chromophore is influenced by the solvent. A striking example of this phenomenon is the difference in fluorescence of the anilinonaphthalenesulfonates in water and when adsorbed to proteins (Weber and Laurence, 1954). A result of this observation is that various aryl-aminonaphthalene-sulfonates have been used as probes for the polarity and conformation of protein binding sites (Stryer, 1965; Laurence, 1966; McClure and Edelman, 1966; Edelman and McClure, 1968; Stryer, 1968). Turner and

Brand (1968) have correlated the observed changes in fluorescence yield, emission wavelength, and band width with an empirical scale of solvent polarity. They found a reasonably close correlation among these parameters, but reservations about ascribing the changes purely to polarity effects remain (Camerman and Jensen, 1969; Seliskar and Brand, 1971).

The application of time decay studies to dye-protein interactions has not resolved the question whether the marked changes in quantum yield are due to the polarity of the dye binding site or to the conformation or rigidity of the bound dye. These studies have however reopened discussion on the topic of excited state dipole moments.

In 1957 Lippert advanced a theory that, for many fluorescing systems, the emission red shift accompanying increases in solvent polarity is due to an excited state dipole moment greater than that in the ground state. The physical mechanism suggested for the observed red shift is that the Frank Condon state reached by excitation is not the state from which emission occurs. During the lifetime of the excited state, reorientation of the polar solvent molecules around the excited solute molecule lowers the energy of the excited state. The more polar the solvent, the greater the stabilization of the excited state.

The change in energy of the excited singlet state could bring it closer to the triplet state and thereby increase the rate of intersystem crossing, affecting both the quantum yield and the lifetime. Environmental rigidity could have a similar effect. If, during the

lifetime of the excited state, only a partial reorientation of the solvent could take place because of solvent viscosity, the stabilization would be decreased, the spectrum blue shifted, and the quantum yield increased. This mechanism has been proposed by Eisinger (1969) to explain his observations on tryptophan quenching in glasses and proteins.

Striking confirmation of these theories has been given by time decay techniques. Ware and coworkers (Ware, Chow, and Lee, 1968; Ware, Lee, Brant, and Chow, 1971; Ware and Chakrabarti, 1970; Chakrabarti and Ware, 1970) showed, for a number of systems, that the emission spectra observed at different times after excitation exhibited a clear shift to the blue as the time between excitation and observation was decreased. This work was done in viscous solutions at low temperatures. Under these conditions, the rate of solvent reorientation is comparable to the excited state lifetime. Brand and Gohlke (1971) have observed similar effects at room temperature for two systems. The dye, 2-p-toluidinylnaphthalene-6-sulfonate, when dissolved in glycerol, and when adsorbed to bovine serum albumin, exhibited spectral shifts in the nanosecond region. Brand and Gohlke measured the apparent lifetime of the dye as a function of emission wavelength, and constructed emission spectra corresponding to Ware's time resolved spectra. Their results indicate nanosecond movements of various groups on the protein close to the dye binding site. The type of information provided by these studies is clearly more detailed than that from steady state measurements and should provide information

about the dye binding sites of proteins and the active sites of enzymes.

When the measured lifetime across the emission band is constant, one may assume that the effects of nanosecond reorientation are negligible. In these cases the measured lifetime yields information about the rigid environment.

While steady state techniques give only an average quantum yield of dyes bound to macromolecules, time decay measurements can indicate the environmental characteristics of a number of different binding sites. Tao, for example, has found that the emission decay curves of 1-anilino-8-naphthalenesulfonate bound to horseradish peroxidase cannot be represented by a single exponential function (Tao, 1969). A double exponential fit yields decay times differing by a factor of three. While this may be expected for dyes adsorbed to protein surfaces, it is also observed for dyes attached to proteins by chemical conjugation. Wahl and Lami (1967) report that dimethylaminonaphthalene sulfonyl chloride when conjugated to lysozyme exhibits a complex fluorescence decay. A double exponential fit in this case yields decay constants differing by a factor of four, indicating significant heterogeneity in dye binding sites.

A final example of the use of time decay measurements as a probe of macromolecular environment is the work of Vaughan and Weber (1970) on pyrene-butyric acid conjugates. Pyrene is very susceptible to oxygen quenching because it has a long radiative lifetime. Using decay measurements at various concentrations of dissolved oxygen,

Vaughan and Weber determined the rate constants of oxygen quenching of pyrene-butyric acid conjugated to a number of proteins and polypeptides. The relative values of the rate constants indicates the degree of shielding of the dye from the oxygen in the environment.

B. Dynamic Polarization

The area of biophysical studies in which time decay fluorometry holds the most promise is that dealing with the rotational motions and internal flexibility of macromolecules. Since many of these motions take place on a time scale comparable with the lifetime of organic fluorophores, they may be studied using time decay techniques. It should be noted, of course, that this order of magnitude agreement between emission rates and the rates of macromolecular rotation is also the basis of the steady state depolarization technique.

As I would like to discuss here the advantages of dynamic over steady state measurements, I will first present a brief review of the classical fluorescence depolarization method.

The theoretical basis of polarized fluorescence was introduced by F. Perrin in 1926. He related the rate of Brownian rotation and lifetimes of fluorescent molecules in solution to steady state measurements of polarized components of emission. The theory was first applied to the determination of fluorescence lifetimes of molecules whose sizes, and hence rotation rates, were known (Perrin, 1929).

With biological macromolecules, though, the parameter of interest is the Brownian rotational rate, and the excited state lifetime is

determined by other means. Weber (1952, 1953) first applied the fluorescence polarization technique in biochemistry, and since its introduction, this technique has seen widespread use (Steiner and Edelhoch, 1962; Chen, 1967).

The experimental determination of Brownian rotation will be described in reference to Figure 1. The sample is a solution of macromolecules having rigidly bound chromophores. Consider the sample placed at the origin of the coordinate system and excited with a beam of light traveling along X and polarized in the OZ direction. At the instant of excitation the transition moments of the excited chromophores will be preferentially oriented in the OZ direction, with a $\cos^2\theta$ dependence. The emission is detected along Y, the components polarized OZ and OX being measured separately. These components, whose relative amplitudes are determined by the orientation of the emission transition moment, are termed I_{\parallel} and I_{\perp} respectively.

If, during the excited state lifetime of the chromophore, rotational motions have randomized the orientation of the emission oscillator, I_{\parallel} and I_{\perp} will be equal. If, however, randomization is incomplete when emission occurs, I_{\parallel} and I_{\perp} will not be equal, and the emission anisotropy*, r , given by

*Note that throughout this thesis the anisotropy of emission, r , will be used. In most earlier literature the parameter commonly used was the polarization, p . Jablonski (1960a) has shown that in all theoretical expressions dealing with the polarization of fluorescence, the use of r , the emission anisotropy, yields more simple equations. r is related to p by $r = 2p/(3 - p)$.

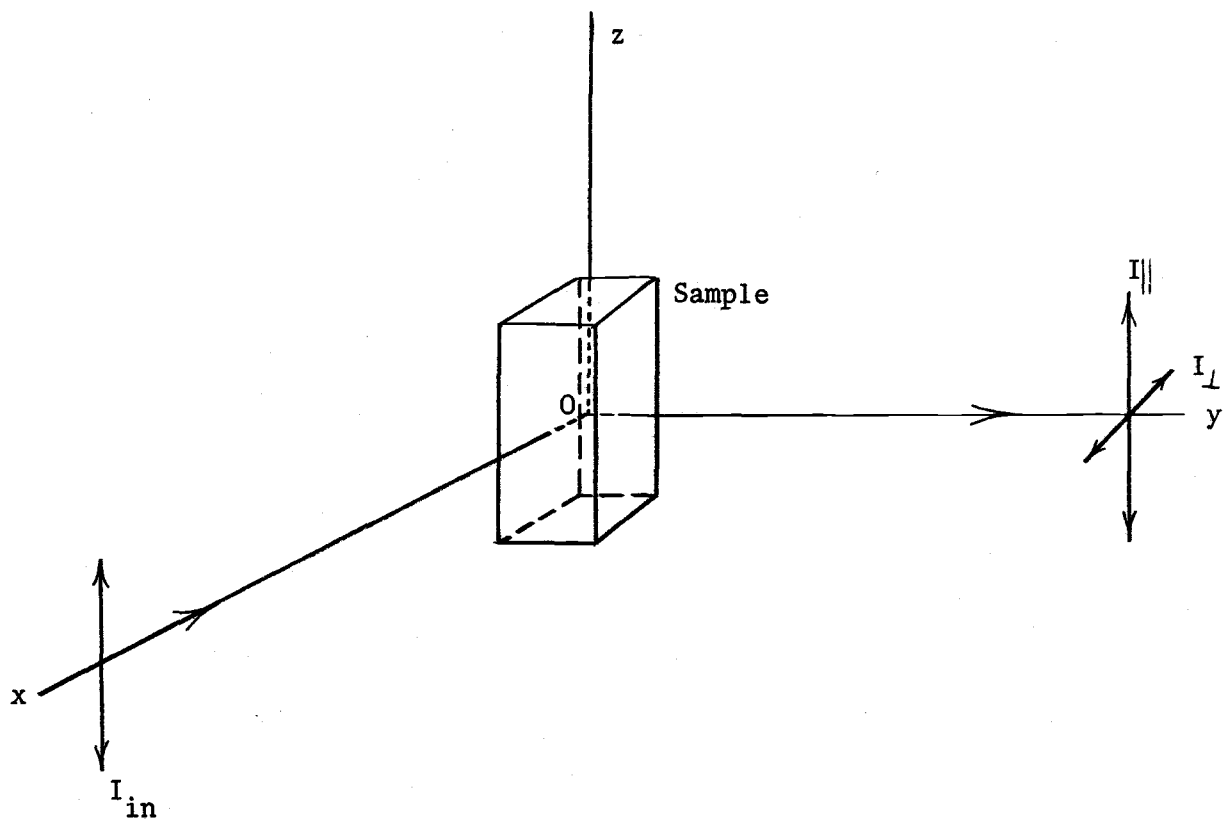


Figure 1. Geometry of a fluorescence polarization experiment.

$$r = \frac{I_{||} - I_{\perp}}{I_{||} + 2I_{\perp}} \quad (13)$$

will not be zero. The emission anisotropy is thus related to the relative values of the rate of rotation of the chromophore transition moment and the excited state lifetime.

For a sphere of volume V undergoing Brownian rotation in a medium of viscosity η at a temperature $T(^{\circ}\text{K})$, the emission anisotropy is given by (Perrin, 1929)

$$r = r_0 / (1 + \frac{kT}{\eta V} \tau), \quad (14)$$

where τ is the lifetime of the excited state, k is the Boltzmann constant, and r_0 is the anisotropy in the absence of rotation. The quantity $kT/\eta V$, which has units of reciprocal time, is a measure of the rate of Brownian rotation. It has been expressed in the literature by a number of constants which are interrelated:

$$\frac{kT}{\eta V} = \frac{1}{\phi} = \frac{3}{\rho} = 6D. \quad (15)$$

ϕ is called the rotational correlation time, ρ is the rotational relaxation time, and D is the rotational diffusion coefficient.

The rotational relaxation time is the time which it takes a given direction in a molecule to make on an average an angle θ with the original direction, such that $\cos^2 \theta = 1/e$ (Weber, 1953). The rotational relaxation time, ρ , is the term most used in fluorescence polarization studies. Yguerabide, Epstein, and Stryer (1970) have suggested that ϕ , the rotational correlation time, might be a better parameter to use because the factor of three is eliminated,

and ϕ is the term used in magnetic resonance and electric birefringence spectroscopy. Doubtless a common term should be agreed upon, but until one is, I will remain with the majority and use ρ , the rotational relaxation time.

The rotational relaxation time of a sphere is determined in the following way. Equation (14) can be written

$$\frac{1}{r} = \frac{1}{r_0} \left[1 + \frac{T}{\eta} \left(\frac{k\tau}{V} \right) \right] \quad (16)$$

It is clear that, if $\frac{k\tau}{V}$ is constant, a plot of $1/r$ versus T/η will be linear with an intercept of $1/r_0$ and a slope of $\frac{k\tau}{r_0 V}$.

The emission anisotropy, r , is measured at several values of T/η . T/η is altered by heating or cooling the solution or by adding sucrose or glycerol to increase the viscosity. The zero point anisotropy is determined from the intercept and the slope is measured. Comparing (16) and (15), the rotational relaxation time is given by

$$\rho = \frac{3\tau\eta}{r_0 T (\text{slope})} \quad (17)$$

If the excited state lifetime is known, ρ is determined for a given temperature and viscosity.

This procedure rests on the assumption that τ , r_0 , and V are invariant over the range of temperatures and viscosities used. This is often a bad assumption. For example, Bernstein, Wilcheck, and Edelhoich (1969) have determined the lifetime of the chromophore at a number of values of T/η and plotted $1/r$ versus $T\tau/\eta$. They observed a 30 to 50 percent increase in the measured lifetime of

tryptophan in going from an aqueous solvent system of 75% to 95% glycerin.

In systems of dyes bound or adsorbed to macromolecules, the emission lifetime is often complex due to binding heterogeneity. The resultant decay parameters may each change with temperature and solvent environment. Wahl (1966b) observed this with dimethylamino-naphthalenesulfonyl conjugates of lysozyme.

Bauer (1963) has demonstrated that r_0 , the zero point anisotropy, is sometimes dependent on the temperature and the nature of the solvent. He has suggested that this might be due to the presence of torsional vibrations (Jablonski, 1950), which cause depolarization in times much shorter than Brownian rotation. Such vibrations would be solvent and temperature dependent and, if present, would cause variations in r_0 .

Finally, possibilities exist for variations in the size and shape of a macromolecule under different solvent conditions. It is often desirable to study these solvent induced variations, but this has not been possible using steady state techniques.

The application of steady state polarization techniques to systems having more than one relaxation time has seldom yielded accurate resolution of the parameters. Such systems include asymmetric macromolecules and those exhibiting internal flexibility.

The case of ellipsoidal molecules was treated theoretically by Perrin (1934, 1936). Weber (1952) simplified the form of Perrin's equations to apply to the case of ellipsoids of revolution, with

chromophores randomly oriented with respect to the ellipsoidal axes. From this simplified theoretical equation Weber showed that elongated molecules with axial ratios less than six would yield Perrin plots whose nonlinearity could not be detected. He also showed that in no case would nonlinearity be detectable in a Perrin plot for a flattened molecule.

Instead of resolving the relaxation times around the principal axes of the molecules, the slope of the linear plots gives the mean harmonic rotational relaxation time, ρ_h .

$$\rho_h = \frac{1}{3} \left(\frac{1}{\rho_1} + \frac{1}{\rho_2} + \frac{1}{\rho_3} \right) \quad (18)$$

where $\rho_{1,2,3}$ are the relaxation times around the principal axes. Memming (1961), in deriving more general equations, again found it necessary to restrict the shape of the rotating particle to a rotational ellipsoid in order to obtain a general solution to the rotational diffusion equation. Random orientation of the chromophore transition moment is, however, not assumed. Memming presents theoretical Perrin plots for systems in which the absorption transition moment lies in the axial plane of the ellipse and shows that the plots are always linear. When the absorption transition moment lies in an equatorial plane, however, nonlinearity is expected for low values of the zero point anisotropy.

The zero point emission anisotropy is related to the angle between absorption and emission transition moments (Jablonski, 1935b). When this angle is greater than 45° , corresponding to r_0 less than

0.1, theoretical Perrin plots give noticeable curvature. As the motion of the chromophore is restricted, the emission anisotropy, r , goes from zero to r_0 . A low zero point anisotropy therefore restricts the range of values which the emission anisotropy may take and leads to less accurate Perrin plots. The Perrin plot technique has thus not yielded information on the shapes of the macromolecules.

Studies have recently been presented, however, which show that, under some circumstances, one may determine the general shape of a body undergoing Brownian rotation and the orientation of the chromophore with respect to the molecular axes (Weber and Anderson, 1969; Witholt and Brand, 1970). The work of Weber and Anderson relates the effects of energy transfer among chromophores to their orientation with respect to the axes of the ellipsoid. This method requires a system in which two or more chromophores are bound to the molecule being studied. The chromophores must also have suitable spectral properties and be close enough to each other to permit radiationless energy transfer.

Witholt and Brand (1970), following the work of Perrin (1934, 1936) and Memming (1961), show that the use of a number of absorption bands of the same chromophore can yield information on preferential orientation. Again it is found that significant deviation from linearity in Perrin plots requires low values of r_0 . This technique however permits one to classify macromolecules as to their general shape; i.e. spherical, oblate, or prolate.

Rotation of a dye molecule around its bond to a macromolecule

has been noted using the steady state polarization technique (Gottlieb and Wahl, 1963; Wahl and Weber, 1967). In all cases to date in which internal flexibility has been studied, the motions resulting from the flexibility are much faster than the overall rotational rate of the macromolecule. For example, a possible internal flexibility on the nanosecond time scale has been suggested for DNA from observations of the emission anisotropy of intercalated proflavine (Ellerton and Isenberg, 1969). Rotational rates of the DNA helix are two orders of magnitude higher. These results are suggestive only, and steady state techniques alone have not yielded quantitative data on the internal motions of macromolecules.

Jablonski recognized in 1935 that it is, in principle, possible to determine the rotational relaxation time, the zero point emission anisotropy, and the excited state lifetime of a rigid sphere by measuring the decay of polarized components of emission. Using the experimental geometry shown in Figure 1, one would observe the following decay characteristics (Jablonski, 1935a, 1936).

$$I_{\parallel}(t) = k[1 + 2r_0 e^{-3t/\rho}]e^{-t/\tau} \quad (19a)$$

$$I_{\perp}(t) = k[1 + r_0 e^{-3t/\rho}]e^{-t/\tau} \quad (19b)$$

k is a constant which depends on instrumental configurations.

If one could accurately resolve either decay curve into the sum of two exponential components, r_0 , ρ , and τ could be determined. From equations (19a) and (19b), the emission anisotropy is

$$r(t) = \frac{I_{\parallel}(t) - I_{\perp}(t)}{I_{\parallel}(t) + 2I_{\perp}(t)} = r_0 e^{-3t/\rho} \quad (20)$$

In 1935, when these equations were first derived, the instrumentation and numerical analysis techniques available did not permit the direct resolution of $I_{\parallel}(t)$ or $I_{\perp}(t)$ into two components, or the construction of $r(t)$. Instead, Jablonski measured the apparent lifetimes of the polarized components of emission with the phase delay technique. Separate measurements of $\langle \tau_{\parallel} \rangle$, $\langle \tau_{\perp} \rangle$, τ , and r at a given temperature and viscosity can be used to determine the rotational relaxation time (Jablonski, 1960). Parenthetically, it should be noted that Jablonski's equations, used to relate $\langle \tau_{\parallel} \rangle$ and $\langle \tau_{\perp} \rangle$ to the phase delay, were wrong and have been corrected by Spencer and Weber (1970).

With the advent of higher precision time decay fluorometers in the early 1960's, Jablonski's equations (19a), (19b), and (20) were revived (Wahl, 1965). The pioneering work of Wahl in dynamic polarization studies has yielded a number of interesting results. For a given experiment $I_{\parallel}(t)$ and $I_{\perp}(t)$ are measured separately and the anisotropy is computed point by point. In this way Wahl (1966) was able to determine a rotational relaxation time from the decay curves of two polarized components of emission. The value was determined in the solvent and at the temperature of interest and is therefore independent of the assumptions required in the steady state technique.

The relaxation time was determined for an assumed spherical molecule. If the molecule exhibits more than one relaxation time,

$r(t)$ becomes

$$r(t) = \sum_i A_i e^{-3t/\rho_i} \quad (21)$$

and the mean harmonic ρ is given by the initial slope of a plot of $\ln r(t)$ vs t (Wahl, 1966). Using these equations, and analyzing his data in terms of a sum of exponential components, Wahl has determined two rotational relaxation times for a γ globulin-dye conjugate (1969) and for a bovine serum albumin conjugate at acid pH (1966). The multiple relaxation times were attributed to internal degrees of freedom. Dynamic polarization experiments on ethidium bromide complexed to DNA have led to the interpretation that DNA also exhibits internal degrees of freedom (Wahl, Paoletti, and LePecq, 1970) as suggested by Ellerton and Isenberg (1969).

Yguerabide, Epstein, and Stryer (1970) have presented equations of the form (21) above, relating the decay of the emission anisotropy to the principal relaxation times of an ellipsoid of revolution and the orientation of the chromophore transition moments to the ellipsoidal axes. Their equations give the dynamic emission anisotropy as a sum of three exponentials for a given orientation of the chromophore transition moment, and two for the case of randomly oriented transition moments. Using techniques similar to Wahl's, they studied the flexibility of an antibody molecule and determined that the nanosecond motions of the antibody represented, again, some internal flexibility of the molecule rather than a characteristic rigid shape. They determined this by comparing the shape of their $r(t)$ versus t

plots with plots calculated for ellipsoids of revolution of various axial ratios. Since the agreement was not good for any assumed axial ratio, an explanation in terms of internal motions was attempted.

Movement of the dye with respect to the macromolecule was ruled out by examining the dynamic polarization of large molecular fragments. These dye labeled fragments exhibited single rotational relaxation times in keeping with their molecular volume and shape, and hence there was no movement of the dye on the protein.

Analysis of the dynamic emission anisotropy in terms to two components, one relating to the Brownian rotational motions of the entire molecule, and the other representing large scale internal flexibility gave results in good agreement with independent investigations of the system using low angle x-ray scattering and electric birefringence. The two relaxation times are 500 and 100 nanoseconds respectively. These results are however different from those of Wahl and Weber (1967), who used steady state polarization methods. Wahl and Weber report a rotational relaxation time of 220 nanoseconds which is approximately the harmonic mean of the values reported by Yguerabide, Epstein, and Stryer. The steady state procedure could not resolve the two relaxation times.

The work discussed above treats the ellipsoid of revolution as the most general case. A complete theory of the dynamic emission anisotropy for general rotators has been presented by Tao (1969). As this represents a significant step in the theory of decay time fluorometry, I will give here a brief outline of Tao's derivation.

The basis of the derivation is the equation,

$$W(\Omega, t) = \int W(\Omega_0) G(\Omega_0 | \Omega, t) d\Omega_0 \quad (22)$$

where $W(\Omega, t)$ is the probability of finding the emission transition moment with an orientation Ω with respect to the laboratory axis at time t , when the initial distribution is $W(\Omega_0)$. $G(\Omega_0 | \Omega, t)$ is a probability evolution function, which is the Green's function of a differential equation satisfied by $W(\Omega, t)$. The differential equation is the diffusion equation for the Brownian rotational diffusion of an asymmetric molecule. The initial distribution and the Green's function are written as an expansion in terms of surface harmonics. Integration of equation (22) is thus simplified, and $W(\Omega, t)$ is obtained. The intensities of the polarized components of emission are obtained by averaging intensities of individual transition moments over the distribution $W(\Omega, t)$. The resulting equations are

$$I_{\parallel}(t) = I_0 \left[\frac{1}{3} + \frac{4}{15} C_{2,0}(t) \right] e^{-t/\tau} \quad (23a)$$

$$I_{\perp}(t) = I_0 \left[\frac{1}{3} - \frac{2}{15} C_{2,0}(t) \right] e^{-t/\tau} \quad (23b)$$

$$r(t) = \frac{2}{5} C_{2,0}(t) \quad (24)$$

Favro (1960) determined $C_{2,0}$ for an asymmetric body, and Tao transformed his result into terms useful in dynamic polarization.

The final equation is

$$\begin{aligned}
r(t) = r_0 & \left[\left(\frac{3\mu_1^2\mu_2^2}{\mu^4} \right) e^{-3(D_3 + D)t} \right. \\
& + \left(\frac{3\mu_1^2\mu_3^2}{\mu^4} \right) e^{-3(D_2 + D)t} \\
& + \left(\frac{3\mu_2^2\mu_3^2}{\mu^4} \right) e^{-3(D_1 + D)t} \\
& + \frac{3}{4} (B + A) e^{-(6D - 2\Delta)t} \\
& \left. + \frac{3}{4} (B - A) e^{-(6D + 2\Delta)t} \right] \quad (26)
\end{aligned}$$

where

$$D = \frac{1}{3} (D_1 + D_2 + D_3)$$

$$\Delta = \left(D_1^2 + D_2^2 + D_3^2 - D_1D_2 - D_1D_3 - D_2D_3 \right)^{1/2}$$

$$A = \frac{D_1}{\Delta} \left(\frac{\mu_1^4 + 2\mu_2^2\mu_3^2}{\mu^4} \right) + \frac{D_2}{\Delta} \left(\frac{\mu_2^4 + 2\mu_1^2\mu_3^2}{\mu^4} \right) + \frac{D_3}{\Delta} \left(\frac{\mu_3^4 + 2\mu_1^2\mu_2^2}{\mu^4} \right) - \frac{D}{\Delta}$$

$$B = \left[\left(\mu_1^4 + \mu_2^4 + \mu_3^4 \right) / \mu^4 \right] - \frac{1}{3}$$

$$\mu = \left(\mu_1^2 + \mu_2^2 + \mu_3^2 \right)^{1/2} .$$

D_1, D_2, D_3 are the diffusion coefficients around the principal axes of the asymmetric body, and μ_1, μ_2, μ_3 are the direction cosines of the emission transition moment with respect to the principal axes. This equation predicts that, in the general case, the emission anisotropy should decay as the sum of five exponentials. With suitable

experimental precision one should be able to determine the diffusion coefficients or rotational relaxation times around the principal molecular axes and thereby parameters which partially characterize the shape of the molecule.

Tao gives the simplifications expected for various assumed orientations of the chromophore and symmetry properties of the rotating body. For random orientation of label, $r(t)$ is the sum of three exponentials. For an assumed ellipsoid of revolution, equation (26) reduces to that of Yguerabide, Epstein, and Stryer (1970), and for a sphere to that of Jablonski (1935a).

In two recent papers (Tao, Nelson, and Cantor, 1970; Beardsley, Tao, and Cantor, 1970) the nanosecond depolarization technique was employed in the study of the shape of transfer ribonucleic acids. Non-linear $\log r(t)$ versus t plots were taken as evidence of ellipsoidal shapes for the rotating molecules. From molecular volumes a crude axial ratio was assigned to the transfer RNA.

It should be noted, though, that unless experiments are undertaken to show that the additional relaxation times are not due to internal flexibility, the assumption of molecular rigidity may be wrong. Experiments at different temperatures may provide this information, but a general theory relating molecular flexibility to the emission anisotropy has not been presented.

C. Energy Transfer

The final area I will discuss in which lifetime techniques may

be applied to studies of biological macromolecules is radiationless energy transfer. Rates of singlet-singlet transfer by the Förster mechanism are competitive with those of other modes of de-excitation and can therefore be studied by time decay fluorometry. Some of the experimental problems associated with steady state studies of energy transfer, for example interference from trivial (radiative) transfer and acceptor absorbance in the donor absorbance band, are obviated when donor decay time methods are used (Ware, 1961; Lamola, 1969). One important use to which this technique can be put is the determination of distances between donor and acceptor chromophores in the region 15-65 Angstrom units (Stryer and Haugland, 1967). I will briefly discuss here the relationship between energy transfer and excited state lifetime and present some theoretical results from the literature, as they seem often to be neglected or misunderstood.

Transfer between chromophores by the Förster mechanism proceeds between a donor and an acceptor when the emission spectrum of the donor overlaps the absorption spectrum of an acceptor. However, the excitation energy of the donor actually transfers to the acceptor without the emission of radiation. The rate of transfer, $k_{D \rightarrow A}$ is given by

$$k_{D \rightarrow A} = \frac{8.8 \times 10^{-25} \kappa^2 q_D}{n^4 \tau_D R^6} \int_0^{\infty} F_D(\nu) \epsilon_A(\nu) \frac{d\nu}{\nu^4} \quad (27)$$

where n is the refractive index of the solvent, τ_D and q_D are the observed lifetime and quantum yield of the donor, κ^2 is a

factor describing the relative orientation of the transition moments of the donor and acceptor, and R is the distance between them.

The overlap integral includes the terms $F(\nu)$, the normalized emission spectrum of the donor, and $\epsilon_A(\nu)$, the molar extinction coefficient of the acceptor. Often equation (27) is expressed in terms of a "critical radius," R_0 , which is the separation between the donor and acceptor molecule at which the rate of energy transfer is equal to the sum of the rates of all other deactivation processes.

$$\text{at } R_0 \quad k_{D \rightarrow A} = k_r + k_1 + k_2 + \dots = \frac{1}{\tau_D} \quad (28)$$

$$R_0^6 = \frac{8.8 \times 10^{-25} \kappa^2 q_D}{n^4} \int F_D(\nu) \epsilon_A(\nu) \frac{d\nu}{\nu^4} \quad (29)$$

In addition, in a solution of randomly dispersed donors and acceptors, a "critical concentration" of acceptor can be defined (Bennett, 1964; Bennett and Kellogg, 1967).

$$C_A^0 = \frac{3\pi^{3/2}}{2N_0 R_0^3} = \frac{4.7 \times 10^{-10} n^2}{k \left[q_D \int F_D(\nu) \epsilon_A(\nu) \frac{d\nu}{\nu^4} \right]^{1/2}} \quad (30)$$

This form will be used later.

Equation (27) represents a simple first order rate process for depopulation of the excited state of the donor for the case where all donor acceptor pairs are separated by a given distance, R . Inclusion of the rate constant for transfer with those for nonradiative and radiative decay serves to decrease the observed lifetime and quantum yield of the donor. These parameters in the absence of

transfer are given by

$$\tau = \frac{1}{k_r + k_n} \quad q = \frac{k_r}{k_r + k_n} \quad (31)$$

and in the presence of transfer to a nonemitting species

$$\tau_{et} = \frac{1}{k_r + k_n + k_{D \rightarrow A}} \quad q_{et} = \frac{k_r}{k_r + k_n + k_{D \rightarrow A}} \quad (32)$$

where k_r is the rate constant for radiative emission and k_n is the sum of the rate constants for nonradiative (excluding energy transfer) degradation. Haugland, Yguerabide, and Stryer (1969) have used relative lifetime and quantum yield measurements to verify the dependence of $k_{D \rightarrow A}$ on the magnitude of the overlap integral as seen in equation (27).

The relationship of lifetime and energy transfer is not as simple in the case where the distances of acceptor molecules from donors assumes a random distribution. Förster (1949) showed that the decay in this case is given by

$$f(t) = e^{-t/\tau_D} e^{-(\pi)^{1/2} N \frac{R_0^3}{R_g^3} (T/\tau)^{1/2}} \quad (33)$$

where τ_D is the lifetime of the donor in the absence of transfer, R_0 is the critical radius, N is Avagadro's number, and R_g is the radius of the total solution assumed to be held in a spherical container.

By employing the concept of "critical concentration" (equation 30) Bennett (1964) derived the relationship

$$f(t) = e^{-t/\tau_D} e^{-2 \frac{C_A}{C_A^0} \sqrt{t/\tau_D}} \quad (34)$$

where C_A is the acceptor concentration. He then obtained decay curves for donor-acceptor pairs in rigid polymer films. The donor was pyrene and the acceptor, the dye sevron yellow. The decay curves were in good agreement with the theory. Equations (33) and (34) predict that at short times the apparent rate of decay would be relatively high and would then slow down. This can be appreciated intuitively; with random distribution of donor and acceptor molecules, those pairs separated by a short distance would cause rapid deactivation of excited donors leaving only the more distant pairs to transfer at a slower rate. The treatment above holds for only rigid distributions, and further complications arise when diffusion is taken into account, as has recently been done (Elkana, Feitelson, and Katchalski, 1968; Steinberg and Katchalski, 1968; Steinberg, 1968).

Weber and Anderson (1969) have pointed out that transfer from a preferentially oriented excited chromophore to another chromophore mimics the effect of Brownian rotation, because memory of the initial orientation is partially lost. Jablonski (1955) derived general equations for the decay of polarized components of emission in the presence of energy transfer. The equations do not specifically relate to transfer by the Förster mechanism. Fayet and Wahl (1969) combined Jablonski's and Förster's equations and found good agreement between the theoretical result and experimental data. The data were obtained

for various numbers of fluorescein molecules attached to γ -globulin. From observations of the decay of the polarized components of emission of the different samples, the average separation of two fluorescein molecules on the protein and the mean harmonic rotational relaxation time of the protein were determined.

III. MEASUREMENT OF TIME DECAY

Two experimental methods have been used in the determination of fluorescence decay. The methods fall into the broad categories of phase and modulation measurements and pulsed excitation techniques.

In the phase delay method, first used by Gaviola (1926), the excitation beam is modulated at a frequency in the megahertz region, and the phase of the emission is measured relative to that of the excitation beam. The measured phase delay is related to the modulation frequency and the lifetime of the excited state of the emitting species. The many phase fluorometers described vary in the methods used to achieve high frequency light modulation and to measure the phase delay. Details on instrumentation appear in the review of Birks and Munro (1967).

The methods used for modulating the exciting light create only a partially modulated beam, which may be represented as an oscillating light signal superimposed on a steady signal. The relative modulation of the excitation and emission provides an independent measurement of the fluorescence lifetime. Some phase fluorometers are designed to permit both phase delay and demodulation measurements (Spencer and Weber, 1969).

In phase fluorometry single exponential decay is usually assumed. Separate measurements of the lifetime by the phase delay and demodulation techniques can indicate, however, whether the assumption is valid.

The expression for the lifetime measured by demodulation gives greater weighting to the longer-lived components than that for phase delay. Thus when more than one component is present in the emitting system, the lifetimes measured by phase delay and demodulation will be different. Heterogeneity can also be detected by measuring the lifetime at two or more modulation frequencies and comparing the results obtained. The components may be specified if one assumes there are only two.

In the pulsed excitation techniques, a short pulse of light excites the sample and the time course of the emitted light is followed in one of a number of ways. Because the form of the decay is directly observed, one can determine whether the decay is a simple exponential function, a sum of exponentials, or a more general function. If the excitation pulse is infinitely narrow, the decay curve may be analyzed directly to yield the parameters of interest. The response to an infinitely narrow (delta function) excitation I will call $f(t)$. If, as is the case with available excitation sources, the exciting pulse has a width that may not be neglected in comparison with $f(t)$, the observed response is given by the convolution

$$F(t) = \int_0^t E(t - u)f(u)du \quad (35)$$

where $F(t)$ is the observed decay, and $E(t)$ is the excitation. The convolution states simply that the amplitude of the observed fluorescence at t is the sum of contributions from the excitation over narrow time intervals, du , from zero to t . In cases where the lamp is narrow with respect to the decay of the fluorescence, one may

often analyze the section of the decay curve which occurs after the lamp has extinguished without using the convolution. For precise analysis of data and the resolution of multi-exponential decay curves, the time decay function must be extracted by a deconvolution technique. In general one must assume a form of $f(t)$, as no useful method of deconvolution has as yet been found which does not yield $f(t)$ as a definite parametric form. Further aspects of the deconvolution will be discussed in Chapter V.

Birks and Munro (1967) briefly review pulsed excitation techniques and I will here mention only a few of the precursors of the monophoton technique.

Excitation with ultraviolet or visible light had to await development of lamps which would provide pulses in the nanosecond region bright enough to generate detectable fluorescence. A more thorough discussion of excitation lamps will be presented in the next chapter, as this has been one of the principal technical problems since the beginnings of pulsed excitation fluorometry.

Using a pulsed hydrogen lamp developed by Malmberg (1957), Brody constructed a fluorometer to study the lifetime of chlorophyll emission. The instrument used a photomultiplier to detect the excitation pulse and provide a trigger for a fast travelling wave oscilloscope. The emission from the sample was viewed by a second photomultiplier and its time course displayed on the oscilloscope. A number of sweeps were photographed to provide the raw data for the decay calculation.

The method was significantly improved by Steingraber and Berlman

(1963) who employed a pulse sampling oscilloscope with a digital interface to a multichannel analyzer. Hundley, et al. (1967) have used the technique by interfacing the sampling oscilloscope to a computer.

Bennett (1960) used a stroboscopic technique to determine decay characteristics. A photomultiplier was gated by the circuit which pulsed the flash lamp. The observation time of the photomultiplier relative to the lamp flash was slowly changed by a motor driven variable delay. In this way a time-intensity profile of sample emission is collected. A variation of this technique has been employed by Dreeskamp and Burton (1959), and Yguerabide (1965) who used an image converter rather than a photomultiplier tube. In this way the effective on-time of the detection circuit is more clearly resolved. These stroboscopic techniques were introduced to overcome the relatively long risetime of photomultipliers, which distorts the early parts of the decay curve. This risetime is due to variations in the interdynode transit time of the secondary electrons (Gatti and Svetlo, 1959). For high gain photomultipliers, risetimes of two to three nanoseconds are common. Information about the tail of the decay curve is also difficult to extract from simple pulse techniques because of low intensity in that region. With the stroboscopic methods, however, data from that region can be easily enhanced.

The shortcomings in simple pulsed excitation fluorometry, which led to the stroboscopic sampling methods, also led to the monophoton method.

In 1961 three independent groups described monophoton fluorometers (Bollinger and Thomas, 1961; Koechlin, 1961; Bennett, 1961). The different requirements of each of these groups illustrate the flexibility and power of the technique. For example, Bollinger and Thomas were interested in a very broad dynamic range of decay and needed a method in which the decay tail could be obtained to high precision. On the other hand, Koechlin was studying the decays of very short lifetime scintillators. For Bennett, the single photon technique was dictated by the very low light level of emission.

The basic design of a monophoton fluorometer is schematized in Figure 2. The excitation source provides a signal which is detected by a photomultiplier which generates a start input for a time to pulse height converter. This input initiates the constant-current charging of a capacitor in the converter. Simultaneously the sample is excited. The emission is attenuated so that a high gain photomultiplier detects, at most, a single photon for each excitation pulse. The anode pulse from this photomultiplier provides a stop input for the time to pulse height converter, and the capacitor ceases charging. The capacitor is discharged, giving a pulse whose voltage is proportional to the time difference between the start and stop inputs. This pulse is then analyzed and stored in the memory of a multichannel pulse height analyzer. After the detection, analysis, and storage of many such events, the memory of the pulse height analyzer represents a histogram of the time-intensity profile of the sample emission. Such a profile is dependent not on the photomultiplier

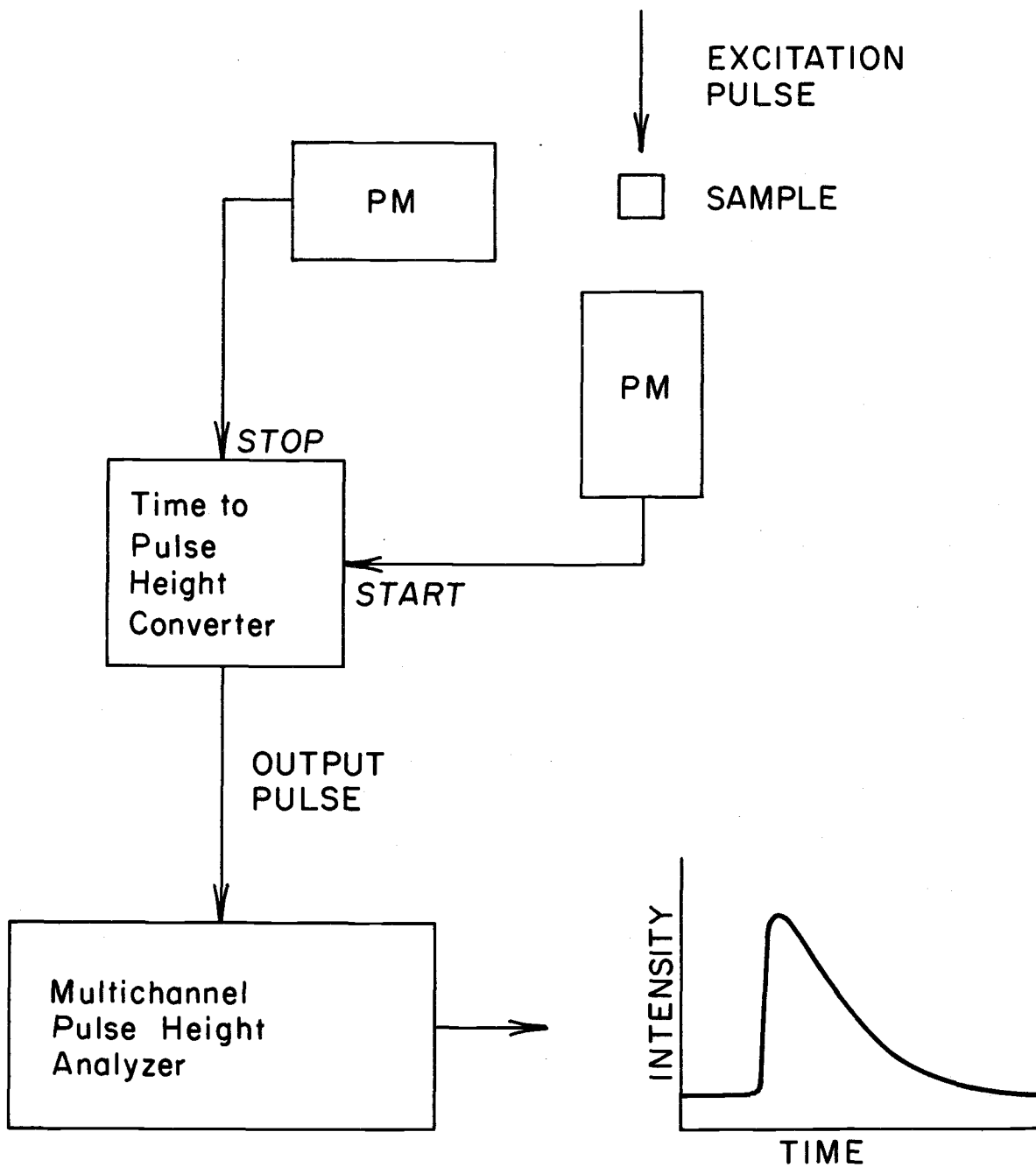


Figure 2. Schematic of the monophoton technique.

risetime, but on a time jitter, which is an order of magnitude smaller (Koechlin, 1961). By increasing the length of the experiment, the precision can be increased to limits set only by the stability of the sample, excitation source, and electronics. Finally, I note that the technique is not only acceptable for low level emission, but actually requires attenuation to the single photon level. These features have made monophoton decay time fluorometry the method of choice among the various pulsed excitation techniques.

Of the monophoton fluorometers described, many employ coincidence circuitry (Bollinger and Thomas, 1961; Koechlin, 1961; McGuire, et al., 1965). This is useful particularly in the case of excitation by nuclear particles when the amplitude of the excitation varies. By accepting as valid excitation events only those within a given pulse height region, the type of excitation can be specified. The usefulness of coincidence circuitry in other systems is questionable, however, because the time to pulse height converter already acts as a coincidence unit. When a trigger pulse starts the time to pulse height converter, an output will be generated only when the pulse from the single photon photomultiplier follows it within the time range of the converter. Only noise occurring within the total time span of the converter will be recorded. This span, typically, is in the one to two hundred nanosecond range, and with an excitation pulse frequency of ten kilohertz, for example, the observed noise rate would be only one to two tenths of one percent of the photomultiplier background count rate.

The background is not negligible, of course, in part due to the low efficiency with which events are collected.

The efficiency (the number of events collected per excitation pulse) is kept low to insure only single photon events, a necessary restriction if the data is to represent truly statistical sampling. When many such events are collected, the relative number recorded in each channel of the pulse height analyzer is proportional to the probability that emission will occur at the time associated with that channel. If multiphoton events were allowed, timing would correspond to the arrival of the first photon generated from a given excitation pulse and would bias the data toward shorter times. The effect is termed pile-up and an example will be discussed and demonstrated in Chapter VI.

A mathematical correction for pile-up, based on the assumption of Poisson statistics, has been suggested for decay curves collected at efficiencies up to 0.2 events per lamp flash (Coates, 1968). The contents N_i of the n channels of the pulse height analyzer are to be corrected to S_i , the true probability of collecting a single photon event in channel i for a single lamp flash. In the derivation of Coates (1968), P_i is the probability of an event of one or more photons occurring in channel i in one cycle. Then

$$N_i = NP_i \prod_{j=1}^{i-1} (1 - P_j) \quad (36)$$

where N is the number of cycles. The number of events collected in channel i is given by the number of times a photon occurs in the

time slice associated with that channel and none earlier. An equivalent expression is

$$P_i = N_i/N - \sum_1^{i-1} N_j \quad (37)$$

The probability of single, double, triple, etc., photon events is described by the Poisson distribution if multiphoton events are rare with respect to single photon events

$$P_i = S_i e^{-S_i} + \frac{S_i^2}{2!} e^{-S_i} + \dots + \frac{S_i^k}{k!} e^{-S_i} \quad (38)$$

$$P_i = 1 - e^{-S_i} \quad (39)$$

$$S_i = -\ln(1 - P_i) \quad (40)$$

By substituting (37) into (40) one can obtain the corrected values, S_i , from the experimental data, N_i .

This correction method has not been widely used. One source of error arises because the anode pulses of photomultipliers are a few nanoseconds in width. Arrival of two photons within this time will distort the shape of the anode pulse, and the timing will not accurately reflect the arrival of the first photon. Distortions of this type will not be corrected by Coates' technique because equations (36) and (37) will not hold. Another problem is the presence of noise on the experimental data. In our experience, for large numbers of counts the observed noise is usually outside the expected counting error, whose standard deviation in a given channel is given by the square root of the number of counts in that channel. While the noise may be

random, it may not be Poisson distributed, and the correction could make it nonrandom. Analysis techniques, such as the method of moments which we use, average away random noise by integration but would not average away nonrandom noise.

Davis and King (1970) have described an inhibit function that under some conditions permits a relatively high collection rate and still retains single photon statistics. They tee the output of the side channel timing discriminator and feed one branch to the stop input of the time to pulse height converter as in other monophoton instruments. The other output goes into a pulse-pair discriminator, which sends an inhibit pulse to the time to amplitude converter when two pulses are detected within the resolution time of the discriminator, which is set equal to the time range of the time to pulse height converter. This technique gives good results and allows high count rates for the relatively long lived emissions with which they deal. However the output pulse width of the photomultiplier and the pulse pair discrimination time of the inhibit module does not permit the rejection of events in which two photons arrive within a few nanoseconds of each other. For decay times less than ten nanoseconds, for example, a large fraction of multiple photon events fall in this category.

Both the theoretical correction technique of Coates and the pulse pair-inhibit function of Davis and King break down in their application to short lifetime decays. Before our instrument, the only alternative to these techniques has been to attenuate the emission so that collection

of even a single photon event per lamp flash is rare and the number of multiple photon events becomes even rarer. Collecting at such low rates, of course, increases the time required to achieve good precision in the data. With currently available lamp repetition frequencies, high precision experiments for the resolution of multiexponential decays, require many hours of collection time. During this time changes in the excitation source or sample can occur and the background level increases, reducing the precision of the data.

In our instrument, described in the following section, we have been able to use a collection efficiency 30 times higher than that demanded by the signal attenuation method to obtain the same high single to multiple photon ratio. The technique employed avoids the problems inherent in the theoretical correction technique and experimental inhibit method described above. Our technique is independent of photomultiplier pulse width and the channel width of the pulse height analyzer. It may be used equally well for very short or long lifetime decays. By thus decreasing the length of time required for high precision experiments, the use of time decay fluorometry as a quantitative experimental method is enhanced.

IV. THE INSTRUMENT--DESIGN, CONSTRUCTION, AND FUNCTION

When working in biochemistry, the power of time decay studies is significantly enhanced if the experimental data can be resolved into a sum of exponential decays. This is clear from the discussion in Chapter II. The determination of the environmental characteristics of binding sites and analysis of flexibility and molecular shape require resolution of multiexponential curves. Because of the precision required in this type of work, we decided to construct a monophoton fluorometer.

Isenberg and Dyson (1969) developed a method of moments for the analysis of monophoton decay time data in terms of a sum of exponential decays, and provided guidelines for the construction of our fluorometer. Using computer synthesized excitation and decay profiles, they demonstrated that the precision required for accurate multiexponential analysis is greater than that customarily achieved in the monophoton techniques, that had been previously used. For example, resolution of a double exponential decay so that the α 's and τ 's were within 10 percent of the known values,

$$f(t) = \sum_{i=1}^2 \alpha_i e^{-t/\tau_i} = 1.00 e^{-t/12.0} + 1.00 e^{-t/18.0} \quad (41)$$

requires more than five million total counts in the decay curve. This analysis assumed no noise above counting noise. With a lamp frequency of ten kilohertz and a collection efficiency of one percent, it would

take thirteen hours to obtain five million counts. The number of total counts to achieve the same precision in the analysis of the three component decay

$$f(t) = 1.00 e^{-t/18.0} + 1.00 e^{-t/12.0} + 1.00 e^{-t/8.0} \quad (42)$$

is approximately 35 million (Isenberg and Dyson, 1969).

The design selected to meet the requirements of high collection rates and low time jitter will now be briefly described, and then individual sections of the apparatus will be described more fully.

Figure 3 is a block diagram of the instrument. The lamp is a low pressure air spark gap pulsed at a constant rate by a hydrogen thyration. The light excites the sample, passes through and produces a multiphoton pulse in a trigger photomultiplier. Two signal channels are employed simultaneously. The decay curves collected in these two channels can differ in either the wavelength or polarization of the emission by insertion of the appropriate filters or rotation of the polarizing prisms. The signals detected in each of the side channels and the trigger channel are separated at the photomultiplier resistor chain into a fast timing signal and a slower linear signal. These signals follow separate paths through the modular electronics.

The timing pulse is amplified and shaped in a timing filter amplifier and fed into a timing discriminator which generates an output pulse timed accurately with respect to an invariant point on the time-intensity profile of the input pulse. Pulses originating in the side channels provide start inputs for the time to pulse height converter and a delayed trigger pulse provides a stop signal.

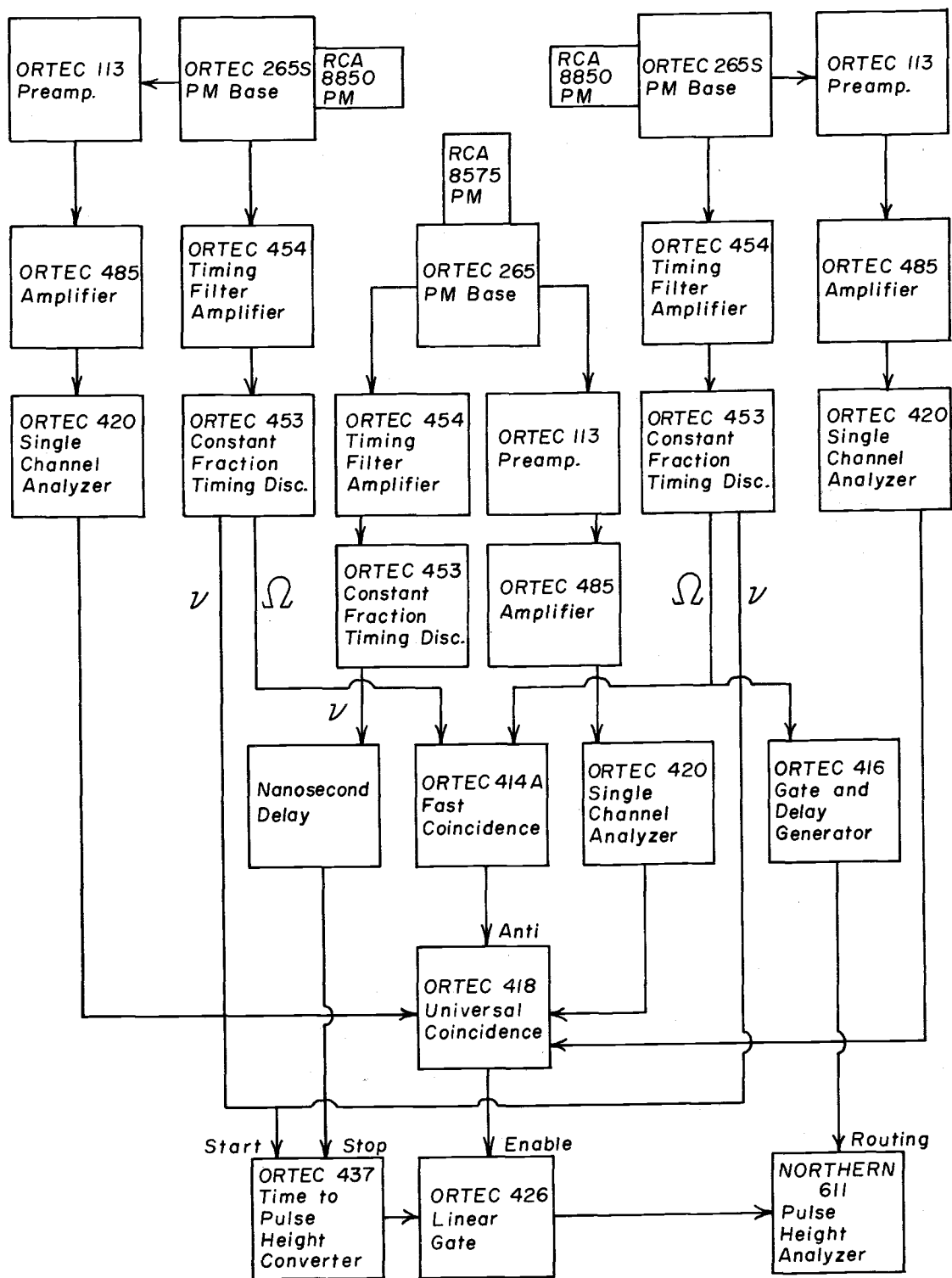


Figure 3. Block diagram of the monophoton fluorometer.

When the coincidence requirements discussed below are met, the voltage pulse generated in the converter is gated to the multichannel pulse height analyzer. Because a delayed trigger signal is used to stop the time to amplitude converter, the memory of the pulse height analyzer provides a time inverted histogram of emission decay.

The memory of the pulse height analyzer is divided into halves, one half reserved for the events collected in each of the side channels. Proper routing of the signals is achieved by the use of a shaped logic pulse from the timing discriminator of one of the side photomultipliers. Any pulse entering the pulse height analyzer will be stored in the second half of memory, if a routing signal is present; otherwise it is stored in the first half.

The linear signals from the photomultiplier bases are integrated and amplified and fed into single channel analyzers. In the trigger channel the single channel analyzer is set to give an output pulse when the input pulse exceeds the amplitude of noise pulses. In a side channel an output from the single channel analyzer is generated only when the input pulse is within the range of amplitudes previously determined for single photon events.

Pulses from the single channel analyzers activate an overlap coincidence, which gates the timing information to the pulse height analyzer. Another coincidence blocks the collection of events if both monophoton detectors are activated by a single excitation pulse. The final coincidence requirement is such that an event is collected when one or the other, but not both, side channels detects a single

photon event in a short time period following a valid excitation pulse.

Because multiphoton events are rejected electronically, data can be collected at rates much higher than those required to insure a negligible number of multiphoton events at the side channel photomultiplier.

A. The Flash Lamp

A suitable excitation source for monophoton time decay fluorometry must meet a number of severe requirements. It must have reasonable intensity in the absorption regions of the chromophores to be studied. In our work to date the region from 300 to 400 nanometers has been of interest, but broadening the available region to the 250 to 550 nanometer range is desirable for greater flexibility. To do high precision experiments a repetition rate in the kilohertz region is necessary. The pulse must also have a duration in the nanosecond region. It was previously believed that decay times shorter than the half width of the lamp could not be determined by the monophoton technique. It will be shown later that this is not true, if the precision of the data is high and the deconvolution method is accurate. The requirement instead is that the shape of the light pulse be stable during long periods of use. Amplitude stability is not as important, if appropriate methods of timing discrimination are used.

One of the major problems in the design and construction of a practical monophoton instrument is the construction of an adequate

flash lamp. Not only must it meet the requirements mentioned above, but it must be carefully designed and shielded so that its pulse will not interfere with the electronics in the remainder of the instrument. Another major problem is the elimination of noise, and our experience with this will be discussed in Section G at the end of this chapter.

Malmberg (1957) was the first to describe nanosecond flash lamps. He used a thyratron triggered spark gap in hydrogen gas at 100 mm Hg pressure. This type of lamp has been used with a number of different gases and has been closely studied (Hundley, et al., 1967; Berlman and Steingraber, 1968; Ware, 1969). A free running spark gap between mercury wetted electrodes filled with high pressure hydrogen has been discussed (D'Alessio, Ludwig, and Burton, 1964; Yguerabide, 1965; D'Alessio and Lanza, 1968). Some lamps of this type have exhibited half widths as small as 0.5 nanosecond (Yguerabide, 1965). Innes and Kerns (1961) have described a lamp in which the spark is formed at the junction of a tungsten wire and a barium titanate dielectric. Among the most promising of the newer techniques is the use of mode locked lasers (Merkelo, et al., 1969). Lasers exhibit high intensity and may be operated at very high frequencies with stable pulse shapes a fraction of a nanosecond in width. The principal drawback at this time is the difficulty in obtaining a wide range of excitation wavelengths. With the present rate of progress in laser technology, however, pulsed lasers may soon replace the spark gap lamps currently in use.

A great deal of time was spent in perfecting an excitation source

for our fluorometer. The first lamp tried was similar to that described by Innes and Kerns (1961). It is commercially produced by PEK Labs (Sunnyvale, California). This lamp in both free running and pulsing modes did not have sufficient intensity for our purposes.

An air spark gap between two stainless steel needles was tried next and exhibited considerable intensity. This lamp had an unstable pulse shape over short periods of time and was therefore unsuitable.

The high pressure hydrogen lamps of D'Alessio, Ludwig, and Burton (1964) were then tried. A number of technical difficulties were encountered in constructing these lamps. The greatest problem was wetting the nickel electrodes with mercury sealed in the lamp. In the cases where the electrodes were well wetted, the useful lifetime of the lamp was short, because mercury gradually coated the inside of the flash tube. We neglected the solution of these technical problems in favor of experimenting with other lamp designs in the literature.

The lamp with which most of our work has been done is based on the design of Ware (1969). The lamp design is shown in Figure 4.

Two Fischer-Porter* threaded glass-teflon needle valves are joined to a one inch diameter pyrex cylinder. They are oriented perpendicular to each other in an equatorial plane. One end of the cylinder is cut off flat one centimeter from the plane of the needle valves. A quartz window is attached to the flat surface with Torr Seal epoxy resin. The other end of the cylinder is tapered and joined

*The names and addresses of all commercial suppliers are found in Appendix I.

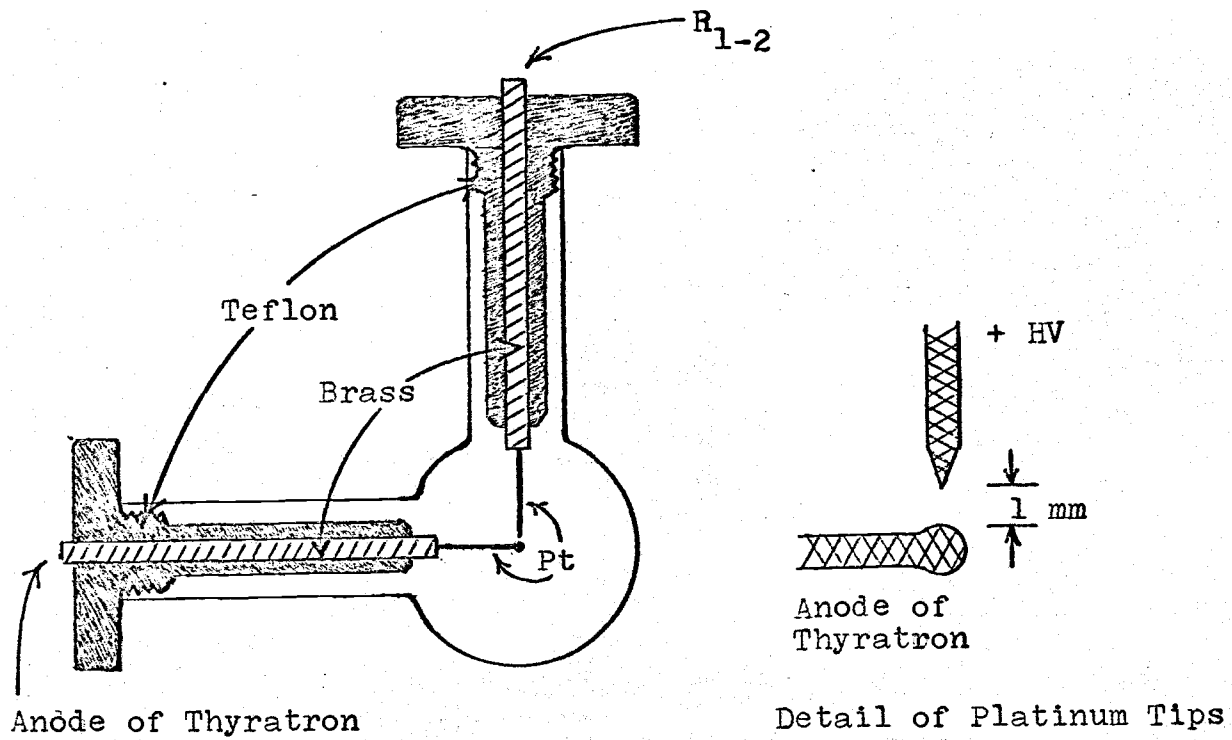


Figure 4. Lamp design.

to a vacuum stopcock which is used for introducing the low pressure gas filling. One eighth inch diameter brass rods are press fitted through the teflon needle valves as indicated. The end of the rod inside the lamp is drilled out to allow a one millimeter diameter platinum wire to be soldered securely. The other end of the rods are also drilled out to facilitate soldering the external leads. The tips of the platinum electrodes are formed as indicated; the ball by carefully melting in a gas-oxygen flame and the point by hand grinding and polishing. A gap of one to two millimeters gives the best results. Wider gaps require higher operating voltages leading to high radio frequency output which creates noise problems. Narrower gaps give lower intensity.

The lamp pulsing circuitry, shown in Figure 5 is enclosed with the lamp in a heavy walled copper box to minimize leakage of radio frequency noise generated by the high voltage pulse. Both electrodes of the lamp are charged to a high voltage, usually 4000 volts, through resistors R_1 - R_3 . One electrode is connected to the anode of an ITT 7621 ceramic-metal hydrogen thyatron. When a pulse from a blocking oscillator is applied to the grid of the thyatron, the anode and one side of the lamp are brought quickly to the cathode potential. This creates a potential difference of four kilovolts between the electrodes. The stray capacitance associated with the positive electrode is then discharged across the spark gap, a small part of the energy appearing as a brief pulse of light. The discharge mechanism is discussed by D'Alessio and Lanza (1968).

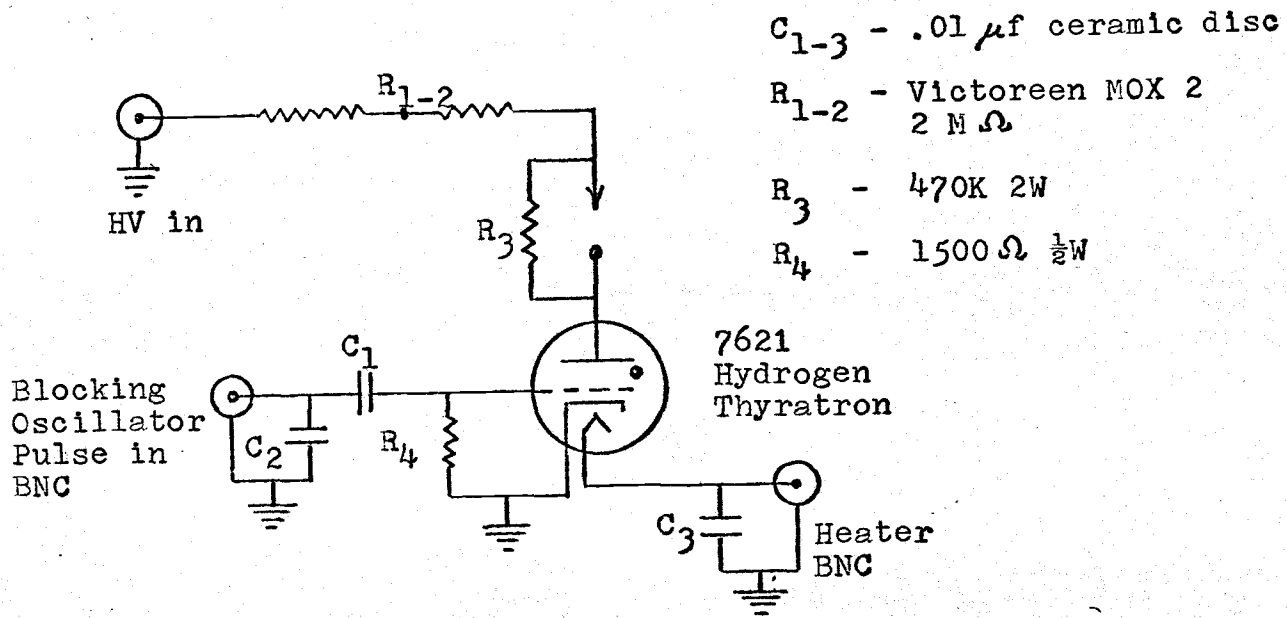


Figure 5. Lamp circuitry.

The schematic of the blocking oscillator, which is of standard design, is given in Appendix IV. The pulse frequency is continuously selectable by adjusting a potentiometer in an RC oscillation circuit. Most of the work described in this thesis was done using a pulse frequency of 10 to 15 kilohertz. Pulse rates higher than this cause a decrease in the intensity of each individual flash and thus no net intensity gain.

The lamp is filled with air at a pressure of 200 mm mercury. We have found that this gives useful intensities in the region 300 to 400 nanometers. Figure 6 is a plot of the relative spectral sensitivity obtained by viewing the intensity through various band pass interference filters with an RCA 8575 photomultiplier. Corrections have been made for the transmittance of the filters used and the wavelength sensitivity of the photomultiplier. The plot thus gives the relative intensity of light available at the sample cuvette, in the absence of an excitation filter. The peak intensity is at 350 nanometers, which is near the absorption peak of most of the chromophores we have studied. The intensity available at the sample was increased approximately 30 fold by placing a quartz collimating lens close to the lamp and focusing the light at the center of the sample cell. Lamps must be evacuated and refilled every few days due to the buildup of nitrogen oxides and slow leakage around the teflon needle valves.

The intensity slowly decreases during the first two hours of operation. The amplitude variation of the repetitive pulses is about

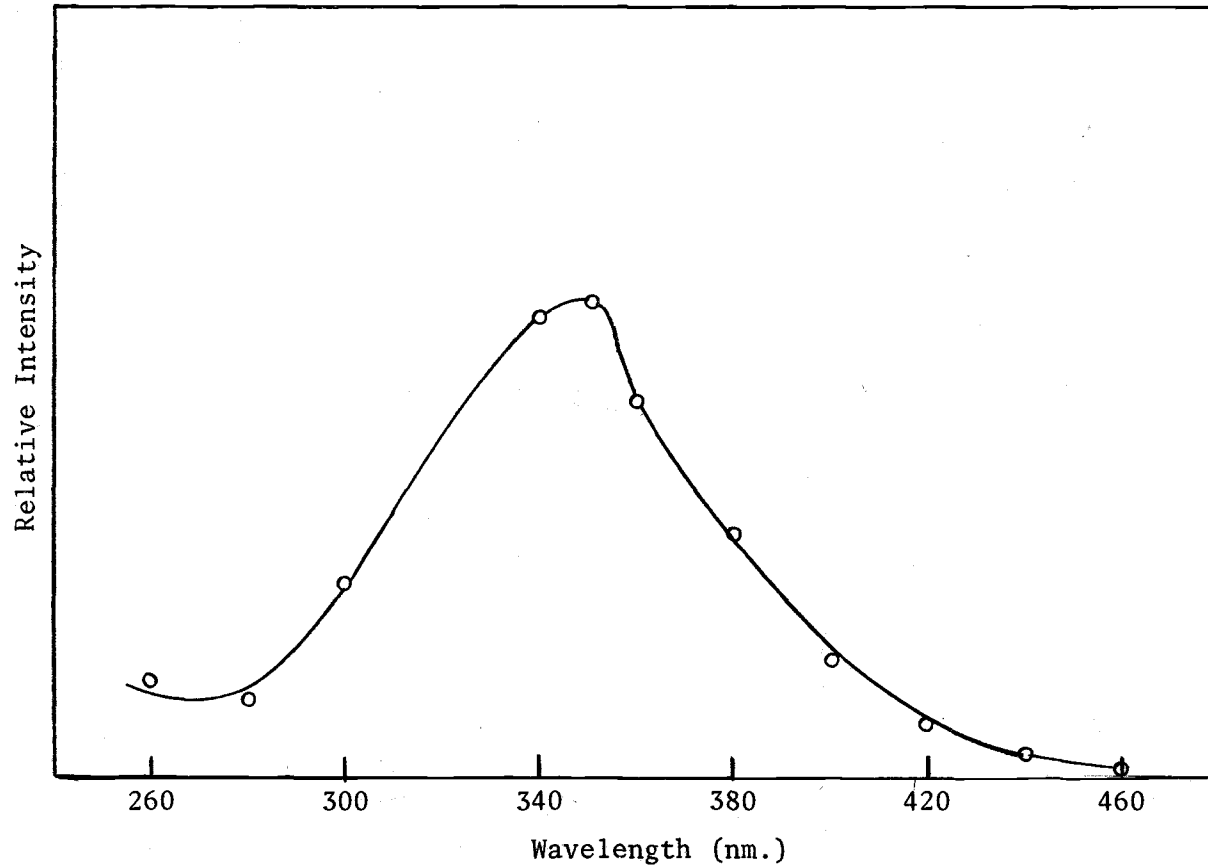


Figure 6. Relative spectral output of the nanosecond flash lamp.

five percent of the pulse height. After the initial warmup the average amplitude decreases about ten percent per day. The lamp has been run steadily for four days with few adverse effects. A slight alteration in output pulse shape is, however, observable on a time scale of hours and the shape is routinely determined before and after each decay curve is collected. A good criterion to see if changes in the lamp profile are significant is to analyze the data with both profiles and see if the analysis is the same.

The pulse shape we obtain is shown in many of the figures in later sections on both linear and logarithmic plots. The origins of the small hump preceding the main peak and the larger hump lagging it are not known, but the response of short lifetime fluorescence samples clearly indicates that the humps are due to light from the lamp (see Figures 17 and 18). These humps and the exponential tail do not adversely affect the analyses.

B. The Sample Chamber

The sample chamber, diagrammed in Figure 7, is a single unit of molded black epoxy designed to be light tight. A lid with overlapping edges and lined with black felt fits snugly on the chamber. The lid contains set screws to open and close shutters between the sample chamber and the various photomultiplier tubes. Removal of the lid automatically closes these shutters.

The cuvette holder, purchased from the American Instrument Company, accommodates a standard square one centimeter path length

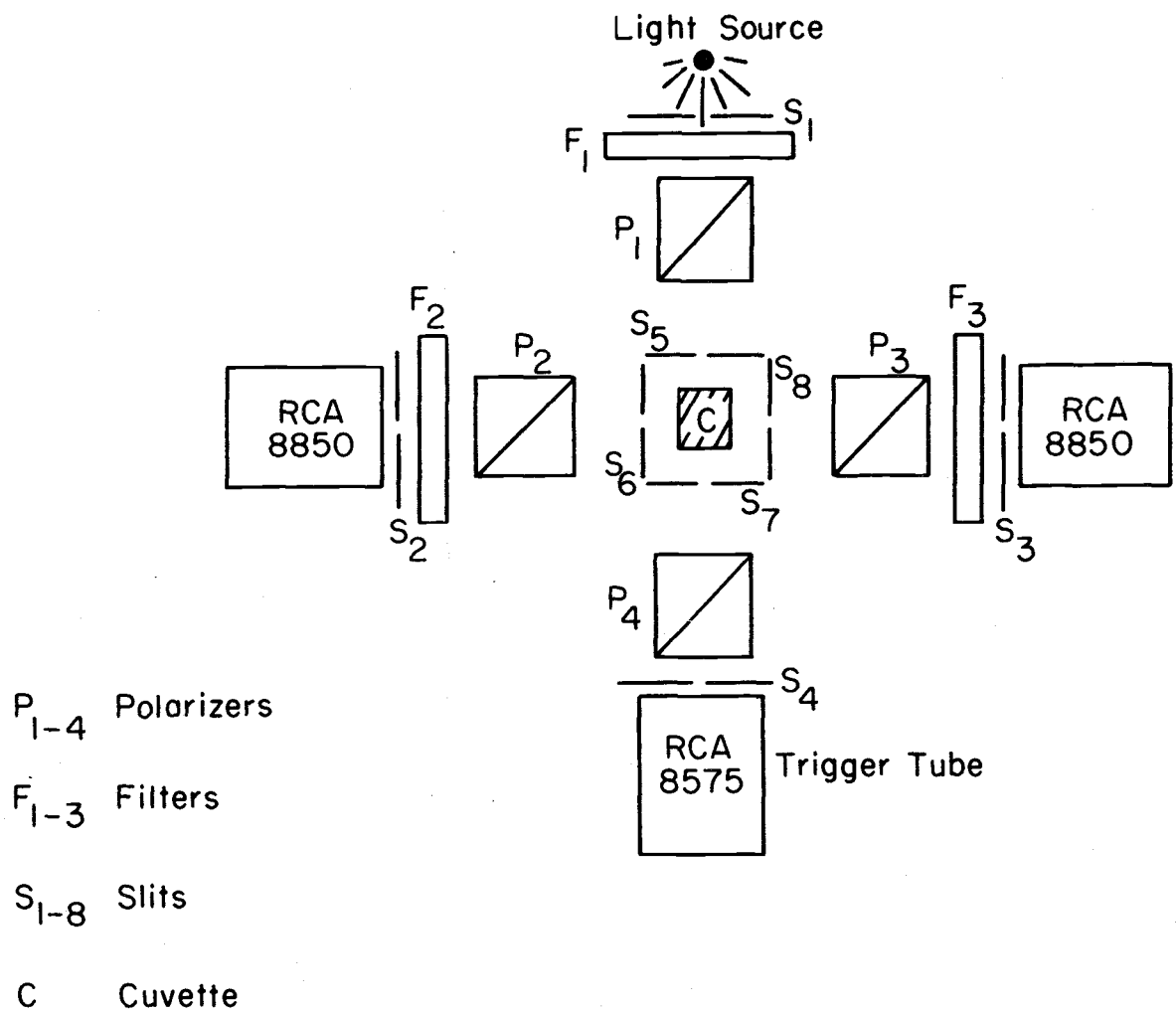


Figure 7. Diagram of the sample chamber.

fluorescence cuvette. Slit holders are present and copper tubing has been soldered to the holder for temperature control. A Yellow Springs Instrument Co. thermister probe is imbedded in the cell holder for temperature read out. For low temperature work a slow stream of dry air can be pumped through the sample chamber to avoid moisture condensation.

Excitation and emission regions are selected by optical filters. Corning colored glass filters and Baird Atomic and Optics Technology interference filters are used. Modern interference filters permit a very narrow wavelength region to be selected for wavelengths greater than 360 nanometers and studies at different emission wavelengths can be accurately performed in this region. The long and short wavelength cutoffs for filters below 360 nanometers are not as precise. In some cases combinations of filters have been used to eliminate spectral overlap and possible scattering artifacts in decay curves.

Four polarizers are used in the sample chamber. Those in Figure 7 labeled P_1 , P_2 , and P_3 are double Glan-Foucault air-gap prisms and are mounted in worm and gear mechanisms to insure accurate and reproducible settings. A rotary counter attached to the control knob indicates the polarization with respect to the experimental plane. Polarizer P_4 is used as a variable attenuator for the trigger photomultiplier tube. The polarizers are used when decay curves of the total intensity are taken, because samples exhibiting any anisotropy of emission will give multiexponential decays unless the appropriate combination of excitation and emission polarizations are used

(Jablonski 1935). The settings we use for collecting decay total intensity are vertical polarization for the excitation beam and 55° from the vertical for the emission beam. The relationship between the polarizer settings and the total intensity is derived in Appendix II. The use of two polarizers attenuates the emission by a factor of ten, but in the monophoton technique, such attenuation is often desirable.

C. The Photomultiplier Tubes

In general, for any monophoton technique, the photomultiplier tubes used must be selected for three principal characteristics. They must have high current amplification, because single photons are being detected. The dark noise should be low, because it is due primarily to thermal emission of individual electrons from the cathode and provides the same signal as a detected single photon. Then again, the tube must have good timing characteristics. By this it is meant that the time between arrival of a photon at the cathode and the time when the current pulse from the anode is detected must be constant from pulse to pulse, typically varying by only a fraction of a nanosecond. In our system we require an additional important characteristic. We discriminate between single and multiple photon events and therefore require high photoelectron pulse height resolution. For this reason we chose RCA 8850 photomultipliers. As described in Chapter VI, the use of single photoelectron pulse height discrimination permits us to obtain high collection rates and hence

good signal to noise.

Most high gain photomultipliers contain 12-14 dynodes, each with a secondary emission ratio of about 4 at the supply voltages used for single photon detection. Low values such as this give rather large statistical fluctuations in the current pulse at the anode. Hyman, Schwarcz, and Schluter (1964) show that, if the multiplication process at each dynode is described by a Poisson distribution, the dispersion, a measure of the pulse height resolution, is given by

$$\text{dispersion} = \frac{\lambda}{\lambda_1(\lambda - 1)} \quad (43)$$

where λ_1 is the mean gain of the first dynode and λ is the mean gain of the other dynodes. A conventional photomultiplier tube has values of λ_1 and λ of eight and four respectively and thus has a dispersion of 1/6. A very high gain dynode has been developed (Simon, et al., 1968), and has been employed as the first dynode in the RCA 8850 photomultiplier. Under normal supply voltages a single photo-electron emitted from the cathode produces about 30 secondary electrons at the first dynode (Morton, Smith, and Krall, 1968). The remaining dynodes have gains of three to four, giving a dispersion of approximately 1/24. This four-fold increase in pulse height resolution enables the tube to clearly resolve the single and double photon peaks. Figure 8a shows the pulse height spectrum we have observed with one of our RCA 8850 photomultipliers.

The pulse height resolution is a sensitive function of the electrostatic focusing between the cathode and first dynode (Coates, 1970). This is illustrated in Figure 8b, which was obtained under

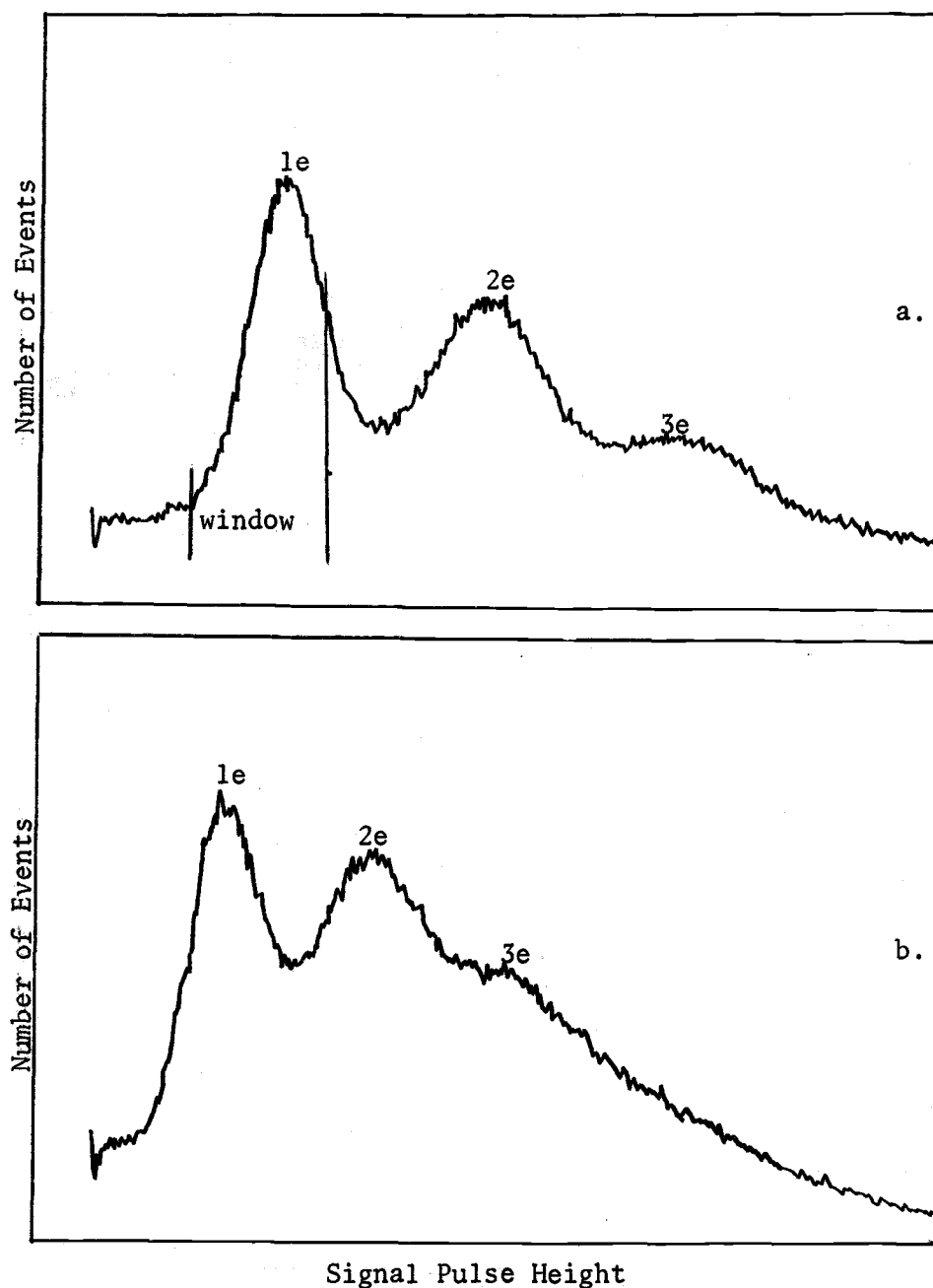


Figure 8a. Photoelectron pulse height resolution of an RCA 8850 photomultiplier. The tube was run at -2200 volts. The values indicated at the pulse height peaks are the number of photoelectrons emitted from the cathode.

8b. Same as 8a, with the electrostatic focus voltage in the photomultiplier slightly altered.

the same conditions as 8a except that the photomultiplier focus was slightly altered. An additional benefit of the high gain dynode is that improved time resolution for single photon pulses is obtained, although the anode rise time remains the same. Present and Scarl (1970) observed a 40% improvement in time resolution when the tubes were operated at 3100 volts. This is due to the relatively large voltage difference between the cathode and first dynode which decreases the transit time.

Although background noise due to random dark pulses in the photomultiplier is minimized in the monophoton technique, for very low signal intensities and for long lifetime materials, it is best to have tubes selected for low dark noise.

The shielding surrounding the tube has a large effect on the observed dark noise. The geometry we now use is shown in Figure 9. The ORTEC tube base has black potting material behind the teflon tube socket to minimize light leaks. The dark noise has been observed to decrease by a factor ten by putting a mu-metal shield at cathode potential tightly around the tube. This is taped over for electrical insulation and taped to the aluminum flange of the tube base to eliminate light leaks. The entire assembly is then inserted into a Ortec 218 magnetic shield, which is secured to the sample chamber. Cooling coils have been provided but have not yet been used because the noise level at ambient temperatures has not yet been found to be excessive for our purposes. Cooling to 0° has been shown to effect only a two fold decrease in noise rate (Coates, 1971).

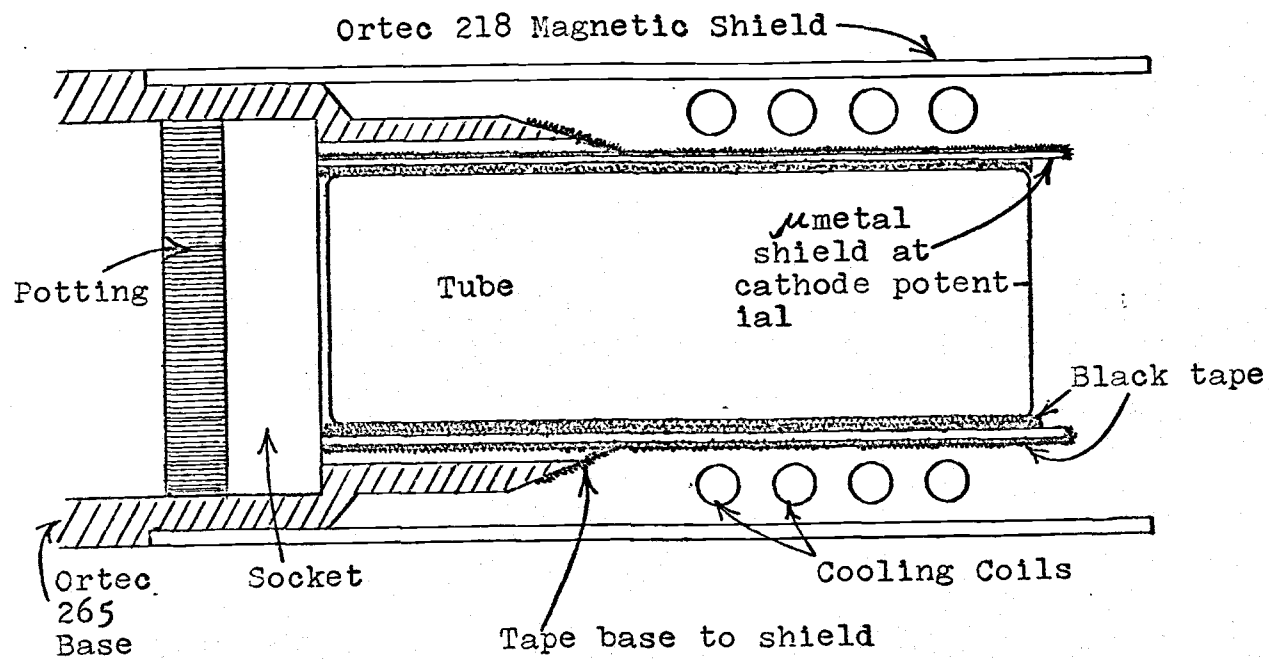


Figure 9. Photomultiplier shielding configuration.

We keep the tubes on at all times. With one tube the dark count rate decreased to one fifth the initial level after two months continuous operation.

The tubes are run at a negative cathode potential of 2200 to 2400 volts, supplied by John Fluke 415 B high voltage sources. The gain varies in different tubes, and the operating voltage must be selected according to the amplifiers and timing discriminators following the photomultiplier. Typically, at 2200 volts, the anode signal into 50 ohms is 10 to 20 millivolts for a single photon input.

The dark noise rate in the single photon region at 2200 volts, at 25°C is 150 to 300 hertz. With a lamp repetition rate of 15 kilohertz and a time to amplitude converter range of 200 nanoseconds the collection rate for random noise will be about one count per second. Signal collection rates vary from 20 to 4000 hertz, and thus background presents little problem.

The RCA 8575 photomultiplier is used as the trigger tube in the time decay fluorometer. Its sensitivity and rise time are the same as the RCA 8850 but the first dynode is not the high gain type, and the overall gain of the tube is lower than the 8850. In most of the work done to date the tube has been run at 1600 volts and has triggered on pulses of about 500 photo-electrons ejected from the cathode. The relatively high incident flux decreases the time jitter of the trigger, and an accurate zero of time is obtained.

D. Pulse Timing

There are many things which affect the timing in monophoton experiments. Some of these were discussed in relation to the photomultipliers. Bearing those considerations in mind, one can take the anode pulse from the photomultiplier as the timing input to the electrical system. The characteristic impedance of the anode circuitry in the photomultiplier is 50 ohms and this impedance is maintained at all fast signal interconnections to reduce reflections. Because the signal amplitude into 50 ohms is low, a wide band amplifier is used to amplify and condition the signal. A comparison of the single photon signals entering and leaving the Ortec 454 timing filter amplifier is shown in Figure 10. The amplifier has clearly introduced additional rise time in the signal, but significant smoothing and amplification has taken place.

The full width at half maximum of the pulses entering the timing discriminator as seen in Figure 10 is eight nanoseconds. From these pulses we would like to extract a timing signal accurate to a small fraction of a nanosecond. Leading edge triggering would create severe problems in the trigger channel, because slow changes in trigger amplitude would introduce systematic changes in the zero time signal relative to the lamp flash. To avoid problems of this type, we have used the recently developed constant fraction of pulse height trigger (Gedcke and McDonald, 1967, 1968). The point on the pulse to which the output timing signal corresponds is always the point at which the pulse reaches a selected fraction of its peak

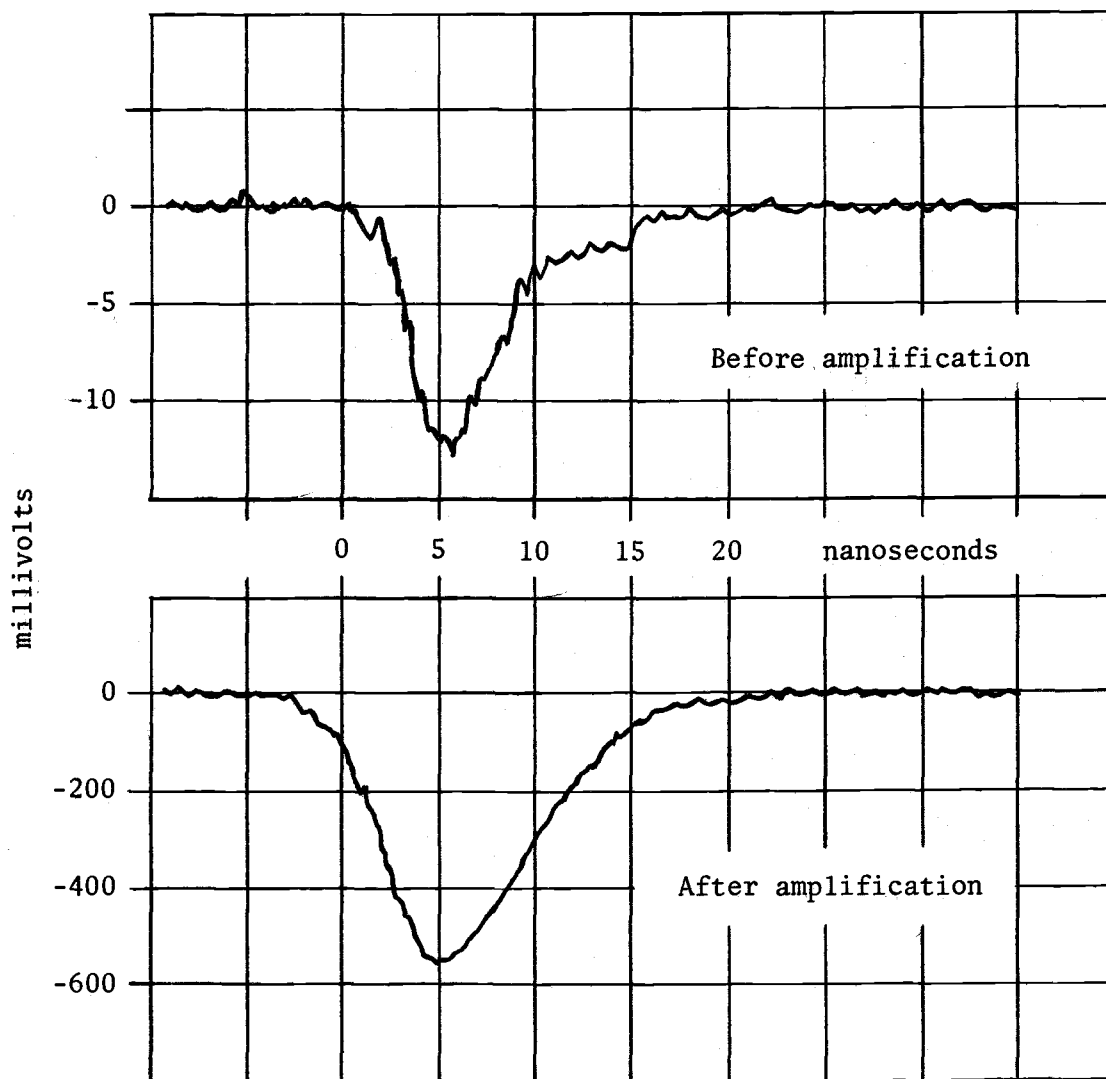


Figure 10. Comparison of the photomultiplier anode pulse resulting from a single photoelectron emitted from the cathode, with the same pulse after amplification and shaping in the Ortec 454 Timing Filter Amplifier.

amplitude. The Ortec 453 timing discriminator has been used in the constant fraction mode with a triggering fraction of three tenths. By carefully tuning the discriminator on the trigger tube we achieved less than 50 picoseconds shift in the time position of a lamp pulse when the trigger amplitude was changed by a factor of two.

Because the single photon channels generate anode signals of randomly varying amplitude, no systematic shift or "walk" is expected in the leading edge timing mode. Leading edge timing does, however, introduce timing jitter because of the wide dynamic range of single photon pulses (Figure 8a). This reduces the resolution of the curves obtained. Figure 11 compares the time intensity profile of the flash lamp collected using leading edge triggering on the side channel timing discriminator, with that obtained using constant fraction of pulse height triggering. The lower time resolution of the leading edge method increased the apparent half width of the pulse by one half nanosecond. When measuring very short lifetimes this loss of resolution becomes important.

The Ortec 453 timing discriminators contain lower level discriminators which prevent generation of timing signals from low level inputs. In practice this lower level discriminator is set at about the same level as the bottom of the single photon window discussed in the next section.

The timing pulse from the discriminators is the NIM standard fast negative logic pulse. It has an amplitude of -800 millivolts into 50 ohms and a rise time of 2.5 nanoseconds. As indicated

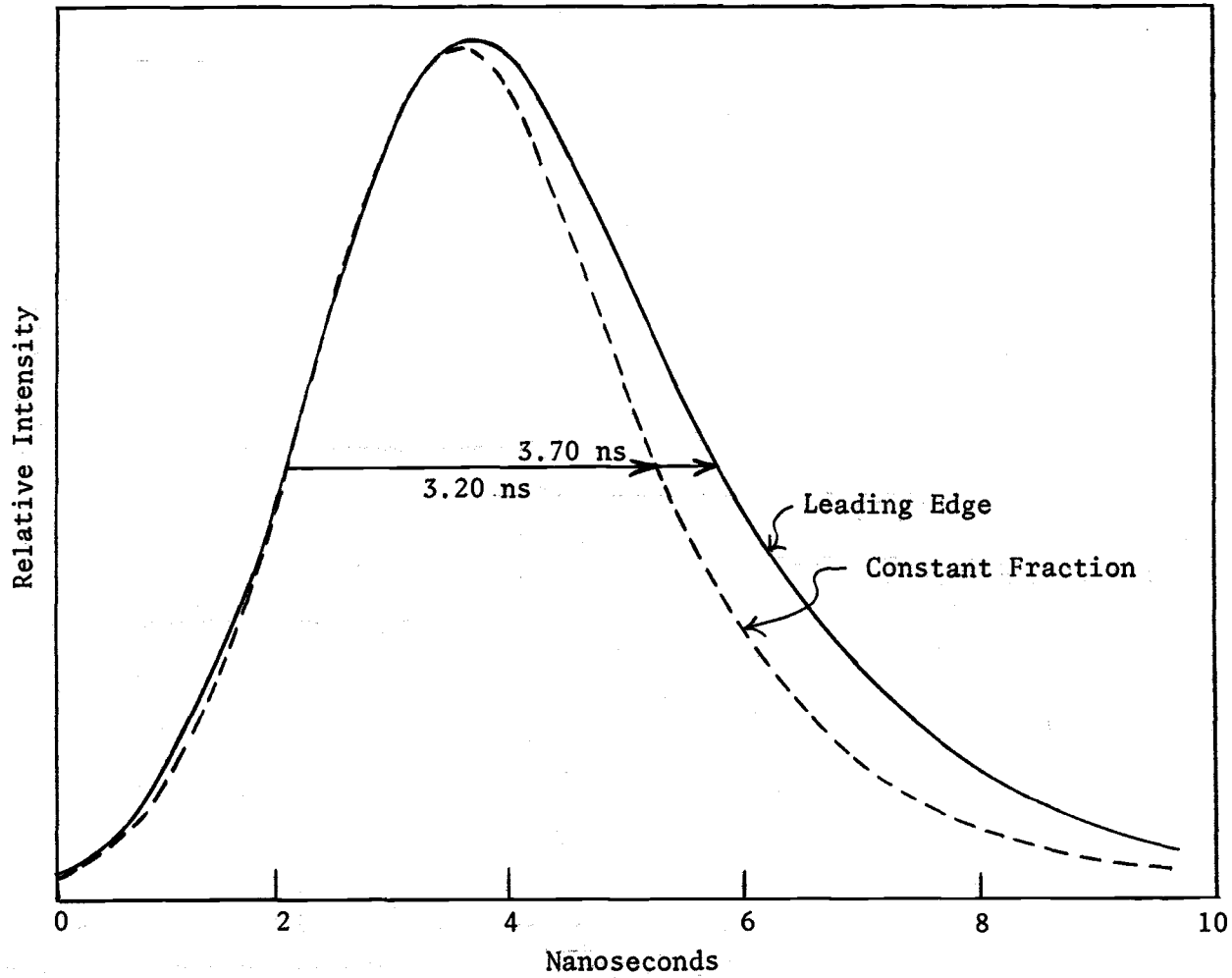


Figure 11. Lamp pulse shape determined using leading edge and constant fraction triggering.

earlier the pulses from the side channel photomultipliers, which in real time occur after the trigger pulse, are used to start rather than stop the time to pulse height converter. To stop the converter the trigger pulse must be delayed. This is accomplished by the use of lengths of 50 ohm coaxial cable, switch selectable in a Science Accessories Corp. variable delay box.

Use of many BNC connectors or switching lines should be avoided, however, because fast pulses can be degraded. This results in decreased amplitude and increased risetime and can affect the timing. We are now using single lengths of low loss RG 8 cable as delay lines, but most of the work described in this thesis employed the variable delay boxes. There is no evidence yet for a systematic error caused by the use of delay boxes, but authorities on fast pulse techniques warn against excessive delay line discontinuities (Dreher, 1967).

E. Linear Channel and Single Photon Window

When using the Ortec 265 photomultiplier base, the origin of the linear signal is usually the ninth dynode. For single photon signals, however, the 113 preamplifier-485 amplifier combination does not give sufficient gain to use a wide region of the single channel analyzer as the single photon window, when extracting the signal from the ninth dynode. We have therefore taken the linear signal from the eleventh dynode, which gives a sixteen fold increase in amplitude.

The preamplifier, amplifier combination has an integrating time

of 1.25 microseconds. Any pulses within 1.25 microseconds of the initial pulse will add to the amplitude of the amplifier output pulse. The single channel analyzer is set so that only amplifier pulses falling within the region marked "window" in Figure 8a generate outputs. Due to an overlap in the pulse height for single and double photon pulses, the top of the window is set to exclude many singles in order to inhibit almost all doubles. A further discussion of the statistics of single and multiphoton pulses and a demonstration of the efficacy of the pulse height discrimination will be given in Chapter VI.

The trigger channel linear signal originates at the ninth dynode of the RCA 8575 photomultiplier and is amplified in a manner similar to the side channels. The function of the single channel analyzer here is to discriminate against low amplitude noise pulses and to provide an input to the coincidence module for each lamp flash. For a given lamp pulse frequency the output of the trigger single channel analyzer is an invariant frequency, indicating that no noise pulses are counted and that all lamp pulses attain the amplitude set by the bottom of the single channel analyzer window. This setting is usually 75% of the Average pulse amplitude.

The pulse from the trigger single channel analyzer is internally regenerated in the coincidence module to provide an effective width of 0.1 to 2 microseconds. The inputs from the side channels are not regenerated and have the NIM standard slow logic width of 0.5 microseconds. Because we are dealing with an overlap coincidence, the

coincidence resolving time between the trigger pulse and either side channel pulse is variable from 0.1 to 2 microseconds. The true coincidence resolving time in an experiment, however, is usually set by the range of the time to pulse height converter. Only stop signals which follow start signals within the conversion time range produce outputs. The resolving time of the coincidence module is made longer than this to fully utilize the range.

F. Signal Routing and Timing

The timing discriminators on all three channels give out a slow logic pulse as well as a fast timing pulse whenever a signal above the lower level discriminator is detected. In order to route events from each side channel to different halves of the pulse height analyzer, the slow output from one side channel discriminator is used as a routing pulse. To route correctly this pulse must be made to bracket the event being analyzed in the pulse height analyzer. A gate and delay generator (Ortec 416) is used to broaden and delay the discriminator output to bracket the event under analysis. Any event unaccompanied by a routing pulse is stored in the first half of the analyzer memory; otherwise it is stored in the second half. At high collection rates there is some probability of getting a single photon event in both side channels for a single lamp flash. Since a routing pulse is generated, the event would be stored in the second half of analyzer memory. The pulse from the time to amplitude converter should, however, be stored in the memory group of the side

channel which first detected an event. This may not be the side channel associated with the second half of analyzer memory, and the event must therefore be rejected. This is accomplished by feeding the slow logic pulses from the two side channel timing discriminators into a second coincidence, an Ortec 414A, and using the output as an inhibit pulse for the first coincidence module. Therefore, whenever events are detected in both side channels for a single lamp flash, no output will occur to gate the time to pulse height converter information to the pulse height analyzer.

The timing of all the signals relative to one another is critical. The pulses from the timing discriminators occur much before the amplifier and single channel analyzer outputs, and circuit changes in the time to amplitude converter had to be made to sufficiently delay the output. The relative timing of pulses is further discussed and illustrated in Appendix IV.

G. Radio Frequency Interference

One of the main problems encountered in the construction of the monophoton fluorometer was signal distortion due to radio frequency interference. The blocking oscillator, hydrogen thyration, and spark-gap lamp can all give out high frequency radiation, which is correlated in time with the scatter or decay curves being collected. A decay curve distorted by radiofrequency interference is shown in Figure 12.

To overcome this difficulty a number of steps were taken. The blocking oscillator was enclosed in copper sheeting and the hydrogen

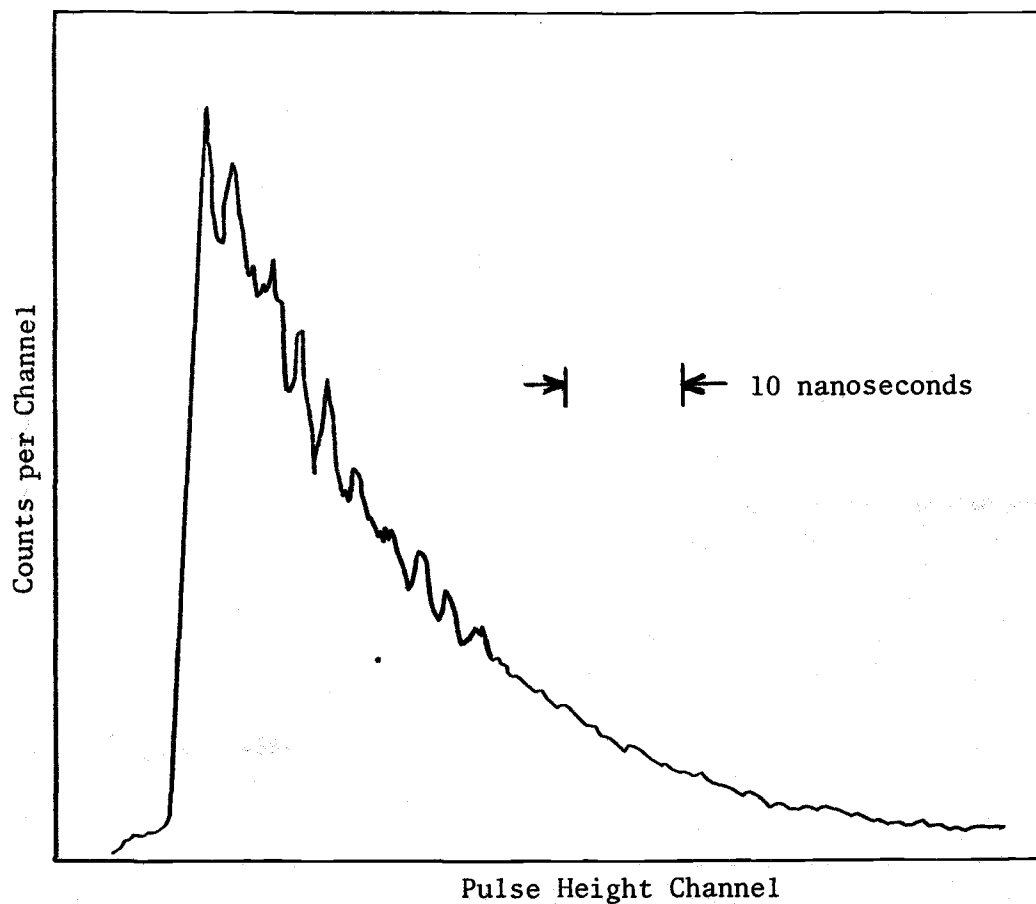


Figure 12. A decay curve of quinine distorted by pickup of radiofrequency interference.

thyration and spark gap were enclosed in a thick walled copper box. All coaxial cables used for signal interconnection are double shielded types. For timing signals RG 55/U cable is used. This has a characteristic impedance of 53.5 ohms. All other cables are RG 71 B/U, having 93 ohm impedance. The efficacy of each of these steps is not clearly known. The most important factor in reducing the effects of radio frequency interference, in our case, has been limiting the applied voltage on the thyration and spark gap to 4000 volts.

V. ANALYSIS OF DATA

All decay curves presented in this thesis have been analyzed by the method of moments described by Isenberg and Dyson (1969). The method has been incorporated into a computer program by Robert D. Dyson. The program is run in the time sharing mode of Oregon State University's Control Data Corporation 3300 computer.

I now return to a discussion of the convolution mentioned earlier (equation 35).

$$F(t) = \int_0^t E(t-u)f(u)du \quad (35)$$

As defined previously $F(t)$ is the observed decay curve, $E(t)$ the system response to the excitation, and $f(t)$ the decay response to delta function excitation. Brody (1957) assumed $f(t)$ was a simple exponential and used a method of moments to determine the lifetime. Wahl and Lami (1967) analyzed dye-protein decay curves in terms of the sum of two exponentials by determining the longer lifetime component from the tail of the decay curve and using a subtraction technique combined with a method of moments to determine the short component. Other workers (Tao, 1969; Tao, Beardsley and Cantor, 1970) have used least squares curve fitting procedures. Such procedures are very untrustworthy in determining parameters of multi-exponential curves (Lanczos 1964).

Figure 13 gives an example of the danger of curve fitting. The noisy curve was synthesized from the parameters indicated with a lamp profile taken on the monophoton instrument. Pseudorandom noise [Moshman, 1967] was added to the data such that the standard deviation of the synthetic data is given by the square root of the number of counts in a given channel. The smooth curve superimposed on the noisy data shows a very good fit to the synthetic curve, but gives very poor decay parameters as indicated.

It was shown by Isenberg and Dyson (1969) that, even by using the method of moments, which involves no normalization of curve fitting in the usual sense, high precision data must be obtained for accurate multiexponential analysis.

In the analysis technique described by Isenberg and Dyson (1969) the decay function $f(t)$ is assumed to be a linear sum of exponential terms.

$$f(t) = \sum_{n=1}^N \alpha_n e^{-t/\tau_n} \quad (44)$$

Moments of $F(t)$ and $E(t)$ are defined by

$$\mu_k = \int_0^{\infty} t^k F(t) dt \quad (45)$$

$$m_k = \int_0^{\infty} t^k E(t) dt \quad (46)$$

It can then be shown that

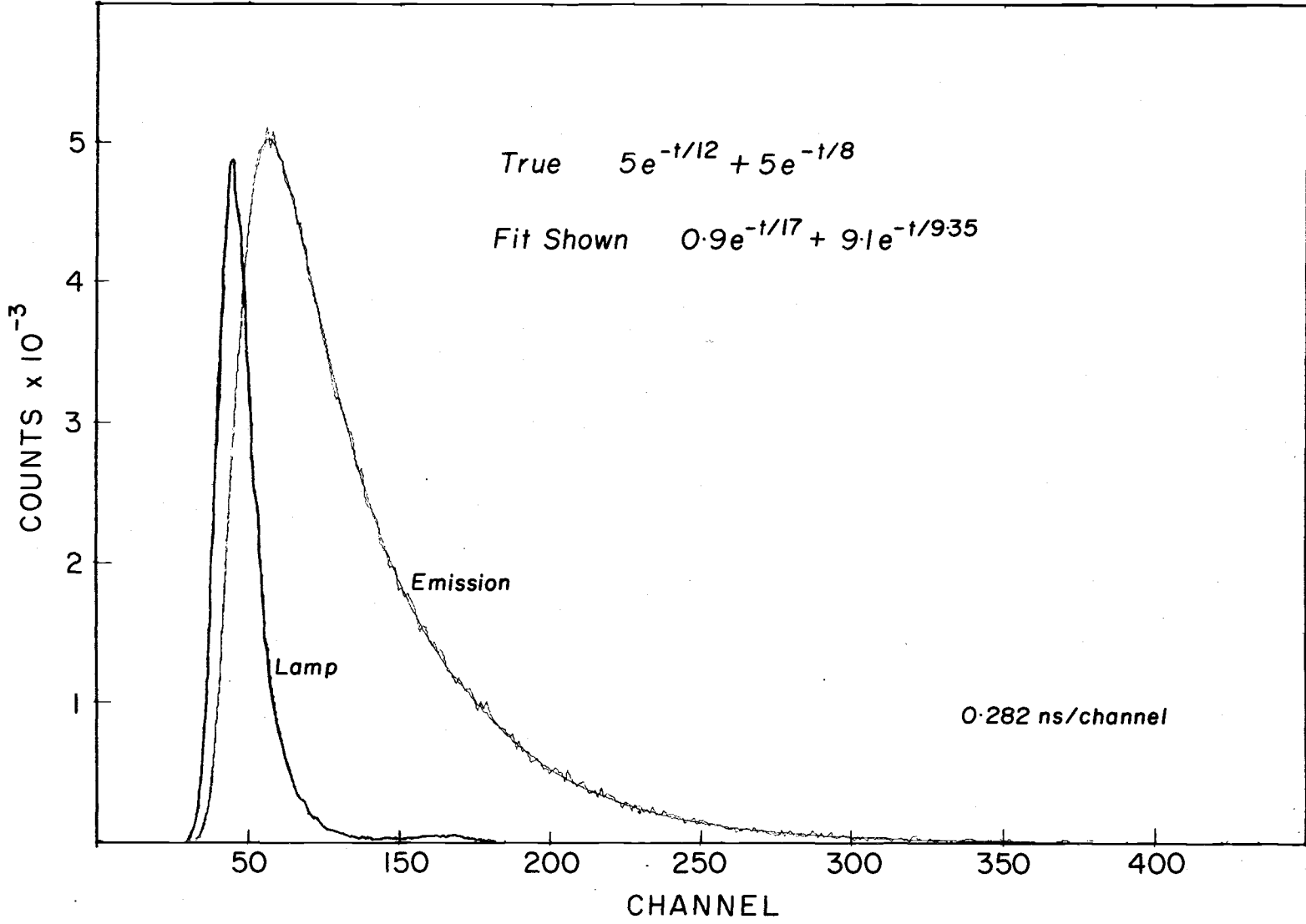


Figure 13. Demonstration of curve fitting with incorrect parameters.

$$\begin{aligned}
\mu_0 &= G_1 m_0 \\
\mu_1 &= G_1 m_1 + G_2 m_0 \\
&\vdots \\
\mu_k &= k! \sum_{s=1}^{k+1} G_s \frac{m_{k+1-s}}{(k+1-s)!}
\end{aligned} \tag{47}$$

where

$$G_s = \sum_{n=1}^N \alpha_n \tau_n^s \tag{48}$$

From the moments of the experimental data one can obtain a set of $2N$ independent G 's, from which the values of $\alpha_1, \alpha_2, \dots, \alpha_N$ and $\tau_1, \tau_2, \dots, \tau_N$ can be determined. The actual number of components contained in the experimental data cannot be unambiguously determined because of the noise on the data. In general, when analysis for an additional component yields a value of α many orders of magnitude lower than the α 's of the previous components, we assume that the new component is not present. We have routinely analyzed to three components, but the presence of additional components cannot be ruled out.

The moments defined by (45) and (46) must be computed to infinite time, but the experimental data stops at some time T . A cut-off correction $\delta\mu_k$ must therefore be added to the approximate moments of the decay data. The approximate moments of $F(t)$ are given by

$$\mu'_k = \int_0^T t^k F(t) dt \quad (49)$$

and from these and the moments of $E(t)$, an initial set of values α_n and τ_n are computed. Cutoff corrections

$$\delta\mu_k = \int_T^\infty t^k \sum_{n=1}^N \alpha_n e^{-t/\tau_n} dt \quad (50)$$

are added to the μ'_k 's to form new moments of $F(t)$ from which new values of α_n and τ_n are computed. This iteration procedure continues until two successive sets of values of μ_k yield α_n 's and τ_n 's different by an arbitrarily small amount. Cutting the experimental data off before the decay curve drops to the baseline is often not only necessary but desirable. The relative noise on the data at long times becomes high and may distort the computed moments so that the resultant analysis is not as accurate as would be obtained using an earlier cutoff (Isenberg & Dyson, 1969).

This is shown in Table I. Synthetic data using an experimental lamp flash were constructed with the decay characteristics

$$f(t) = .40e^{-t/18.0} + 1.60e^{-t/4.0} + 1.60e^{-t/10.0} \quad (51)$$

The nanoseconds per channel is 0.28 and the number of counts in the peak channel is 300,000. The background is set to 200 counts.

Well defined limits of analysis are not yet known, and factors such as time per channel, analyzed parameters, and background level are all important. Some experience with computer analysis should be obtained to determine the data requirements of a given experiment.

Table I. Effect of Cutoff Point on Decay Analysis

| Cutoff Channel | Counts at Cutoff | Iterations | Analysis |
|----------------|------------------|------------|---|
| 520 | 412 | 200 | $.48e^{-t/17.4} + 1.50e^{-t/3.9} + 1.6e^{-t/9.5}$ |
| 560 | 307 | 112 | $.41e^{-t/17.9} + 1.61e^{-t/4.0} + 1.57e^{-t/10.0}$ |
| 600 | 265 | 250 | $.01e^{-t/32.8} + 2.24e^{-t/5.2} + 1.26e^{-t/13.8}$ |

The only guide, however, to the reliability of an analysis so far is that the computed parameters do not change with increased precision of the data.

For the determination of very short lifetimes, that is, those of the order of the lamp's lifetime or smaller, the lamp should be cut off at the same point as the fluorescence. An additional, though insufficient, guide to the reliability of the analysis in this case is that it not change with the cutoff point chosen. Analysis of a short lifetime decay will be presented in the next chapter.

Although we can determine time decays much shorter than the width of our excitation pulse with the method of moments, there is still some impetus toward developing a very fast lamp. For example, Dyson and Isenberg (1971) have recently developed a data smoothing technique for data in the form of sums of exponentials without a convolution. This technique may be applied to the portion of fluorescence decay curves falling after the lamp is extinguished, and considerably smooths noisy data while retaining the same time constants. This technique will be illustrated with long lifetime data in Chapter VI.

IV. TESTING AND PERFORMANCE

The performance of the monophoton fluorometer was checked with a number of tests. The efficacy of the single photon window was determined. Short and long lifetimes were measured, sub-nanosecond resolution was demonstrated, and resolution of a double exponential decay was rigorously demonstrated. Finally, the excited state lifetime, the zero point anisotropy, and the rotational relaxation time of a spherical protein were determined from a single polarized component of decay according to Jablonski's equation (19a).

A. Single Photon Window

The statistics of photon counting may be approximated using the Poisson distribution. The Poisson distribution is derived in relation to the parameters of the photon counting experiment in Appendix III.

If one pulses a flash lamp at a given rate and attenuates the excitation beam so that the mean number of photons detected per flash is n , the distribution of integral photon events is given by

$$e^{-n} + ne^{-n} + \frac{n^2}{2!} e^{-n} + \dots + \frac{n^k}{k!} e^{-n} + \dots$$

In this expression the value of the k^{th} term gives the fractional number of events due to the detection of k photons. The probability of no event being observed is e^{-n} and thus the number of events

occurring per flash is $(1 - e^{-n})$. Figure 14 is a plot of the frequency of given events (single photon, multiple-photon) versus the frequency of all events. Theoretical curves calculated from the Poisson distribution are indicated by solid lines. Figure 14 also gives the results of an experiment showing the frequency of events within the single photon window as a function of total events. The experiment was performed by inserting a scattering suspension of Ludox (Dupont) in the excitation beam and varying the light level to the side channel photomultiplier by adjusting the shutter aperture to the tube. The lamp was run at a constant frequency, and the number of events per flash was determined by measuring the frequency of events from the side channel timing discriminator in coincidence with a lamp flash, and dividing by the lamp frequency. The events per flash satisfying the single photon window were determined simultaneously by counting the lamp flash-single channel analyzer coincidence rate. The data obtained are indicated by the dotted line in Figure 14. These data lie on a curve representing an attenuated curve of the theoretical single photon rate. The reason for the attenuation is that the overlap of the pulse height of single and multiple photon events requires that the window be chosen to cut off some single photon events in order to discriminate against multiple photon events in the same pulse height region.

Figure 15 shows this overlap. The curve marked A is the pulse height distribution of events obtained at a high collection frequency, so that a large percentage of the events are due to more than one

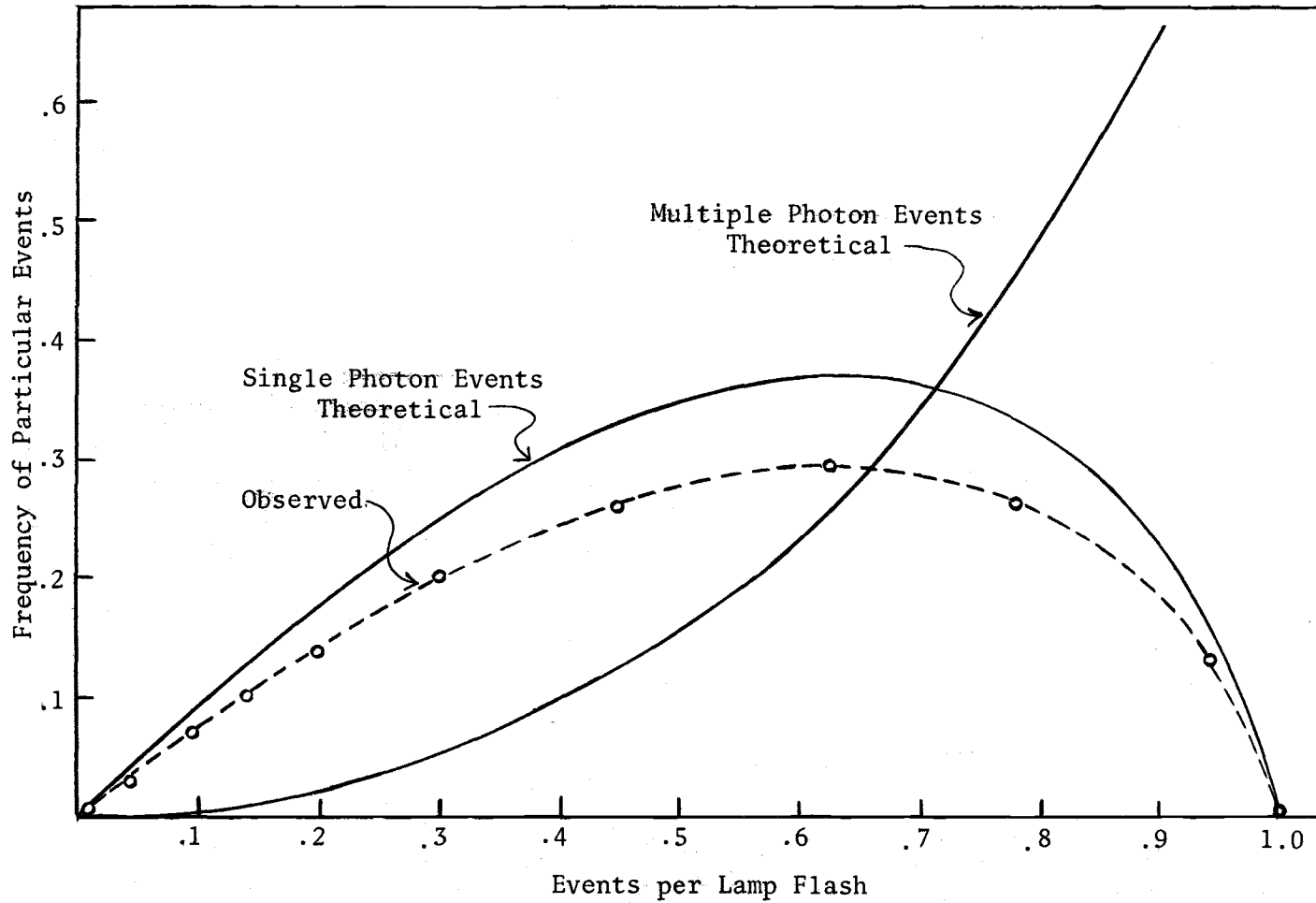


Figure 14. Frequency of single and multiple photon events versus the fraction of events collected per lamp flash according to the Poisson distribution law (solid lines). The dotted line is the frequency of events satisfying the single photon window versus the fraction of events that would be collected without the window.

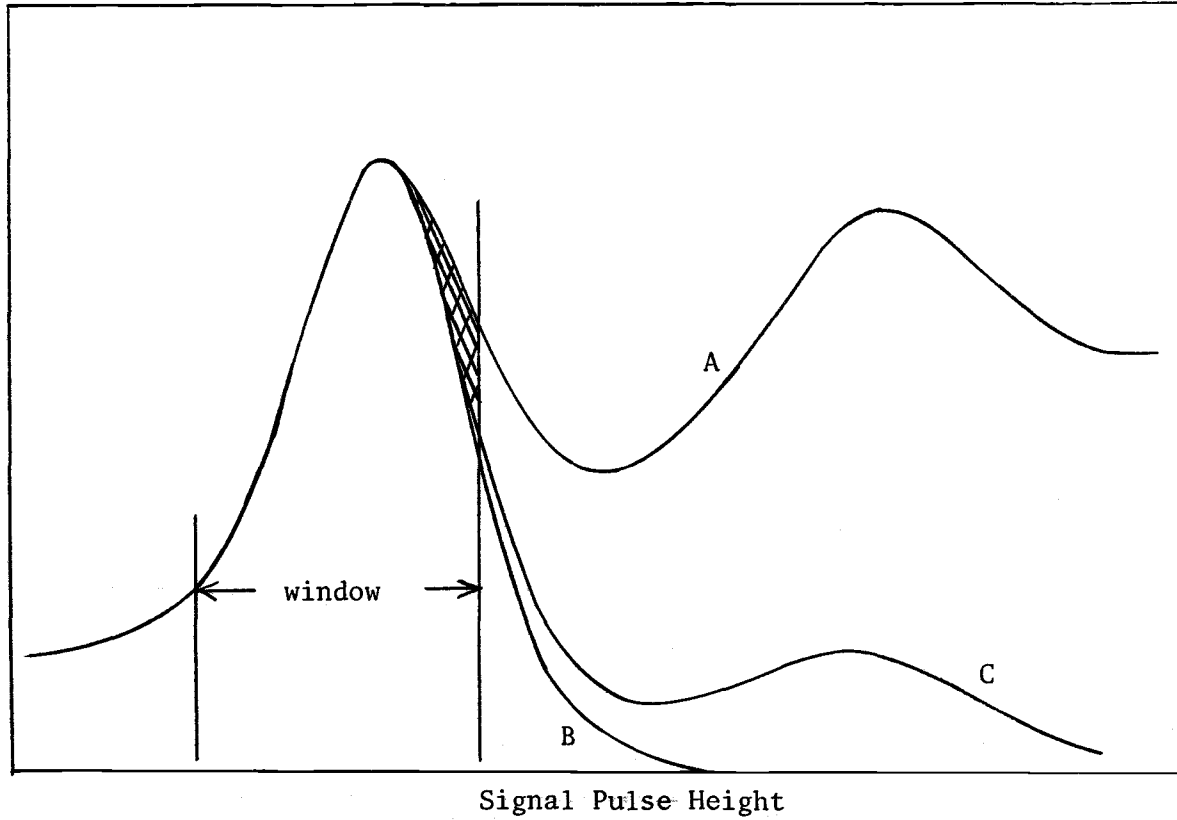


Figure 15. Signal pulse height spectra at different collection efficiencies. Curve A efficiency = .90; curve B efficiency = .01; curve C efficiency = .50.

photoelectron emitted from the photomultiplier cathode. Curve B was collected under conditions where less than one in 200 events is due to multiple photoelectrons. For curve A the fraction of multiphoton events which would not be rejected by the single photon window is given by the ratio of the cross hatched region to the total area within the window. This curve was taken at a collection efficiency of 90%, and approximately three out of 100 events within the window are due to two or more photons. Curve C was collected at an efficiency of 50% and the number of multiple photon events that would not be rejected by the single photon window is a small fraction of one percent. Using the single photon window, such a curve would collect at a rate of 0.28 counts per lamp flash. To achieve the same low percentage of multiphoton events without the window, the emission beam would have to be attenuated to give a collection rate of 0.01 counts per lamp flash.

Figure 16 shows decay curves of anthranilic acid in methanol. The solid line is a curve collected at an efficiency of one percent with no single photon pulse height discrimination. The dotted curve was collected at an efficiency of 50 percent, again with no single photon windowing. The crosses are data points from a curve collected with the same photon flux as the dotted curve but with multiple photon events rejected by single photon pulse height discrimination. The collection efficiency was 28 percent. Analyses of these decay curves using a lamp profile and the method of moments gives a lifetime of 8.11 nanoseconds for the low efficiency data, 6.70 nanoseconds

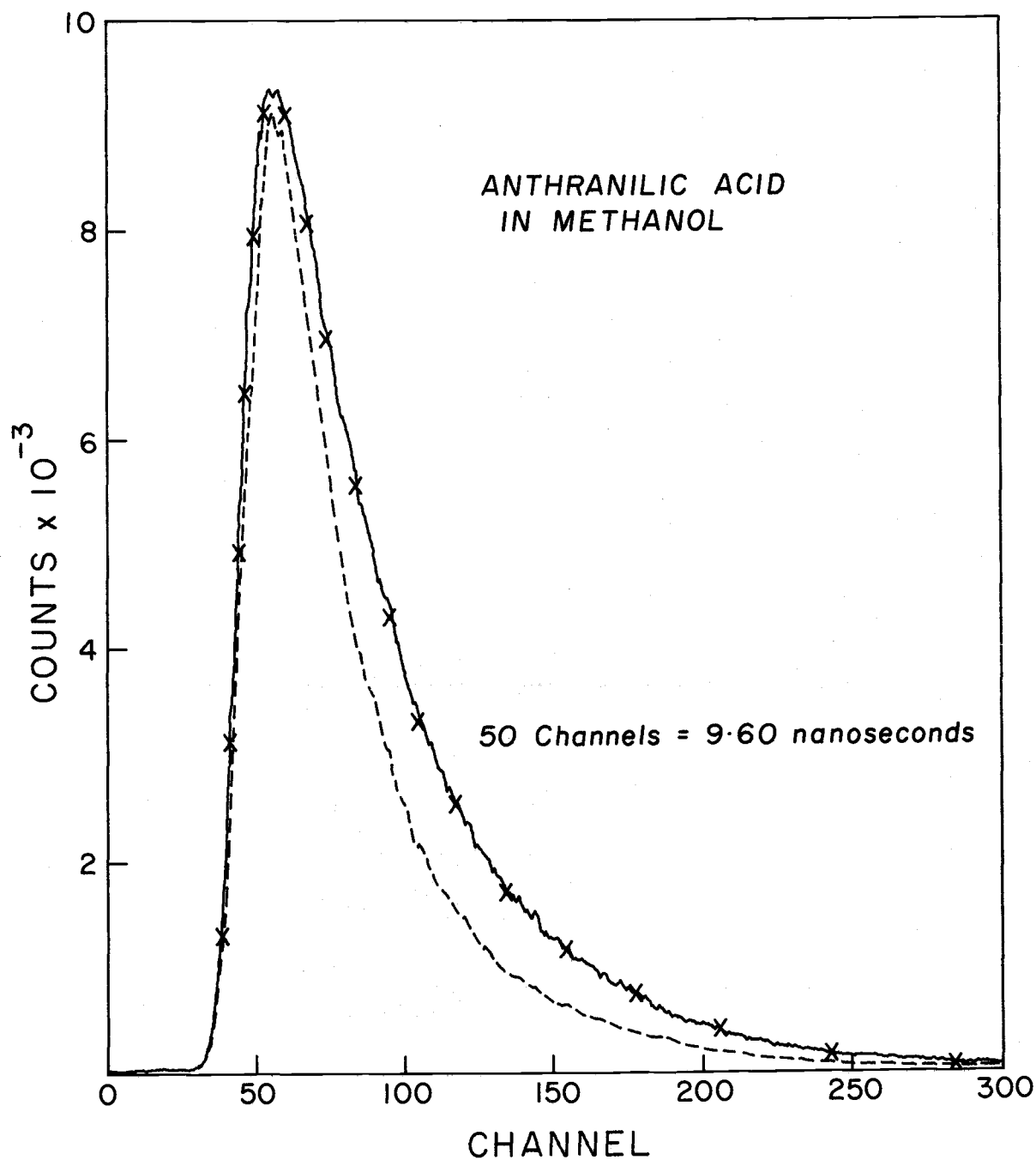


Figure 16. Decay curves of anthranilic acid in methanol. Solid line - data collected at 1% efficiency. Dotted line - data collected at 50% efficiency. Crosses - data points from a curve collected under the same conditions as the dotted curve but using the single photon window.

for the unwindowed data, and 8.06 nanoseconds for the windowed data. The values 8.11 and 8.06 nanoseconds are within our range of reproducibility, ± 0.05 nanoseconds. Thus the discrimination employed in the instrument described here markedly increases the collection efficiency while retaining single photon statistics.

B. Short Lifetime Decay

The analysis of data for decay times shorter than the half width of the excitation pulse has long been thought impossible. In theory, however, the limitation is not the lamp width but the time jitter in the electronics and photomultiplier and the power of the deconvolution technique. Although the half width of the flash lamp described here is 3.2 nanoseconds, the method of moments makes it possible to analyze subnanosecond lifetimes, provided reasonably precise data are available.

Reduced nicotinamide adenine dinucleotide (NADH) was selected as the test substance for a short lifetime determination because of its importance in biochemical studies and its very short lifetime in aqueous solution. Spencer and Weber (1969) and Scott et al. (1970) report a lifetime for NADH in water of $0.40 \pm .05$ nanoseconds. This value is consistent with that obtained from the intrinsic lifetime calculation and the measured quantum yield and may be considered reasonably accurate.

The sample we used was the disodium salt of β -NADH obtained from Sigma Chemical Co. (Lot no. D-7380). It was prepared at 10^{-4}

molar with 10^{-3} M tris buffer, pH 8.3. The excitation was selected by a Baird Atomic interference filter having a 338 nanometer peak and 25 nm. half width. The emission filter was an Optics Technology 3468 high pass filter with an 80 percent transmission point at 450 nm.

The experimental data are shown in Figure 17 along with the fluorescence computed by the method of moments.* The computed decay for a two exponential analysis is

$$f(t) = .13e^{-t/.48} + .00012e^{-t/7.90} \quad (52)$$

The result shown in equation (52) was obtained for analysis with the data cutoff at channel 800. With the same cutoff point the one component analysis yields a lifetime of 0.59 nanoseconds. The one component lifetime however decreases as the data is cutoff earlier. This is due to the higher weighting of the long lived portions of the curve in the calculation of the first moment. A two component analysis allows this weighting to be absorbed into a very low amplitude, long-lifetime, evidently spurious component. The amplitude and lifetime of the short lifetime (0.48 nanosecond) component do not vary with cutoff points ranging from channel 500 to 1000. The results of these analyses are discussed more completely elsewhere (Schuyler, Isenberg, and Dyson, 1971). The lifetime is $0.48 \pm .05$ nanoseconds, where .05 nanoseconds is the range of reproducibility

*Figures 13, 17-19 and 21 are reproductions of plots drawn by a computer driven Calcomp plotter. The experimental lamp and fluorescence decay data are shown. The smooth curve superimposed on the decay data is the fluorescence computed by convoluting the decay parameters, obtained from the method of moments analysis, with the experimental lamp flash.

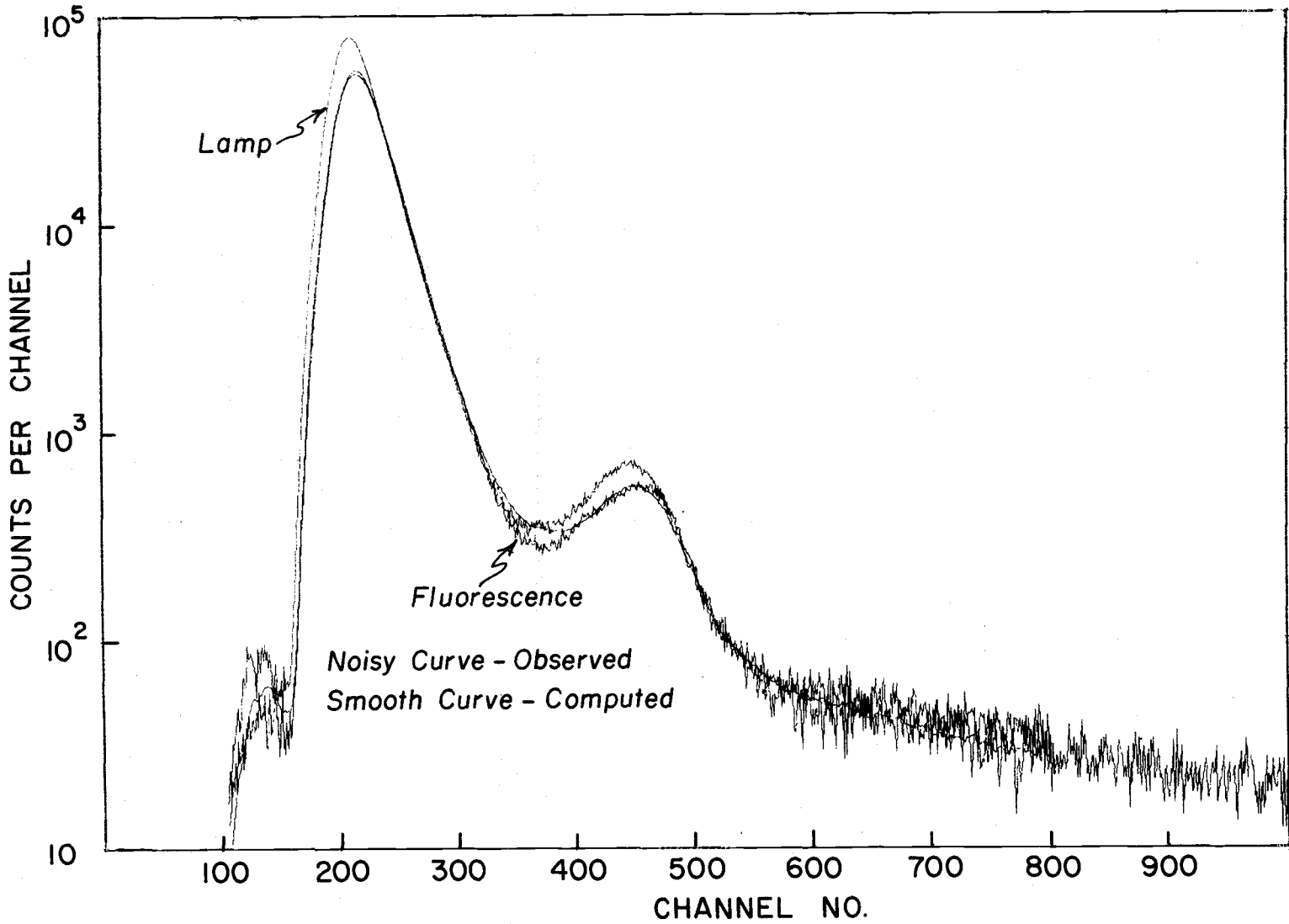


Figure 17. Decay of NADH in aqueous solution.

of the different samples run. This value is in good agreement with that of Spencer and Weber (1969) and demonstrates that lifetimes as short as one half nanosecond can be measured with the instrument and analysis described. Clearly the width of the excitation pulse does not interfere with the determination of these lifetimes.

C. Subnanosecond Resolution

As a test of the resolution of the data obtained, decay curves of deoxygenated anthracene solutions and solutions equilibrated with air were measured. Anthracene was obtained from Eastman Organic Chemicals (no. 480, lot 89A) and purified by sublimation. A 6×10^{-5} molar solution in spectro-quality benzene was used. Corning colored glass filter 7-54 was used in the excitation beam, and the emission was selected with the Corning 3-73 filter. Analysis of decay curves of samples equilibrated with air yielded a lifetime of $3.65 \pm .05$ nanoseconds. The solution was deoxygenated in a cuvette of Corning 9741 glass by a series of three freeze-pump-thaw cycles (Parker, 1968) and sealed. The experimental and computed curves for this sample appear in Figure 18. The lifetime determined is 4.00 nanoseconds, in agreement with the value of Metcalf, et al. (1965) determined by phase fluorometry. The work with oxygenated and deoxygenated anthracene in benzene clearly shows that the instrument is capable of subnanosecond resolution.

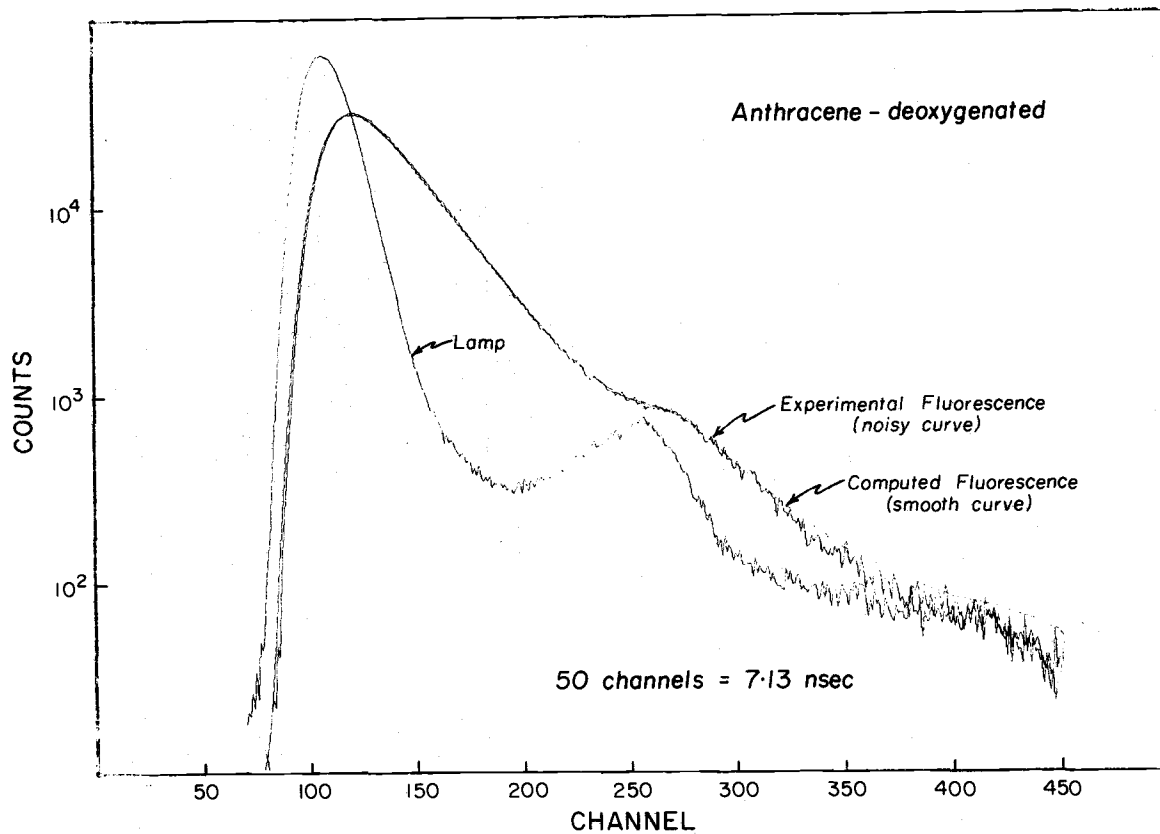


Figure 18. Decay of deoxygenated anthracene in benzene.

D. Double Exponential Decay

A number of workers have reported the resolution of time decay curves into the sum of two exponential components (Chen, et al., 1967; Wahl and Lami, 1967; Tao, 1969; and Yguerabide, Epstein and Stryer, 1970). No one however has demonstrated that the precision of his data or the power of his analysis technique warrants the assignment of two well defined exponentials. Furthermore, in view of the curve fit shown in Figure 13, least squares curve fitting without further justification is highly suspect.

To test the instrument and the method of analysis for the resolution of a two component decay, two separate samples were used, successively, with the emissions added in the pulse height analyzer. To avoid the possibility that two species in the same sample might interact, two separate samples were used. By recording the data in the analyzer before the addition of the data for the second sample, we also determined independently the decay parameters of the two samples. Decay data from 10^{-4} molar quinine in 0.1 N sulfuric acid were first collected and the curve analyzed to give α_1 and τ_1 . A sample of 10^{-4} molar anthranilic acid in methanol was substituted for the quinine and counts were added to the data already present. The values of α_2 and τ_2 were determined from the data generated by point by point subtraction of the quinine curve from the double decay curve. These values of α_n and τ_n and the values obtained from the analysis of the double decay curve are compared in Table II.

Table II. Test of Double Exponential Decay

| | | Expected | Found |
|------------------|------------|----------|-------|
| Quinine | α_1 | 4.21 | 4.10 |
| | τ_1 | 19.4 | 19.3 |
| Anthranilic Acid | α_2 | 8.34 | 8.47 |
| | τ_2 | 8.0 | 8.15 |

Linear plots of the experimental and computed curves for the double exponential decay are shown in Figure 19.

The number of counts per channel indicated on the ordinate of Figure 19 is higher than the number conventionally used in the mono-photon technique. The number of counts required to achieve a given level of accuracy is a function of many parameters. The time per channel, the shape of the lamp, the stability of the lamp, and the true decay characteristics all strongly influence the analyses, and no simple rule of thumb is available. It is clear, however, that taking many more counts than is necessary can have a detrimental effect, because, during the longer time required for data collection, the lamp characteristics may slowly change.

Such a situation is illustrated by the data shown in Table III. The data shown are for the observed double exponential decay of N-methyl-2-anilino-6-naphthalenesulfonate adsorbed to histone IV. The dye was prepared by Cory, et al. (1968) and adsorbs to regions on

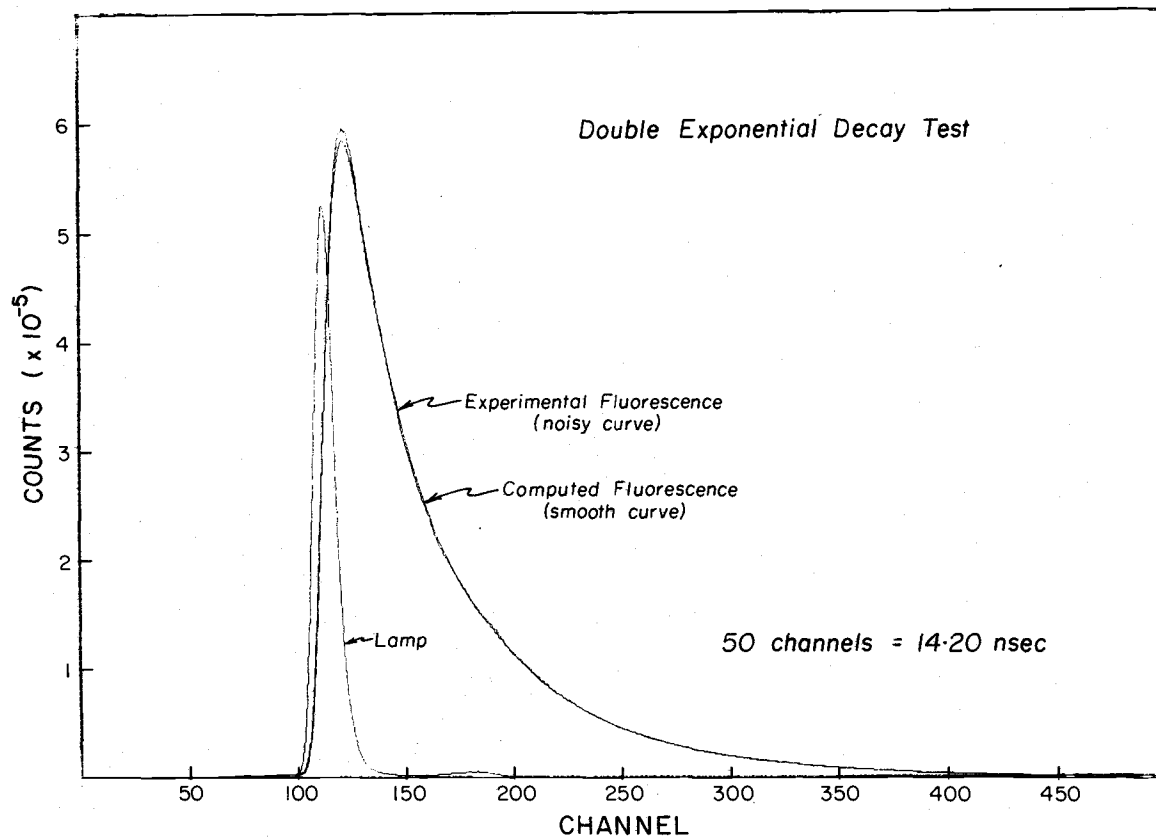


Figure 19. Double exponential decay test. The experimental fluorescence is the sum of a quinine and an anthranilic acid decay curve.

proteins and there exhibits a large increase in quantum yield. The histone was prepared according to Starbuck, et al. (1968), and diluted to 7×10^{-5} molar with .005 molar cacodylate buffer, pH 6.2. Sodium N-methy-2-anilino-6-naphthalene-sulfonate was added to a concentration of 5×10^{-6} molar. A combination of Corning 7-54 and 7-51 filters was used for excitation and a Baird Atomic 440 nanometer peak, 20 nanometer band pass filter selected the emission. Under these conditions, I found that the dye emission decay approximated a double exponential decay curve. The computed parameters are indicated in Table III along with the number of counts in the peak channel of the decay curve and the time required for collection. These data were obtained by continually adding decay data and reading out the analyzer memory at different peak count values corresponding to longer collection times.

Table III. Decay Parameters versus Peak Count

| Peak ($\times 10^{-3}$) | Time ($\times 10^{-3}$ sec.) | α_1/α_2 | τ_1 | τ_2 |
|---------------------------|----------------------------------|---------------------|----------|----------|
| 2.7 | 2.0 | .14 | 19.5 | 6.9 |
| 5.2 | 4.0 | .21 | 16.6 | 5.1 |
| 7.6 | 6.0 | .22 | 16.2 | 4.9 |
| 11.4 | 9.0 | .24 | 15.7 | 4.7 |
| 20.9 | 16.6 | .24 | 15.6 | 4.8 |
| 35.9 | 28.9 | .24 | 15.8 | 5.0 |
| 63.6 | 50.0 | .23 | 16.2 | 5.5 |

The analysis stabilizes around 11,000 counts and 9000 seconds to a decay function given by

$$f(t) = .24e^{-t/15.7} + e^{-t/4.8}$$

With fewer than 8000 counts at the peak the analysis is bad, presumably due to insufficient precision. Above this value the analysis stabilizes with parameters that are presumably accurate. However, at 50,000 seconds, the analysis changes again due to instabilities of the lamp, electronics, or perhaps even the sample. Regardless of the source of instability, however, it is clearly important for any instrument to be capable of collecting highly precise data rapidly, and the significance of single photon windowing is here emphasized.

E. Long Lifetime Decays--Analysis Without Convolution

For fluorescence lifetimes that are much longer than the decay of the flash lamp, the data may be directly analyzed at times after the point where the lamp has extinguished. The analysis in this case requires no deconvolution, and the smoothing technique developed by Dyson and Isenberg (1971) may be used. The technique was applied to a double exponential decay curve of pyrene fluorescence. The curve was constructed in the same way as the double exponential decay trial above, except that the two species were samples of pyrene with different concentrations of dissolved oxygen. The pyrene was recrystallized twice from ethanol and dissolved in spectral grade cyclohexane to a concentration of 3×10^{-5} molar. One sample was equilibrated with 0.05 atmosphere of air and the other was subjected to a

freeze-pump-thaw cycle giving a lower concentration of dissolved oxygen. Analysis of the single component curves, using the region beyond the lamp cutoff, yielded lifetimes of 125 and 332 nanoseconds respectively. The analysis for the sum of the two curves, again without the convolution, gave two lifetimes of 103 and 286 nanoseconds. When data smoothing was employed an analysis of 125 and 324 nanoseconds was achieved. A plot of the experimental and computed curves appears in Figure 20.

F. Dynamic Polarization

Four groups have presented dynamic polarization data in the literature (Wahl, 1969; Tao, 1969; Yguerabide, Epstein, and Stryer, 1970; Schuyler and Isenberg, 1971). In the first three papers, normalized curves of $I_{||}(t)$ and $I_{\perp}(t)$ were used for a point by point reconstruction of $r(t)$, the dynamic emission anisotropy. The drawback of this method is the problem of normalizing $I_{||}(t)$ and $I_{\perp}(t)$, that is obtaining the correct relative intensities of the two components. The same problem is encountered in steady state polarization work and has been discussed by Azumi and McGlynn (1962). The inherent difficulties in steady state polarization measurements with single beam instruments has led to the development of double beam polarization fluorometers (Weber & Bablouzian, 1966; Deranleau, 1966; Evett and Isenberg, 1969). Using these instruments, one can measure $I_{||}$ and I_{\perp} simultaneously, and thus obtain the emission anisotropy to greater accuracy. It is possible to do the same with

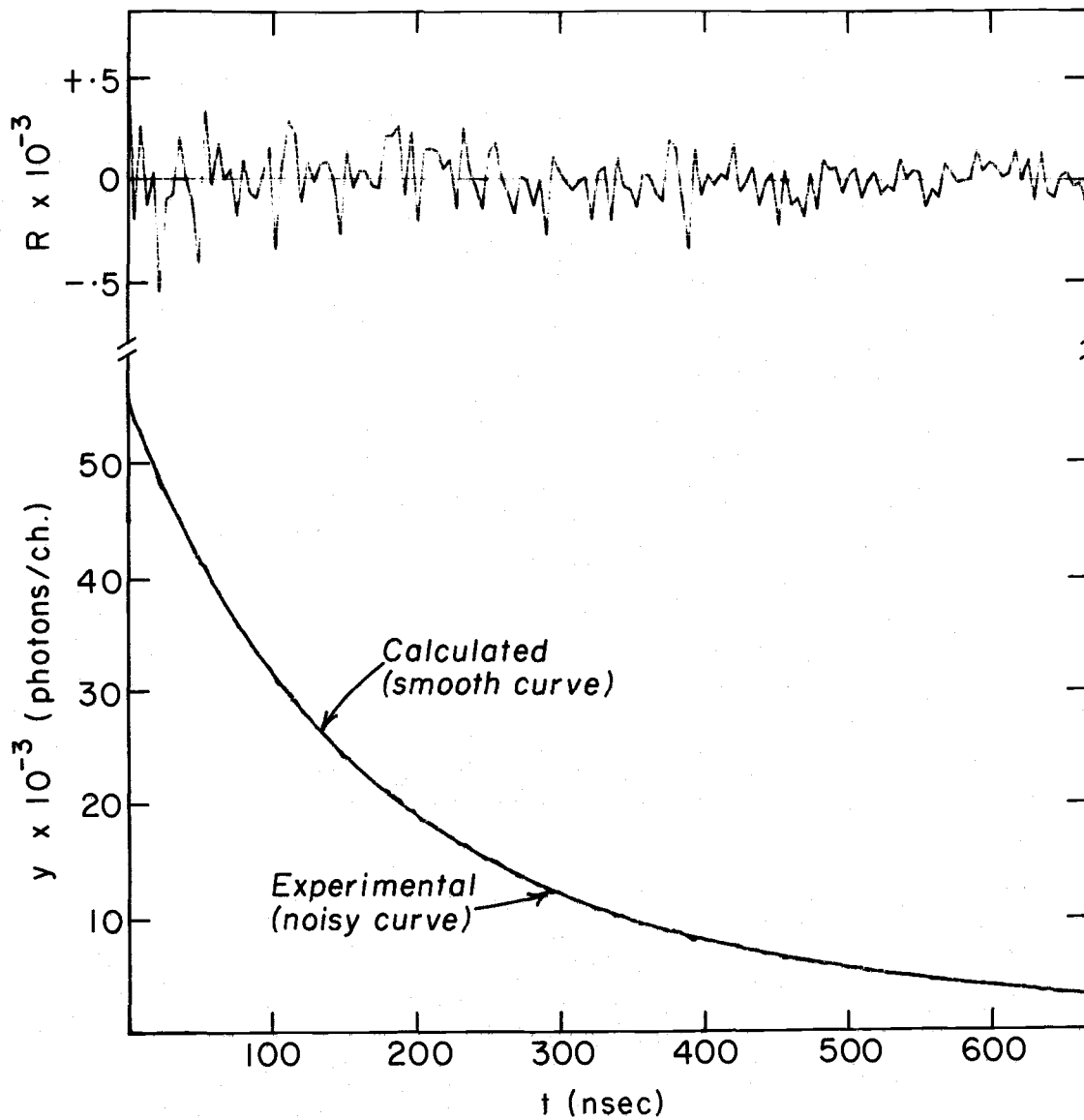


Figure 20. Summed decays of pyrene in cyclohexane at two different oxygen concentrations. The upper plot is the difference between the calculated and experimental curves.

dynamic polarization measurements, and our instrument was designed with this capability as an inherent feature. However, the small differences in the timing characteristics among photomultipliers has not yet permitted this application. Careful photomultiplier selection and timing should, in the future, permit the simultaneous collection of normalized components of decay.

The normalization techniques of each of the groups mentioned above are different. Wahl collects an $I_{||}(t)$ decay for a period of time and then $I_{\perp}(t)$ for the same period. This is repeated and if the decay profiles appear consistent, they are averaged to yield normalized decay curves of $I_{||}(t)$ and $I_{\perp}(t)$. Yguerabide, Epstein and Stryer recognize that lamp intensity changes occur in the time required to collect the decay of a polarized component to suitable precision. They therefore determine the frequency ratio of inputs to the time to amplitude converter from the single photon channel and from the trigger channel. This is done for $I_{||}(t)$ and $I_{\perp}(t)$ in succession, so that the time separating the determination of the two ratios is short enough to assume negligible change in the excitation intensity. The areas under the decay curves of the two polarized components subsequently collected are then scaled relative to these ratios, and the normalized amplitude of $I_{||}(t)$ and $I_{\perp}(t)$ are determined. Tao uses the fact that the equations representing the decay profiles of the polarized components (equations 19a and 19b) at long times reduce to a single component equal to the lifetime of the excited state. He determines the amplitude of this component

and scales the two polarized decay curves accordingly. All these procedures have yielded reasonable results for the systems described but involve some uncertainty. The technique of Wahl relies on a stable lamp intensity, which in many cases is not observed. Yguera-bide, Epstein, and Stryer's method cannot be applied to decay measurements using the single photon window, and Tao's method requires that the rotational relaxation time be shorter than the excited state lifetime.

The most straightforward way to avoid the problems of normalization is to analyze a single polarized component of decay in terms of a sum of exponential terms as in Tao's equations. For asymmetric molecules, given a single exponential excited state lifetime, the expression for $I_{\parallel}(t)$ and $I_{\perp}(t)$ is the sum of six exponential terms. As certain symmetry features are assumed, the expression reduces to two exponentials in the simplest case, that of a sphere, and is identical with Jablonski's equation (19a).

$$f(t) = k[1 + 2r_0 e^{-3t/\rho}]e^{-t/\tau} \quad (19a)$$

We chose to use this form for the analysis of a spherical macromolecule.

The system selected was apomyoglobin tagged with the dye 1-anilino-8-naphthalenesulfonate. This system has been studied using steady state techniques (Stryer, 1965; Anderson, Brunori, and Weber, 1971) and by the dynamic technique (Tao, 1969). Among the attractive features are: 1) the dye binds exclusively in the crevice from which the heme is extracted (Stryer, 1965), 2) the dye has a quantum yield

of 0.004 in aqueous solution and 0.99 in the heme binding site (Stryer, 1965), and 3) the protein is closely spherical (Kendrew, et al., 1960). The magnesium salt of 1-anilino-8-naphthalenesulfonate was obtained from Dr. S.R. Anderson and the spermwhale myoglobin was a product of Sigma Chemical Co. The apomyoglobin was prepared by the acid-acetone extraction method of Rossi-Fanelli, Antonini, and Caputo (1958). The dye and apoprotein were dissolved in 0.1 molar potassium phosphate buffer, pH 7.0, to a final concentration of 1.3×10^{-4} molar and 4×10^{-5} molar respectively. From the binding constant of 3×10^5 liters per mole (Stryer, 1965) the concentration of the dye-protein complex was computed to be 4×10^{-5} molar. A Corning 7-60 filter was used for excitation, and a 3-73 filter for emission. The excitation polarizer was oriented vertical to the plane of the excitation and emission beams. On one side channel the polarizer was also oriented vertical to this plane in order to measure the decay of $I_{||}(t)$. The polarizer in the other side channel was oriented 55° from the vertical to determine the lifetime of the dye emission without the contribution from Brownian rotation (see Appendix II). The sample was kept at 15°C and the experiment was run for 16 hours. A logarithmic plot of the two component analysis of the $I_{||}(t)$ data is shown in Figure 21. The analysis obtained is

$$f_{||}(t) = .13e^{-t/16.50} + 0.087e^{-t/6.01} \quad (51)$$

The parameters determined by substitution of (51) into (19a) are compared in Table IV with the values obtained by Anderson, Brunori, and Weber (1970) from a Perrin plot and a lifetime measured by phase

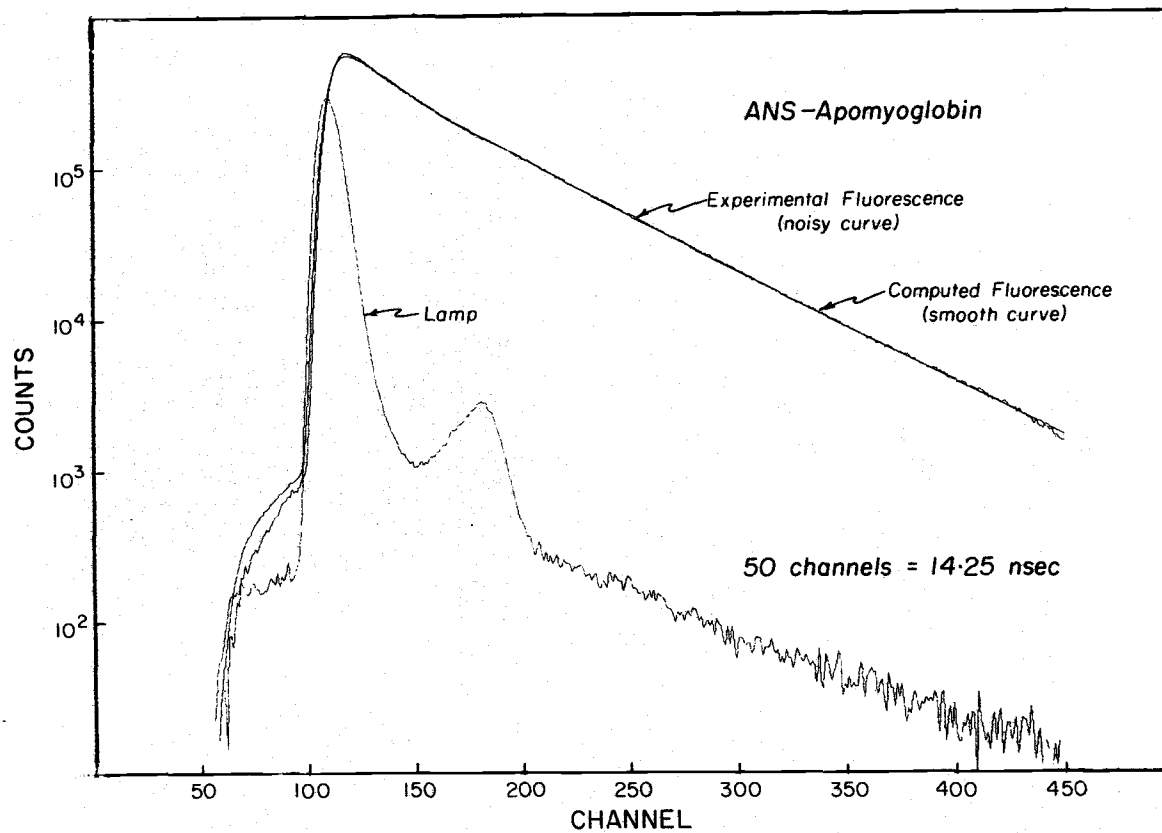


Figure 21. Decay of the ANS-apomyoglobin complex. The component of emission polarized parallel to the polarization of the excitation beam is shown.

delay. Values obtained by Tao (1969) using normalized $I_{\parallel}(t)$ and $I_{\perp}(t)$ are also given.

Table IV. Fluorescence lifetime, intrinsic anisotropy, and rotational relaxation time of the apomyoglobin-anilinonaphthalenesulfonate complex.

| | Our result | Anderson et al. | Tao |
|----------------|---------------|-----------------|---------------|
| r_0 | .33 | .34 | — |
| τ (nsec.) | $16.5 \pm .2$ | $16.4 \pm .4$ | $16.4 \pm .2$ |
| ρ (nsec.) | 28.4 | 31 | 27.5 |

The decay of total intensity determined from the $I_{\text{total}}(t)$ channel is 16.4 nanoseconds. Our result is in good agreement with the others and demonstrates the precision of the instrument and analysis technique discussed here.

The results of the tests of performance of the instrument described in this thesis can be summarized briefly. The most significant design feature, single photon pulse height discrimination has been shown to allow a 30 fold increase in the rate of data collection, while retaining high precision single photon statistics. Our work on the decay times of deoxygenated and air equilibrated anthracene indicates the subnanosecond resolution of the instrument. The timing jitter in the electronics is low enough to allow the determination of the decay time of NADH in water, a value less than one half nanosecond. We present also the first rigorous demonstration of accurate resolution

of a double exponential decay curve. This is shown for species of moderate lifetime, where a convolution of the lamp and decay profiles must be considered, and for long lifetime species, where the convolution is unnecessary. Finally, we give the first example of the analysis of a single polarized component of emission yielding the zero point anisotropy excited state lifetime, and the rotational relaxation time of a dye protein complex.

The flexibility and resolution of the instrument and analytical techniques described here will, it is hoped, enhance the value of fluorescence time decay method in the physical characterization of macromolecules.

References

1. Anderson, S.R., M. Brunori, and G. Weber. 1970. Fluorescence studies of aplysia and sperm whale apomyoglobins. *Biochemistry* 9:4723-4729.
2. Anderson, S.R., and G. Weber. 1969. Fluorescence polarization of the complexes of 1-anilino-8-naphthalenesulfonate with bovine serum albumin. Evidence for preferential orientation of the ligand. *Biochemistry* 8:371-377.
3. Azumi, T. and S.P. McGlynn. 1962. Polarization of the luminescence of phenanthrene. *Journal of Chemical Physics* 37:2413-2420.
4. Bauer, R.K. 1963. Polarization and decay of fluorescence of solutions. *Zeitschrift für Naturforschung* 18a:718-724.
5. Beardsley, K., T. Tao, and G.R. Cantor. 1970. Studies on the conformation of the anticodon loop of phenyl alanine transfer ribonucleic acid. Effect of environment of the fluorescence of the Y base. *Biochemistry* 9:3524-3532.
6. Bennett, R.G. 1960. Instrument to measure fluorescence lifetimes in the millimicrosecond region. *Review of Scientific Instruments* 31:1275-1279.
7. Bennett, R.G. 1964. Radiationless intermolecular energy transfer. I. Singlet \rightarrow singlet transfer. *Journal of Chemical Physics* 41:3037-3040.

8. Bennett, R.G., and R.E. Kellogg. 1967. Mechanisms and rates of radiationless energy transfer. *Progress in Reaction Kinetics* 4:215-238.
9. Bennett, W.R. 1961. Radiative lifetimes and collision transfer cross sections of excited atomic states. In: *Advances in quantum electronics*, ed. by J. Singer. Columbia University Press, New York, p. 28-43.
10. Berlman, I.B. and O.J. Steingraber. 1965. Further evidence of a hidden singlet transition in biphenyl. *Journal of Chemical Physics* 43:2140-2141.
11. Berlman, I.B., O.J. Steingraber and M.J. Benson. 1968. Hydrogen flash lamps. *Review of Scientific Instruments* 39:54-61.
12. Bernstein, R.S., M. Wilchek, and H. Edelhoch. 1969. Structural studies on polypeptide hormones. II. Polarization of fluorescence. *Journal of Biological Chemistry* 244:4398-4405.
13. Birks, J.B. and D.J. Dyson. 1963. The relations between the fluorescence and absorption properties of organic molecules. Royal Society (London), *Proceedings* A275:135-148.
14. Birks, J.B., and I.H. Munro. 1967. The fluorescence lifetimes of aromatic molecules. *Progress in Reaction Kinetics* 4: 239-303.
15. Brand, L., and J.R. Gohlke. 1971. Nanosecond time resolved fluorescence spectra of a protein-dye complex. *Journal of Biological Chemistry* 246:2317-2324.

16. Brody, S.S. 1947. Instrument to measure fluorescence lifetimes in the millimicrosecond region. Review of Scientific Instruments 28:1021-1026.
17. Camerman, A., and L.H. Jensen. 1969. 2-p-toluidinyl-6-naphthalene sulfonate: Relation of structure to fluorescence properties in different media. Science 165:493-495.
18. Chakrabarti, S.K., and W.R. Ware. 1970. Nanosecond time-resolved emission spectroscopy of 1-anilino-8-naphthalene sulfonate. Minneapolis. 27p. (University of Minnesota. Technical Report no. 8 on U.S. Office of Naval Research Contract N00014-67-A-0113-0006)
19. Chen, R.F. 1967. Extrinsic and intrinsic fluorescence in the study of protein structure: A review. In: Fluorescence: Theory, instrumentation and practice, ed. by G.G. Guilbault. New York, Marcel Dekker. p. 443-509.
20. Chen, R.F., G.G. Vurek, and N. Alexander. 1967. Fluorescence decay times: Proteins, coenzymes, and other compounds in water. Science 156:949-951.
21. Coates, P.B. 1968. The correction for photon pileup in the measurement of radiative lifetimes. Journal of Physics E. Scientific Instruments 1:878-879.
22. Coates, P.B. 1970. The edge effect in electron multiplier statistics. Journal of Physics D. Applied Physics 3:1290-1296.
23. Coates, P.B. 1971. Noise sources in the C31000D photomultiplier. Journal of Physics E. Scientific Instruments 4:201-207.

24. Cory, R.P., R.R. Becker, R. Rosenbluth, and I. Isenberg. 1968. Synthesis and fluorescent properties of some N-methyl-2-anilino-6-naphthalene sulfonyl derivatives. American Chemical Society, Journal 90:1643-1647.
25. D'Alessio, J.T., and H. Lanza. 1968. Discharge mechanism in gases in the subnanosecond region. Review of Scientific Instruments 39:1029-1035.
26. D'Alessio, J.T., P.K. Ludwig, and M. Burton. 1964. Ultraviolet lamp for the generation of intense, constant-shape pulses in the subnanosecond region. Review of Scientific Instruments 35:1015-1017.
27. Davis, C.C. and T.A. King. 1970. Correction methods for photon pile-up in lifetime determination by single photon counting. Journal of Physics A. General Physics 3:101-109.
28. Deranleau, D.A. 1966. A recording fluorescence polarization photometer. Analytical Biochemistry 16:438-449.
29. Dreeskamp, H., and M. Burton. 1959. Measurement of fast luminescence decay times. Physical Review Letters 2:45-46.
30. Dreher, T. 1967. Fast Pulse Techniques. Oakland, E.H. Research Laboratories. 47p.
31. Dyson, R.D., and I. Isenberg. 1971. The analysis of exponential curves by a method of moments, with special attention to sedimentation equilibrium and fluorescence decay. Biochemistry 10:3233-3241.

32. Edelman, G.M. and W.O. McClure. 1968. Fluorescent probes and the conformation of proteins. *Accounts of Chemical Research* 1:65-70.
33. Ellerton, N.F. and I. Isenberg. 1969. Fluorescence polarization study of DNA-proflavine complexes. *Biopolymers* 8:767-786.
34. Einstein, A. 1917. Zur Quantentheorie der Strahlung. *Physikalische Zeitschrift* 18:121-128.
35. Eisinger, J. 1969. Fluorescence quenching of tryptophan and proteins. In: *Molecular luminescence*, ed. by E.D. Lim. New York, W.A. Benjamin, p. 185-201.
36. Eisinger, J., B. Feuer, and A.A. Lamola. 1969. Intramolecular singlet excitation transfer. Applications to polypeptides. *Biochemistry* 8:3908-3915.
37. Elkana, Y., J. Feitelson, and E. Katchalski. 1968. Effect of diffusion on transfer of electronic excitation energy. *Journal of Chemical Physics* 48:2399-2404.
38. Evett, J. and I. Isenberg. 1969. DNA-polylysine interaction as studied by polarization of fluorescence. New York Academy of Sciences, *Annals* 158:210-222.
39. Favro, L.D. 1960. Theory of the rotational brownian motion of a free rigid body. *Physical Review* 119:53-62.
40. Fayet, M. and P. Wahl. 1969. Etude du declin de la fluorescence polarisée de la γ -globuline de lapin conjuguée avec l'isothiocyanate de fluoresceine. *Biochimica et Biophysica Acta* 181:373-380.

41. Förster, T. 1949. Experimentelle und theoretische Untersuchung des zwischenmolekularen Übergangs von Elektronenanregungsenergie. Zeitschrift für Naturforschung 4a:321-327.
42. Förster, T. 1951. Fluoreszenz organischer Verbindungen. Göttingen, Vandenhoeck & Ruprecht, 1951. 312p.
43. Gatti, E. and V. Svetlo. 1959. Theory of time resolution of scintillation counters. Nuclear Instruments and Methods 7:189-201.
44. Gaviola, E. 1926. Die Abklingungszeiten der Fluoreszenz von Farbstofflösungen. Annalen der Physik. 81:681-689.
45. Gedcke, D.A. and W.J. McDonald. 1967. A constant fraction of pulse height trigger for optimum time resolution. Nuclear Instruments and Methods 55:337-380.
46. Gedcke, D.A. and W.J. McDonald. 1968. Design of the constant fraction of pulse height trigger for optimum time resolution. Nuclear Instruments and Methods 58:253-260.
47. Gill, T.J. 1965. Crosslinked synthetic polypeptides. II. Evaluation of the internal structure of intramolecularly crosslinked polymers by polarization of fluorescence measurements. Biopolymers 3:43-55.
48. Gottlieb, Y.Y., and P. Wahl. 1963. Etude théorique de la polarisation de fluorescence des macromolécules portant un groupe émetteur mobile autour d'un axe de rotation. Journal Chimie Physique 60:849-856.

49. Haugland, R.P., J. Yguerabide, and L. Stryer. 1969. Dependence of the kinetics of singlet-singlet energy transfer on spectral overlap. National Academy of Sciences, Proceedings 63:23-30.
50. Hevesi, J. 1969. Relative yield of luminescence of quenched viscous solutions. In: Molecular luminescence, ed. by E.C. Lim. New York, W.A. Benjamin, p. 39-52.
51. Hundley, L., T. Coburn, E. Garwin, and L. Stryer. 1967. Nanosecond fluorometer. Review of Scientific Instruments 38: 488-492.
52. Hyman, L.G., R.M. Schwarcz, and R.A. Schluter. 1964. Study of high speed photomultiplier systems. Review of Scientific Instruments 35:393-406.
53. Innes, T.G. and O.A. Kerns. 1961. A pulsed nanosecond light source. U.S. Atomic Energy Commission. (UCRL-9726)
54. Isenberg, I. and R.D. Dyson. 1969. The analysis of fluorescence decay by a method of moments. Biophysical Journal 9:1337-1350.
55. Jablonski, A. 1935a. Eine Theorie der zeitlichen Abklingung des Leuchtens bei polarisierter Fluoreszenz von Farbstofflösungen. Zeitschrift für Physik 95:53-65.
56. Jablonski, A. 1935b. Zur Theorie der Polarisation der Photolumineszenz von Farbstofflösungen. Zeitschrift für Physik 96:236-246.
57. Jablonski, A. 1936. Über die Abklingungsgesetze der polarisierten Fluoreszenz. II. Zeitschrift für Physik 103:526-535.

58. Jablonski, A. 1950. Fundamental polarization of photoluminescence and torsional vibrations of molecules. *Acta Physica Polonica* 10:193-206.
59. Jablonski, A. 1955. Self-depolarization and decay of photoluminescence of solutions. *Acta Physica Polonica* 14:295-307.
60. Jablonski, A. 1960a. On the notion of emission anisotropy. *Bulletin de L'Académie Polonaise Des Sciences. Série des sciences mathématiques, astronomiques et physiques VIII*: 259-264.
61. Jablonski, A. 1960b. Über die Abklingsvorgänge polarisierter Photolumineszenz. *Zeitschrift für Naturforschung* 16a:1-4.
62. Jablonski, A. 1962. Decay and polarization of fluorescence of solutions. In: *Luminescence of organic and inorganic materials*, ed. by H.P. Kallmann and G.M. Spruch. New York, John Wiley and Sons, p. 110-114.
63. Kendrew, J.C., R.E. Dickerson, R.E. Strandberg, B.E. Hart, R.G. Davies, D.R. Phillips, and V.C. Shore. 1960. Structure of myoglobin. *Nature* 185:422-427.
64. Koechlin, Y. 1961. Sur une nouvelle méthode d'étude des scintillations ultrabrèves. *Académie des Sciences, Paris. Comptes rendus hebdomadaires des séances* 252:391-393.
65. Lami, H., G. Pfeffer, and G. Laustriat. 1966. Rendements quantiques de fluorescence et durées de vie radiative de quelques solutés utilisés dans les scintillateurs liquides. *Journal de Physique* 27:398-404.

66. Lamola, A.A. 1969. Electronic energy transfer in solution: Theory and applications. In: Techniques of organic chemistry, ed. by P.A. Leermakers and A. Weissberger. Vol. 17. Organic photochemistry. New York, Wiley. p. 17-132.
67. Lanczos, C. 1964. Applied analysis, Englewood Cliffs, New Jersey, Prentice Hall, 539p.
68. Laurence, D.J.R. 1966. Interactions of calf-thymus histone fractions in aqueous solution with 8-anilinonaphthalene-1-sulfonic acid. Biochemical Journal 99:419-426.
69. Lippert, E. 1957. Spektroskopische Bestimmung des Dipolmoments aromatischer Verbindungen im ersten angeregten Zustand. Zeitschrift für Electrochemie 61:962-975.
70. McClure, W.O., and G.M. Edelman. 1966. Fluorescent probes for conformational states of proteins. I. Mechanism of fluorescence of 2-p-tolindinyl-naphthalene-6-sulfonate, a hydrophobic probe. Biochemistry 5:1908-1919.
71. McGuire, R.L., E.C. Yates, D.G. Crandall, and C.R. Hatcher, 1965. Apparatus for precise measurement of scintillator decay times. IEEE Transactions on Nuclear Science 12:24-27.
72. Malmberg, J.H. 1957. Millimicrosecond duration light source. Review of Scientific Instruments 28:1027-1029.
73. Merkelo, H., B.R. Hartman, T. Mar, G.S. Singhal, and Govindjee. 1969. Mode locked lasers: Measurements of very fast radiative decay in fluorescent systems. Science 164:301-302.

74. Memming, R. 1961. Theorie der Fluoreszenz-polarisation für nicht kugelsymmetrische Moleküle. Zeitschrift für Physikalische Chemie, Neue Folge 28:168-189.
75. Metcalf, W.S., D.R.S. Nautsch, S.G. Page, E.D. Shipley, and P.M. Wiggins. 1965. Measurement of the decay of fluorescence. Journal of Scientific Instruments 42:603-606.
76. Morton, G.A., H.M. Smith, and H.R. Krall. 1968. Pulse height resolution of high gain first dynode photomultipliers. Applied Physics Letters 13:356-357.
77. Muller, A., R. Lumry, and H. Kokubun. 1965. High performance phase fluorometer constructed from commercial subunits. Review of Scientific Instruments 36:1214-1226.
78. Moshman, J. 1967. Random number generation. In: Mathematical methods for digital computers, vol. 2, ed. by A. Ralston and H.S. Wilf. New York, Wiley and Sons, p. 249-263.
79. Munro, T.H., and I.A. Ramsay. 1968. Instrumental response time corrections in fluorescence decay measurements. Journal of Physics E. Scientific Instruments 1:147-148.
80. Parker, C.A. 1968. Photoluminescence of solutions. New York, Elsevier. 544p.
81. Perrin, F. 1926. Polarisation de la lumiere de fluorescence. Vie moyenne des molécules dans l'etat excité. Journal de Physique 12:390-401.
82. Perrin, F. 1929. La fluorescence des solutions. Annales de Physique 12:169-275.

83. Perrin, F. 1934. Mouvement Brownien d'un ellipsoide I.
Dispersion dielectrique pour des molecules ellipsoideale.
Journal de Physique et le Radium 5:497-511.
84. Perrin, F. 1936. Mouvement Brownien d'un ellipsoide II.
Rotation libre et depolarisation des fluorescences. Trans-
lation et diffusion de molecules ellipsoidales. Journal
de Physique et le Radium 7:1-11.
85. Present, G. and D.B. Scarl. 1970. Single photon time resolu-
tion of photomultipliers with gallium phosphide first
dynodes. Review of Scientific Instruments 41:771-772.
86. Rossi-Fanelli, A., E. Antonini, and A. Caputo. 1958. Studies
on the structure of hemoglobin, I. Physicochemical pro-
perties of human globin. Biochimica et Biophysica Acta
30:608-615.
87. Schmillen, A. 1954. Zur Löschung der Fluorescein-fluoreszenz.
Zeitschrift für angewandte Physik 6:260-262.
88. Schuyler, R. and I. Isenberg. 1971. A monophoton fluorometer
with energy discrimination. Review of Scientific Instru-
ments 42:813-817.
89. Schuyler, R., I. Isenberg, and R.D. Dyson. 1971. Manuscript
in preparation.
90. Scott, G.T., R.D. Spencer, N.J. Leonard, and G. Weber. 1970.
Emission properties of NADH. Studies of fluorescence
lifetimes and quantum efficiencies of NADH, AcPyADH, and
simplified synthetic models. American Chemical Society,
Journal 92:687-695.

91. Seliskar, C.J., and L. Brand. 1971. Solvent dependence of the luminescence of N-arylamino-naphthalene-sulfonates. *Science* 171:799-800.
92. Seliskar, C.J., D.C. Turner, J.R. Gohlke, and L. Brand. 1969. The ultraviolet absorption and fluorescence properties of N-arylamino-naphthalene-sulfonates and related molecules. In: *Molecular luminescence*, ed. by E.C. Lim. New York, W.A. Benjamin, p. 677-696.
93. Simon, R.E., A.H. Sommer, J.J. Tietjen, and B.F. Williams. 1968. New High gain dynode for photomultipliers. *Applied Physics Letters* 13:355-356.
94. Spencer, R.D. 1970. Fluorescence lifetimes: Theory, instrumentation, and application of nanosecond fluorometry. Ph.D. thesis. Urbana, University of Illinois 308p.
95. Spencer, R.D. and G. Weber. 1969. Measurements of subnanosecond fluorescence lifetimes with a cross-correlation phase fluorometer. *New York Academy of Science, Annals* 158:361-376.
96. Spencer, R.D. and G. Weber. 1970. Influence of Brownian rotations and energy transfer upon the measurements of fluorescence lifetime. *Journal of Chemical Physics* 52:1654-1663.
97. Starbuck, W.C., C.M. Mauritzen, C.W. Taylor, I.S. Saroja, and H. Busch. 1968. A large scale procedure for isolation of the glycine-rich, arginine-rich histone and the arginine-rich, lysine-rich histone in a highly purified form. *Journal of Biological Chemistry* 243:2038-2047.

98. Steinberg, I.Z. 1968. Nonradiative energy transfer in systems in which rotatory brownian motion is frozen. *Journal of Chemical Physics* 48:2411-2413.
99. Steinberg, I.Z., and E. Katchalski. 1968. Theoretical analysis of the role of diffusion in chemical reactions, fluorescence quenching, and nonradiative energy transfer. *Journal of Chemical Physics* 48:2404-2410.
100. Steiner, R.F. and H. Edelhoich. 1962. Fluorescent protein conjugates. *Chemical Reviews* 62:457-483.
101. Steingraber, O.J. and I.B. Berlman. 1963. Versatile technique for measuring fluorescence decay times in the nanosecond region. *Review of Scientific Instruments* 34:524-529.
102. Stern, O. and M. Volmer. 1919. Über die Abklingungszeit der Fluoreszenz. *Physikalische Zeitschrift* 20:183-188.
103. Strickler, S.J. and R.A. Berg. 1962. Relationship between absorption intensity and fluorescence lifetime of molecules. *Journal of Chemical Physics* 37:814-822.
104. Stryer, L. 1965. The interaction of a naphthalene dye with apomyoglobin and apohemoglobin. A fluorescent probe of nonpolar binding sites. *Journal of Molecular Biology* 13: 482-495.
105. Stryer, L. 1968. Fluorescence spectroscopy of proteins. *Science* 162:526-533.
106. Stryer, L., and R.P. Haugland. 1967. Energy transfer: A spectroscopic ruler. *National Academy of Science, Proceedings* 58:719-726.

107. Tao, T. 1969. Time-dependent fluorescence depolarization and Brownian rotational diffusion coefficients of macromolecules. *Biopolymers* 8:609-632.
108. Tao, T., J.H. Nelson, and C.R. Cantor. 1970. Conformational studies on transfer ribonucleic acid. Fluorescence lifetime and nanosecond depolarization measurements on bound ethidium bromide. *Biochemistry* 9:3514-3524.
109. Tolman, R.C. 1924. Duration of molecules in upper quantum states. *Physical Review* 23:693-701.
110. Turner, D.C., and L. Brand. 1968. Quantitative estimation of binding site polarity. Fluorescence of N-arylamino-naphthalenesulfonates. *Biochemistry* 7:3381-3390.
111. Vaughan, W.M., and G. Weber. 1970. Oxygen quenching of pyrenebutyric acid fluorescence in water. A dynamic probe of the micro-environment. *Biochemistry* 9:464-473.
112. Wahl, P. 1965. Sur l'étude des solutions de macromolécule par la décroissance de la fluorescence polarisée. Académie des Sciences, Paris. *Comptes rendus hebdomadaires des séances* 260:6891-6893.
113. Wahl, P. 1966a. De termination du temps de relaxation brownienne de la sérum-albumine en solution par la mesure de la décroissance de la fluorescence polarisée. Académie des Sciences, Paris. *Comptes rendus hebdomadaires des séances* 263:1525-1528.
114. Wahl, P. 1966b. Depolarisation de fluorescence du lysozyme-DNS. *Journal de Chimie Physique* 63:1011-1014.

115. Wahl, P. 1969. Mesure de la décroissance de la fluorescence polarisée de la γ -globuline-1-sulfonyl-5-diméthylamino naphthalene. *Biochimica et Biophysica Acta* 175:55-64.
116. Wahl, P. and H. Lami. 1967. Etude du déclin de la fluorescence du lysozyme-1-dimethyl-amino-naphtalene-5-sulfonyl. *Biochimica et Biophysica Acta* 133:233-242.
117. Wahl, P., J. Paoletti, and J.B. LePecq. 1970. Decay of fluorescence emission anisotropy of the ethidium bromide-DNA complex. Evidence for an internal motion in DNA. *National Academy of Sciences, Proceedings* 65:417-421.
118. Wahl, P. and G. Weber. 1967. Fluorescence depolarization of rabbit gamma globulin conjugates. *Journal of Molecular Biology* 30:371-382.
119. Ware, W.R. 1961. An experimental study of energy transfer between unlike molecules in solution. *American Chemical Society, Journal* 83:4374-4377.
120. Ware, W. 1969. Fluorescence lifetime measurements by time correlated single photon counting. Minneapolis. 28p. (University of Minnesota. Technical Report no. 3 on U.S. Office of Naval Research Contract N00014-67-A-0113-0006)
121. Ware, W.R. and B.A. Baldwin. 1964. Absorption intensity and fluorescence lifetimes of molecules. *Journal of Chemical Physics* 40:1703-1705.
122. Ware, W.R., and S.K. Chakrabarti. 1970. Nanosecond time resolved emission spectroscopy of 9-amino-acridine. Minneapolis. 31p. (University of Minnesota. Technical Report no. 9 on Office of Naval Research Contract N00014-67-A-0113-0006)

123. Ware, W.R., P. Chow, and S.K. Lee. 1968. Time-resolved nanosecond emission spectroscopy: Spectral shifts due to solvent-solute relaxation. *Chemical Physics Letters* 2: 356-358.
124. Ware, W.R., S.K. Lee, G.J. Brant, and P.P. Chow. 1971. Nanosecond time-resolved emission spectroscopy: Spectral shifts due to solvent-excited state solute relaxation. *Journal of Chemical Physics* 54:4729-4737.
125. Ware, W.R., and J.S. Novros. 1966. Kinetics of diffusion-controlled reactions. An experimental test of the theory as applied to fluorescence quenching. *Journal of Physical Chemistry* 70:3246-3253.
126. Wawilow, S.I. 1921. Die Lebensdauer der angeregten Moleküle in den wässrigen fluoreszierenden Lösungen. *Zeitschrift für Physik* 53:665-674.
127. Weber, G. 1952a. Polarization of the fluorescence of macromolecules. I. Theory and experimental method. *Biochemical Journal* 51:145-155.
128. Weber, G. 1953. Rotational brownian motion and polarization of the fluorescence of solutions. *Advances in Protein Chemistry* 8:415-459.
129. Weber, G. and S.R. Anderson. 1969. The effects of energy transfer and rotational diffusion upon the fluorescence polarization of macromolecules. *Biochemistry* 8:361-371.

130. Weber, G. and B.B. Bablouzian. 1966. Construction and performance of a fluorescence polarization spectrophotometer. *Journal of Biological Chemistry* 241:2558-2561.
131. Weber, G. and D.J.R. Laurence. 1954. Fluorescence indicators of adsorption in aqueous solution and on the solid phase. *Biochemical Journal* 56:xxxi.
132. Weller, A. 1961. Fast reactions of excited molecules. *Progress in Reaction Kinetics* 1:187-214.
133. Witholt, B. and L. Brand. 1970. Multioscillator fluorescence depolarization. Anisotropy of dye binding. *Biochemistry* 9:1948-1956.
134. Yguerabide, J. 1965. Generation and detection of subnanosecond light pulses: Application to luminescence studies. *Review of Scientific Instruments* 36:1734-1742.
135. Yguerabide, J., H.F. Epstein, and L. Stryer. 1970. Segmental flexibility in an antibody molecule. *Journal of Molecular Biology* 51:573-590.

APPENDICES

Appendix I

Products and names and addresses of principal commercial sources of equipment used in the construction of our monophoton fluorometer.

| <u>Product</u> | <u>Source</u> |
|-----------------------|--|
| Coaxial Cable | Belden @ Almac/Stroum Electronics 8888 S.W. Canyon Rd. Portland, Oregon 97225 Ph. (503)292-3534 |
| Cable Connectors | Kings @ Allied Electronics 4000 Aurora Ave. North Seattle, Wash. 98103 Ph. (206)632-5935 General Radio (17361 Armstrong Ave.) Santa Ana, Calif. 92705 Ph. (714)540-9830 ITT Gremar Inc. @ Dave Miller Sales Co. 2323 N. 45th Street Seattle, Washington 98103 Ph. (206)632-2070 |
| Delay Boxes | Science Accessories Corp. 65 Station St. Southport, Conn. 06490 Ph. (203)259-8329 |
| Electronic Components | Allied Electronics (see under Cable Connectors) |

| <u>Product</u> | <u>Source</u> |
|----------------------------|--|
| Epoxy (molding resin) | Hysol Resin @ Fiberchem Inc. P.O. Box 625 Beaverton, Ore. 97005 Ph. (503)646-6891 |
| Epoxy (low vapor pressure) | Torr Seal @ Varian Associates Vacuum Sales 611 Hanson Way Palo Alto, California 94303 |
| Gears and Counters | Veeder Root Co. 70 Sargent St. Hartford, Conn. 06102 Ph. (203)527-7201 Pic Design Corp. P.O. Box 3278 Van Nuys, Calif. 91407 Ph. (213)782-6702 |
| Modular Instruments | ORTEC 100 Midland Rd. Oak Ridge, Tenn. 37830 Ph. (615)483-8451 Canberra Industries 45 Gracey Avenue Meriden, Conn. 06450 Ph. (203)238-2351 Nuclear Chicago 333 E. Howard Avenue Des Plaines, Ill. 80018 Ph. (312)827-4458 |
| Optical Filters | Corning Glass Works Color Filter Sales Section Corning, New York Baird Atomic, Inc. System Components Division 125 Middlesex Turnpike Bedford, Mass. 01730 Ph. (617)276-6420 |

| <u>Product</u> | <u>Source</u> |
|-------------------------------------|--|
| | Optics Technology Co. 901 California Avenue Palo Alto, California 94304 Ph. (415)327-6600 |
| Oscilloscopes and Probes | Tektronix, Inc. 8845 S.W. Center Court Tigard, Oregon 97223 Ph. (503)639-7691 |
| Photomultipliers | RCA (W.D. Lindley) Electronic Components 975 Marshall Avenue Lancaster, Pa. 17601 Ph. (717)397-7661 |
| Polarizers | Crystal Optics Co. 3959 N. Lincoln Avenue Chicago, Illinois 60613 |
| Power Supplies (photomultiplier) | John Fluke Mfg. Co. @ Instrument Specialists Inc. 7101 220th St. S.W. Mountlake Terrace, Wash. 98043 Ph. (206)774-2211 |
| (high voltage) | Raytheon Co. - Sorensen Operation Richards Avenue Norwalk, Conn. 06856 Ph. (203)838-6571 |
| Pulse Generators | E.H. Research Labs Inc. 163 Adeline St. Oakland, Calif. 94607 Ph. (413)834-3030 |
| Pulse Height Analyzers | Northern Scientific Co. 2551 West Beltline Middleton, Wisc. 53562 Ph. (608)836-6511 |
| Resistors (metal oxide) | Victoreen Instrument Division 10101 Woodland Avenue Cleveland, Ohio 44104 Ph. (216)795-8200 |

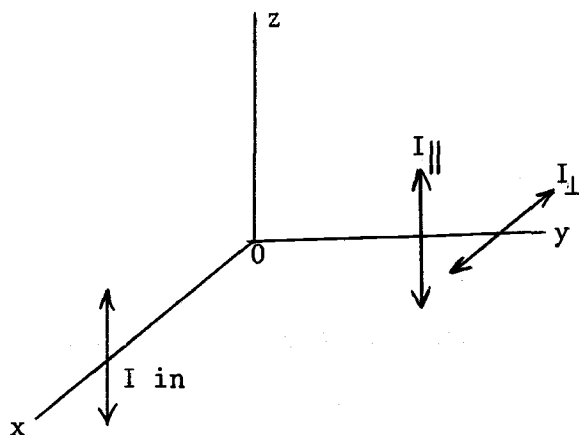
| <u>Product</u> | <u>Source</u> |
|-------------------------------|--|
| Temperature Bath (circulator) | Lauda Instruments Division Brinkmann Instruments Inc. Cantiague Road Westbury, New York 11590 Ph. (516)334-7500 |
| Thermister Probes | Yellow Springs Instrument Co. @ Scientific Supplies Co. 3950 N.W. Yeon Avenue Portland, Oregon 97210 Ph. (503)222-1721 |
| Thyratron Tubes | ITT and Tungsol @ Deeco, Inc. 2500 16th Ave. S.W. Cedar Rapids, Iowa 52406 Ph. (319)365-7551 |
| Valves and Fittings (metal) | Swagelok and Whitey Portland Valve and Fitting Co. 112 N.E. Holladay Portland, Oregon Ph. (503)236-2171 |
| Valves (glass-teflon) | Fischer Porter @ Scientific Supplies Co. (see under Thermister Probes) |

Appendix II

Polarizer Settings for Observing Total Intensity

In the coordinate system shown here, let the excitation beam travel along x and be polarized oz .

Let the emission be viewed along y .



In order to determine the excited state lifetime one must view a component proportional to the total intensity of emission integrated over a sphere. This is proportional to the sum of the three components of emission polarized ox , oy , and oz . Because of the symmetry around oz , the ox and oy components are equal. The expression for the total intensity is then

$$I_{\text{total}} \propto I_{ox} + I_{oy} + I_{oz} = I_{||} + 2I_{\perp}$$

We therefore seek a component of emission polarized at an angle θ from oz such that

$$I \propto I_{\parallel} + 2I_{\perp}$$

Since the intensity is given by the square of the orientation vectors,

$$I_{\theta} = I_{\parallel} \cos^2 \theta + I_{\perp} \sin^2 \theta.$$

The appropriate value of θ is given by the solution to the equation

$$2 \cos^2 \theta = \sin^2 \theta.$$

$$\theta = \tan^{-1} \sqrt{2}$$

$$\theta = 54.72^{\circ} \cong 55^{\circ}$$

This expression was first derived by Jablonski (1935a) and states that with vertically polarized excitation, total emission is viewed only when the emission polarizer is oriented 55 degrees from the vertical.

Spencer and Weber (1970) have derived a more general expression which states that, for the experimental geometry shown above, total emission is viewed when

$$\cos^2 \alpha \cos^2 \beta = 1/3$$

where α and β are the angles made by the excitation and emission polarizers with respect to the oz direction.

Appendix III

Derivation of the Poisson Distribution
for a Photon Counting Experiment

If a large burst of photons directed toward a detector is attenuated to such a degree that only a few photons are detected, the statistical distribution of the number of photons detected in many such bursts may be derived in the following way.

Let each of the N available photons be an event.

Let n be the average number of photons detected per burst of N photons, so that n/N is the probability of detecting a photon.

Let $P_k(n, N)$ = probability of detecting exactly k photons when N are available.

This probability is given by the binomial formula,

$$P_k(n, N) = \frac{N!}{k!(N-k)!} \left(\frac{n}{N}\right)^k \left(1 - \frac{n}{N}\right)^{N-k}$$

$$= \frac{N(N-1) \dots [N-(k-1)]}{k!} \left(\frac{n}{N}\right)^k \frac{\left(1 - \frac{n}{N}\right)^N}{\left(1 - \frac{n}{N}\right)^k}$$

From the definition of e ,

$$\lim_{N \rightarrow \infty} \left(1 - \frac{n}{N}\right)^N = e^{-n}.$$

For large N , then,

$$P_k(n, N) = \frac{n^k}{k!} e^{-n} \cdot \frac{N(N-1)(N-2) \dots [N-(k-1)]}{N^k \left(1 - \frac{n}{N}\right)^k}$$

The factor

$$\frac{N(N-1)(N-2) \dots [N-(k-1)]}{N^k \left(1 - \frac{n}{N}\right)^k}$$

becomes

$$\frac{\left(1\right) \left(1 - \frac{1}{N}\right) \left(1 - \frac{2}{N}\right) \dots \left(1 - \frac{k-1}{N}\right)}{\left(1 - \frac{n}{N}\right) \left(1 - \frac{n}{N}\right) \left(1 - \frac{n}{N}\right) \dots \left(1 - \frac{n}{N}\right)}$$

because there are exactly k factors in the numerator. The limit of this expression when N is large and n is a small fixed number is one. The distribution then becomes Poisson with a mean n .

$$P_k(n) = \frac{n^k}{k!} e^{-n}$$

Appendix IV
Operating Instructions and General Tuning
Procedures for the Monophoton Fluorometer

In order to make this appendix as self contained as possible, that is to avoid excessive cross referencing to the body of the thesis, some discussion and figures will be reproduced here. This, it is hoped, will enhance the value of this appendix as an instruction manual for the operation and tuning of the monophoton fluorometer described in the thesis.

Contents

| | Page |
|---|------|
| Operation and Adjustments | |
| I. Excitation System | 133 |
| A. Operating the Flash Lamp | 139 |
| B. Adjustments on the Excitation System | 141 |
| C. Troubleshooting the Excitation System | 141 |
| II. The Sample Chamber | 143 |
| A. Operations and Adjustments | 143 |
| III. Photomultiplier Tubes and Shields | 146 |
| A. Handling the PM Tubes | 148 |
| B. Bleeder Chain and High Voltage Supply | 149 |
| C. Tuning the PM Bases | 149 |
| IV. The Modular Electronics | 151 |
| A. Module Interconnections | 154 |
| B. Module Settings | 155 |
| C. Single Curve Operation | 157 |
| D. Timing | 157 |
| V. Special Tuning Procedures | 160 |
| A. Single Photon Window | 161 |
| B. Setting the Timing Discriminators | |
| Leading Edge Timing | 163 |
| C. Constant Fraction Triggering - Side Channels | 165 |
| D. Constant Fraction Triggering - Trigger Channel | 166 |
| VI. The Pulse Height Analyzer | 166 |
| A. Invariant Settings | 167 |
| B. CRT Controls | 167 |
| C. Multiplier and Time Base Controls | 168 |
| D. Erasure | 168 |
| E. Collecting Data | 169 |
| F. Readout - CRT | 169 |
| G. Readout - Pen | 170 |
| H. Teletype Readout | 171 |

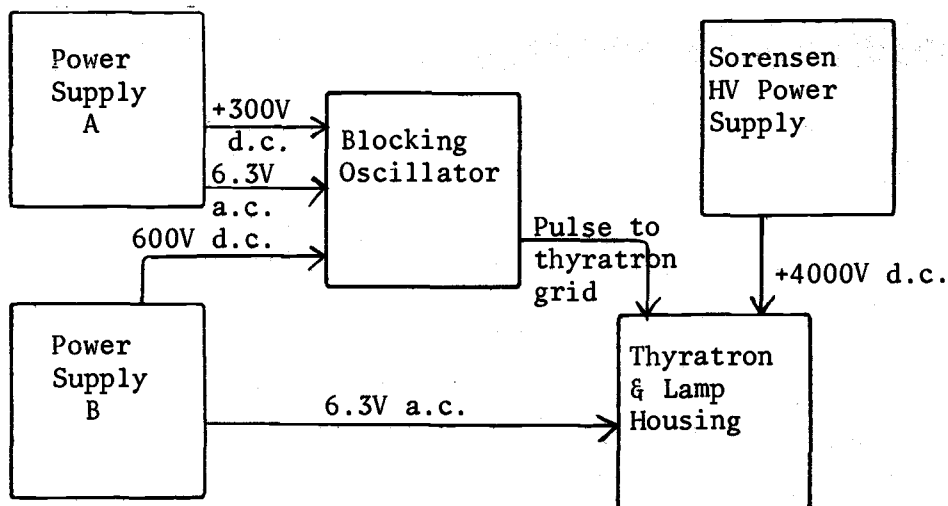
| | Page |
|--|------|
| VII. Setting the Time Range | 171 |
| A. Useful Settings | 172 |
| B. Obtaining the Settings | 173 |
| C. Determining the Nanoseconds per Channel | 173 |
| D. Using 1024 Channels | 174 |
| VIII. Step by Step Procedure | 175 |

Operation and Adjustments

The instrument is conveniently divided into a number of sections, each of which should be understood prior to operation.

I. Excitation System--

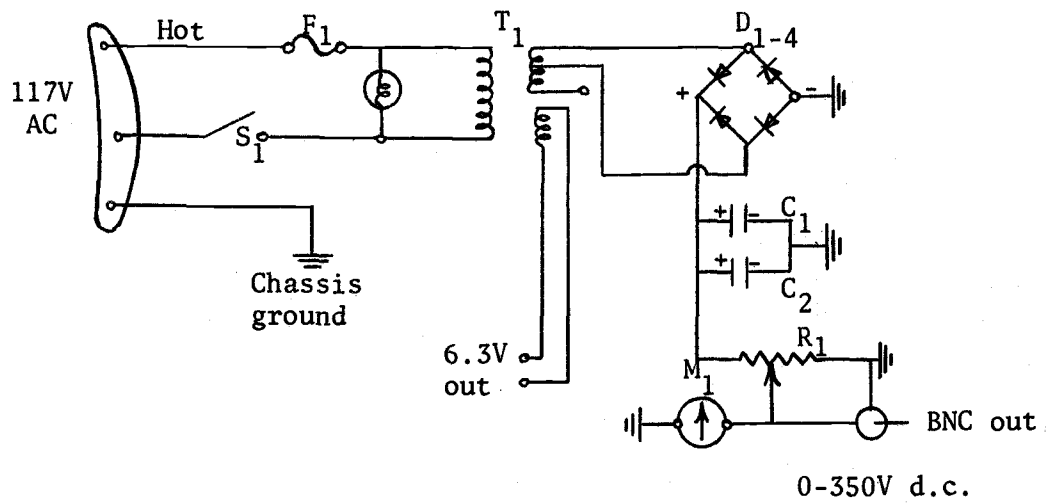
The lamp is a low pressure air spark gap pulsed by a ceramic-metal hydrogen thyration, which in turn is pulsed by a blocking oscillator. A block diagram of this system is shown below.



Block Diagram of Excitation System

Figure 1

On the following pages are schematics of each of the components of the excitation system except the Sorenson 1020-30 HV power supply.



T_1 - Stancor PC 8419 Power Transformer

F_1 - 250V, 2 amp

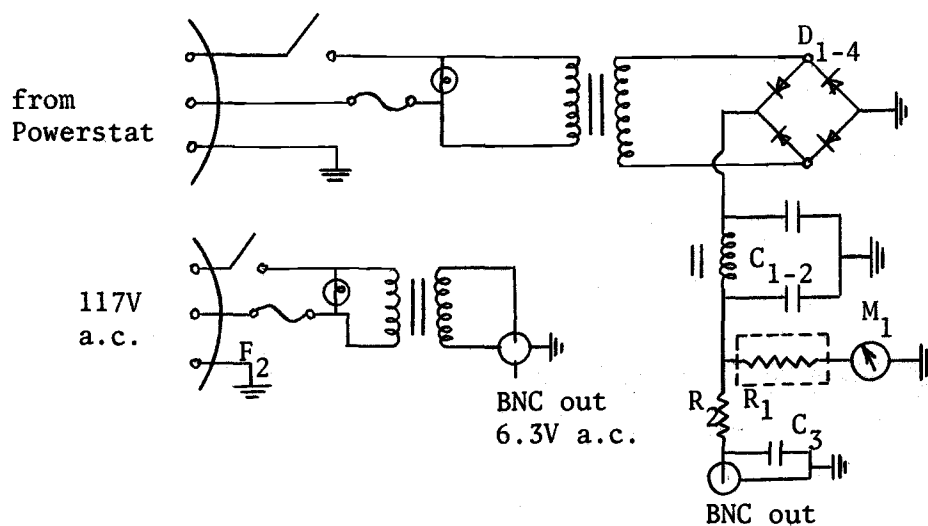
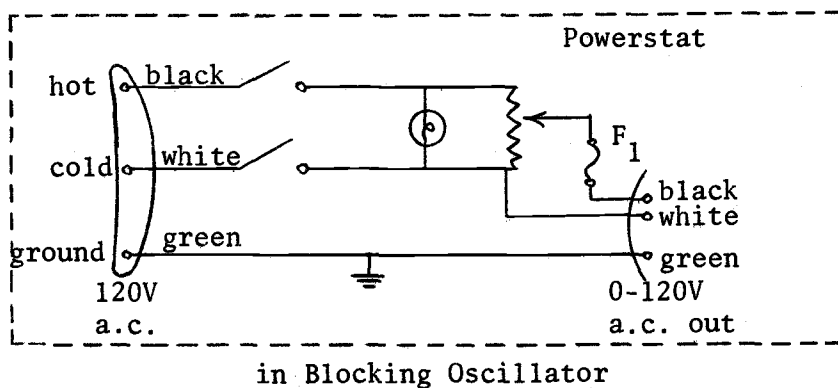
D_{1-4} - S 2484

C_{1-2} - 16 μ f 450V electrolyte

R_1 - 75K pot

M_1 - 0-500V

Figure 2. Power Supply A.



- R_1 - 2 M Ω
- R_2 - 30K
- C_{1-2} - 16 μ f, 700V
- C_3 - .1 μ f 1kV disc
- M_1 - 0-1000V meter
- $F_{1,2}$ - 4 amp sloblo

Figure 3. Power Supply B.

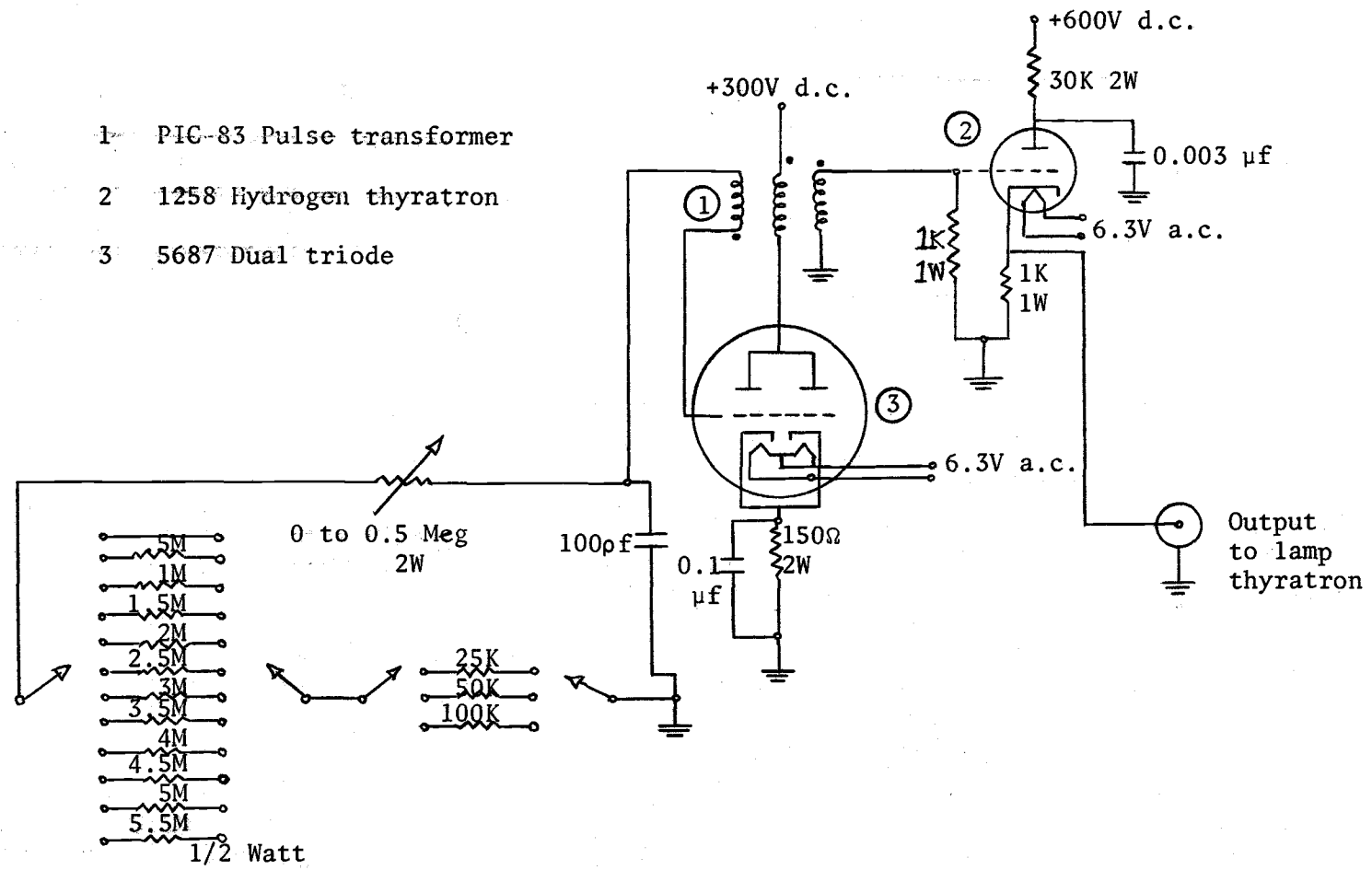


Figure 4. Blocking Oscillator Pulse Generator.

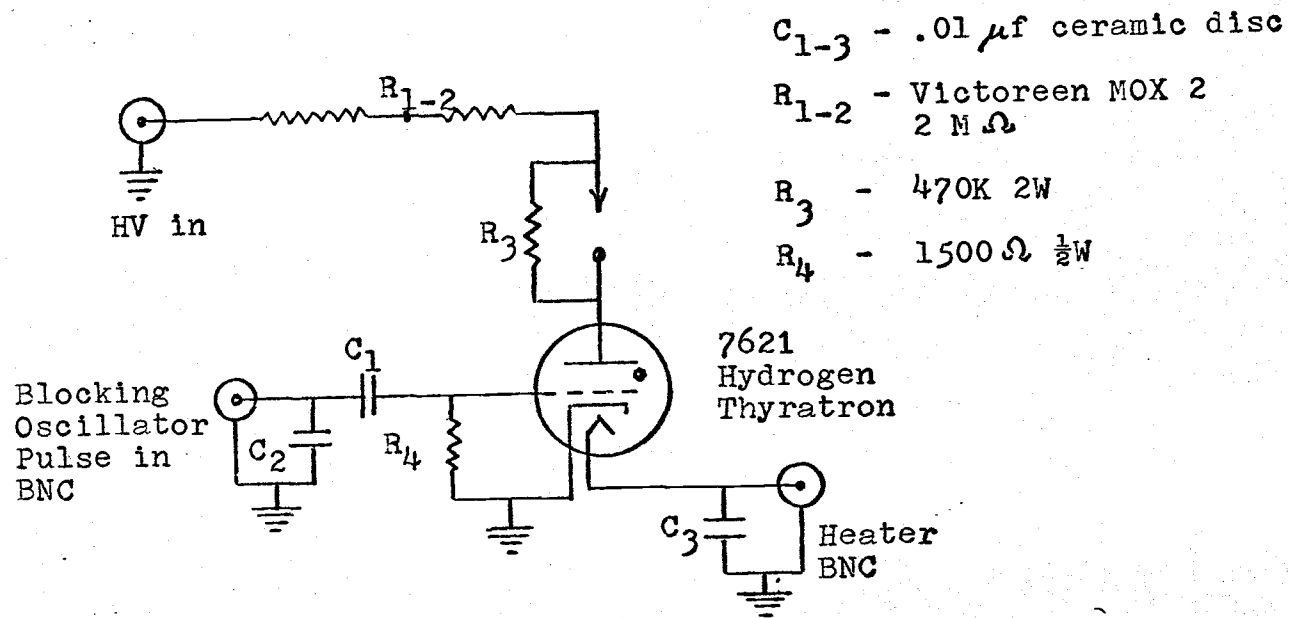


Figure 5. Lamp circuitry.

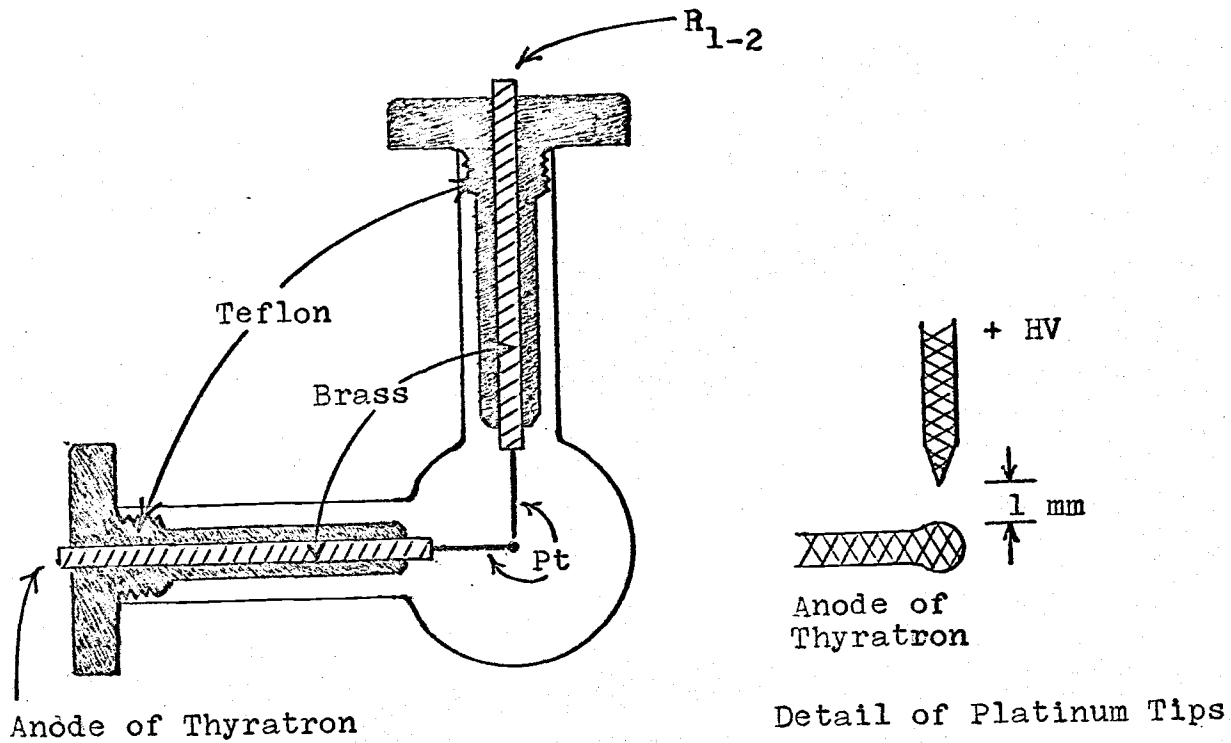


Figure 6. Lamp geometry.

Power supply A supplies voltage (~ 300 v) to the anode of the 5687 dual triode in the blocking oscillator. It also supplies the heater current for both the 5687 and the 1258 miniature hydrogen thyratron. Line voltage for the d.c. output of power supply B comes from the Powerstat mounted in the blocking oscillator panel. The d.c. output (~ 600 v) is applied to the anode of the 1258 miniature hydrogen thyratron. Power supply B also independently provides the heater current for the 7621 ceramic-metal hydrogen thyratron. The blocking oscillator provides a pulse for the grid of the 7621 and the Sorensen 1020-30 high voltage source provides the anode voltage for the 7621.

A. Operating the Flash Lamp

1. Insure that all connections are made as shown in the block diagram.
2. Turn the coarse high voltage control on the Sorensen to "0". Set the "Meter Selectors" as follows: "Voltage", "high"; "Polarity", "+"; "Current", "low".
3. Switch on Power supplies A, B (two toggle switches), the variac, and the Sorensen.
4. Adjust potentiometer on "A" to give a meter reading of 300 v. This may not require adjustment, as it is usually left at the correct position.
5. Adjust powerstat to give a "B" meter reading of 600 v (a setting of ~ 70). May not require adjustment.

6. Allow 3 minutes warm up.

7. If the lamp is set to excite the trigger photomultiplier, ignition and operation can be monitored by placing the lid on the sample chamber and opening the shutter to the trigger PM. One triggers the oscilloscope with the slow logic pulse from the trigger tube (A) timing discriminator (Ortec 453), and views the signal from the tap point of the output from the channel A amplifier (Ortec 485). The scope settings should be 1 v/cm and 1 μ sec/cm.

8. Turn on the Sorensen high voltage by pressing the button marked "on". If a loud buzzing noise is heard, press "off reset" and press "on" again. If the high voltage monitor light does not come on, the high voltage control may not be set to "0".

9. Turn the high voltage control until the lamp fires, as evidenced by a bipolar pulse trace on the oscilloscope, or the voltage reading reaches 10 KV -- Do not exceed 10 KV! Turn the high voltage back down so that the meter reads 4 KV (you may want to switch the meter selector to "medium"). For example, the lamp may ignite at 8 KV and be run at 4 KV. The lamp should remain firing. If the amplifier pulse has a positive portion greater than three volts in amplitude, close the shutter. If this amplitude is not achieved, it may be necessary to remove the polarizer (see II, A, 3).

10. The lamp is turned off by turning the high voltage control on the Sorensen to "0" and pushing the "stop-reset" button. The toggle switches on Power supplies A, B, the Sorensen, and the powerstat are then turned off.

B. Adjustments on the Excitation System

1. The "Fine Frequency Adjust" on the blocking oscillator front panel is usually set to give 15 kHz repetition rate and need not be changed. If a different rate is desired, one can simply turn this screwdriver adjust while watching the oscilloscope trace of the lamp output.

2. One must remove the top of the blocking oscillator compartment to make additional changes on the resistor switch settings. This is not recommended.

3. The d.c. outputs of "A" and "B" are usually not varied or turned down when turning off the lamp. Variations of 20% from the values 300 and 600 volts seem to have little effect on the lamp pulse characteristics.

4. Lamp operating voltages higher than 4 KV may introduce serious radio frequency interference.

5. The electrode spacing of the flash lamp should be $1.0 \pm .2\text{mm}$. The geometry is as shown in Figure 6. The lamp should be evacuated and refilled every four to five days or whenever the amplitude appears jittery.

C. Trouble shooting the Excitation System

1. If the lamp output is not seen on the oscilloscope trace, turn the Sorensen high voltage off. Leaving the three cables attached, remove the side plate, and carefully place lamp and electronics on a wooden surface with the lamp pointing upwards. Repeat steps A, 8-9

above. If the lamp lights, carefully reinsert it in the copper housing and put the housing into position on the sample chamber.

2. If lamp does not fire, refill with 20 cm air and try again. Do this also if the lamp output appears jittery on the oscilloscope trace.

3. If lamp still fails to fire check:

a. Thyatron heater input (6.3 v a.c.).

b. Blocking oscillator output. This can be viewed on the sampling scope with the following setup:

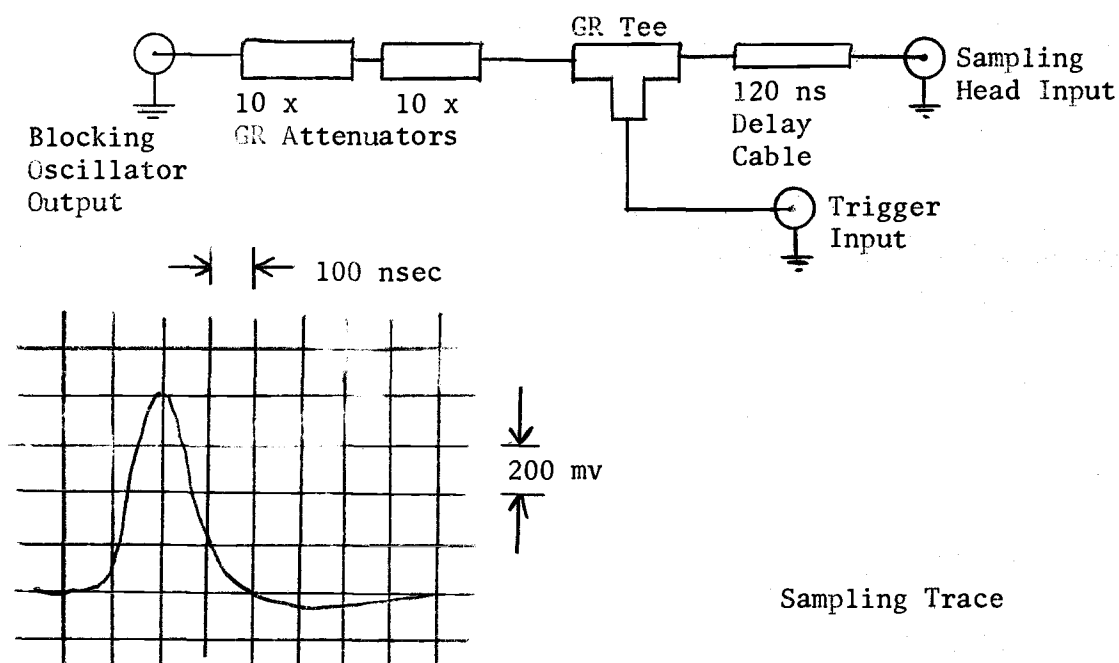
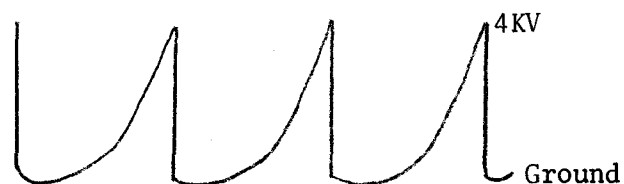


Figure 7. Blocking oscillator output.

Be sure to use enough attenuation!

c. Check the anode of the 7621 thyatron with a high voltage probe and a real time oscilloscope. The oscilloscope trace should appear like this:



At 15 KH_3 rep. rate pulses
are 65 μsec apart

Figure 8. Thyatron anode
voltage.

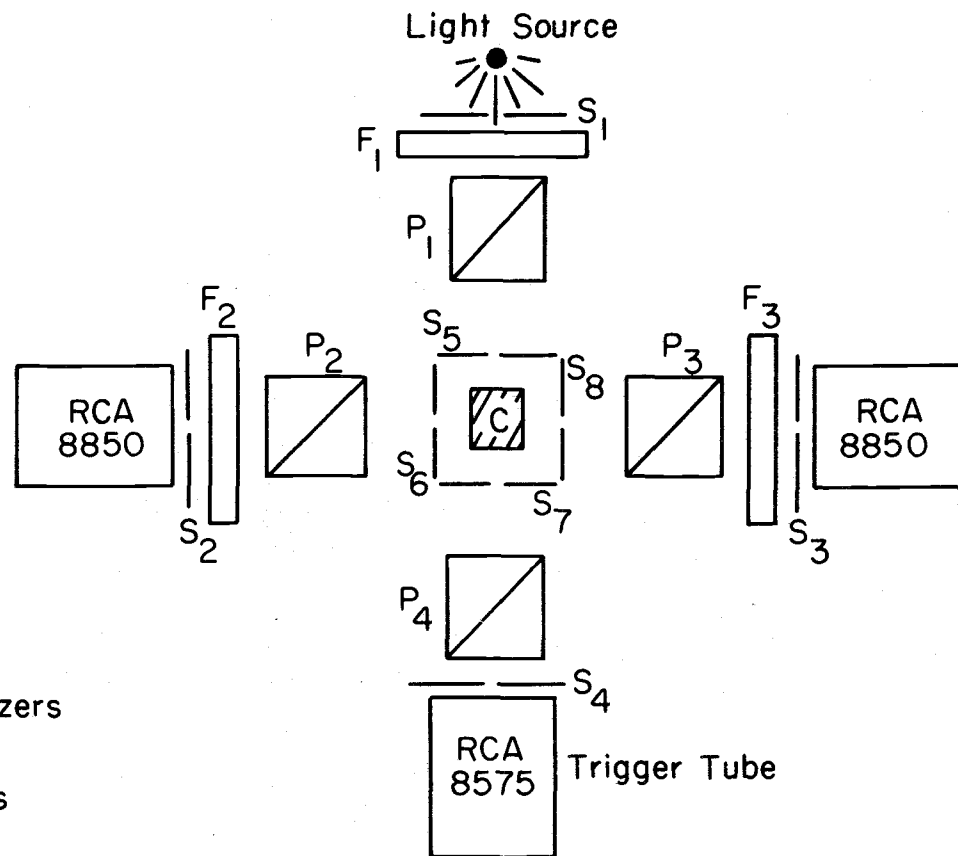
d. If checks a, b, and c look okay, and the lamp fails to fire, look for leakage paths in the lamp housing, or remove and clean the lamp.

II. The Sample Chamber--

The sample chamber is a single unit of molded black epoxy (Hysol). In it are the excitation and two emission polarizers mounted in gear and counter mechanisms for accurate setting. There are filter holders, a fourth polarizer for the trigger phototube, a thermostated cuvette holder, and shutters between the sample and the phototubes. The lid is provided with a tall cap for long cuvettes and with set screws for depressing the shutter pins. Figure 9 shows a diagram of the components.

A. Operation and Adjustments

1. A counter setting of 000.0 indicates vertical polarization. A setting of 525.0 indicates horizontal polarization. To collect a decay curve representing total intensity, the excitation polarizer



P₁₋₄ Polarizers

F₁₋₃ Filters

S₁₋₈ Slits

C Cuvette

Figure 9. Diagram of the sample chamber.

is set at 000.0 and the emission polarizer at 319.0 (see Appendix II). The polarizers may be rotated by removing the external black plastic knob from the counter shaft and attaching it to the shaft of a 300 rpm reversible motor with thick wall rubber tubing. The motor is hand held and switched on to rotate the counter in the appropriate direction. Always return to vertical polarization by counting down, and to a more horizontal position by counting up. In no case should it be necessary to rotate the counter past 525.0. When the appropriate polarizer setting has been nearly reached, turn off the motor, remove it from the counter shaft, replace the knob, and do the fine setting by hand.

2. Select the excitation and emission filters and insert them in the filter holder or attach them to the holder by carefully tightening the 4-40 screws. The filter holders are then slipped into the sample chamber. Care should be taken to orient interference filters perpendicular to the light beam.

3. The polarizer for the trigger tube can be removed if necessary, but for most work serves as a variable attenuator for the trigger light pulse. It is set so that the amplified anode pulse from the trigger photomultiplier is of optimum amplitude for the timing discriminator. The settings most often used call for a three volt pulse height from the Ortec 485 amplifier with the photomultiplier voltage set at 1600 v and the amplifier set at a gain of 160. The Ortec 454 amplifier should be at minimum (x2) gain. The appropriate amplitude can be "fine tuned" with the shutter pin set screw.

4. The sample chamber is attached to metal base supported in a wooden frame. Coils for photomultiplier cooling and leads to the cuvette holder for temperature control are connected to Swagelok fittings on the frame under photomultiplier B. Photomultiplier cooling is not usually used. The sample temperature, however, is controlled by circulating liquid through the cuvette holder. The grey cable and jack exiting the frame below photomultiplier A plugs into a YSI Model 42SC Tele-thermometer for monitoring sample temperature.

5. Because the photomultipliers remain on at all times, the shutter set screws should be raised and the room light dimmed before removing the sample chamber lid.

6. When extensive cooling of either the cuvette holder or PM's is used, a slow flow of dry air should be introduced at the fitting below photomultiplier C.

III. Photomultiplier Tubes and Shields

Three photomultiplier tubes are used in the instrument. The trigger tube is an RCA 8575, and the two side tubes are RCA 8850's (previously C31000D-developmental types). The 8850's have very high gain first dynodes giving them excellent photo-electron resolution in the single electron region. The tube envelopes are pyrex and the spectral responses are shown in the RCA data sheets. The configuration of shielding around the tubes is shown in Figure 10.

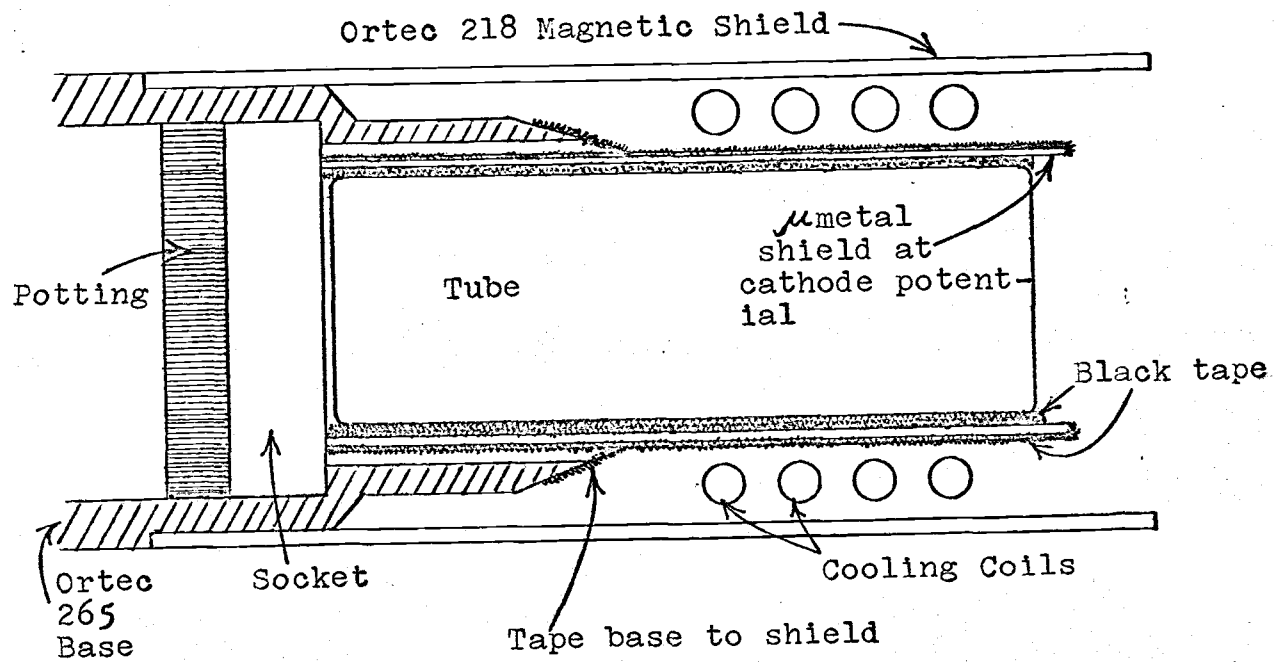


Figure 10. Photomultiplier shielding configuration.

The two side tubes (8850's) were selected for low noise. The addition of the μ -metal shield kept at cathode potential reduces the noise rate in the single photon region by a factor of 10. The tubes when left at -2400 v for two to three months exhibit a further decrease in background pulse rate.

A. Handling the Photomultiplier Tubes

1. To remove the tubes from the instrument, disconnect all cables from the tube base and remove the three screws fastening the Ortec 265 base to the Ortec 218 magnetic shield.
2. Close door and turn out all lights except a dim red darkroom lamp.
3. Carefully rotate back and forth and simultaneously pull the base and tube out of the magnetic shield.
4. Place the foam rubber cup provided in the RCA photomultiplier box over the exposed cathode end of the tube.
5. Remove tape attaching base to phototube. See Figure 10.
6. Carefully pull (using a small amount of lateral motion) the tube out of the socket in the base.
7. Remove the tape from the inner μ -metal shield and slip it off the tube. Be careful not to loose the small brass lead connecting the shield to pin 21 of the tube.
8. Reassembly and insertion is done in the reverse order. Insure that the tube pins enter the correct socket holes and that the tube is pressed all the way into the socket.

B. Bleeder Chain and High Voltage Supply

All three tubes employ the Ortec 265 base and bleeder chain.

The bases on the side channels (B & C) have been changed as indicated in the Ortec 265 manuals marked "Side Channel". The dynode output has been moved from the 9th to the 11th dynode. The resistance between the cathode and first dynode has been increased, and the indicator lamp has been replaced by a 68K resistor.

Each tube is supplied with high voltage by a Fluke 415B regulated power supply. The trigger tube runs at -1600 v, and the side tube B at -2200 v. Photomultiplier C has usually been run at -2400 v. Varying these voltages requires readjustment of amplifier and single channel analyzer settings.

C. Tuning the Photomultiplier Bases--

As indicated in the Ortec 265 manual this need be done only when the photomultiplier voltage is changed by more than 200 v.

1. The lamp should be firing with a scattering sample in place.
2. It is preferable to leave the PM high voltage on, but extreme caution must be exercised. (If the high voltage is turned off, the tube should stay in the dark for one day after reapplying the voltage. This is precautionary only. The effect of transients during reestablishment is not known.) If one is very careful and uses an insulated screwdriver, adjustments done with the high voltage on involves little risk.

3. Check the dark noise rate by applying the output of the associated single channel analyzer (PM shutter closed) to a frequency meter.

4. Remove the tape and screws from the cylindrical cover of the 265 base. Disconnect the anode and dynode outputs (Not the High Voltage connector).

5. Carefully slide the cylindrical cover over the high voltage cable. Reconnect the anode and dynode connections and recheck the count rate. A large increase indicates light leaks through the base.

6. Open the shutter to the tube while viewing the amplifier output on an oscilloscope. Adjust the shutter so that many single and very few double photon events occur (side channel), or the pulse amplitude is about 3 volts (trigger channel).

7. Trigger the sampling scope on a fast negative output from the 453 and connect a sampling head through the RG8 delay cable to the bottom bridging input of the 453.

8. Set the differential and integral time constants of the 454 amplifier at the "out" position and vary the gain on the 454 so that the scope trace has an amplitude of about 1 volt.

9. Refer to the Ortec 265 manual and carefully (insulated screwdriver) perform steps 3.3 - 4 & 5 on the top of page 3. Refer to photograph p. 12 of the manual.

10. Disconnect the anode and dynode leads, replace the cylindrical cover, and reconnect the leads.

11. The single photon window must be reset following bleeder

chain tuning. See Section V.

IV. The Modular Electronics

The timing, pulse height discrimination, and coincidence functions of the nanosecond fluorometer are carried out with NIM standard modules. The block diagram (Figure 11) shows the signal paths through these modules. The paths will now be briefly traced. The individual modules are discussed in greater detail in the Ortec manuals. Specific adjustments will be mentioned later.

The signals may be divided into two classes: timing signals and linear signals. The timing signal originates at the anode of a given photomultiplier. It is amplified and shaped in the 454 amplifier and triggers the 453 timing discriminator. The pulse generated there serves as a stop or start for the time to pulse height converter depending on whether the pulse originated in the trigger photomultiplier (A) or one of the side photomultipliers (B or C). A delay is introduced between the timing discriminator and the time to pulse height converter (TPHC) for the trigger tube, so that the pulse arrives later than the side channel pulse. The time difference between the arrival of the start and stop inputs is linearly represented by the amplitude of the TPHC output pulse.

The linear signal paths differ for the trigger and side PM's.

The linear trigger signal originates at the ninth dynode of the 8575 photomultiplier. The pulse is integrated, amplified, and pulse shaped in the 113 preamplifier and the 485 amplifier. The amplified

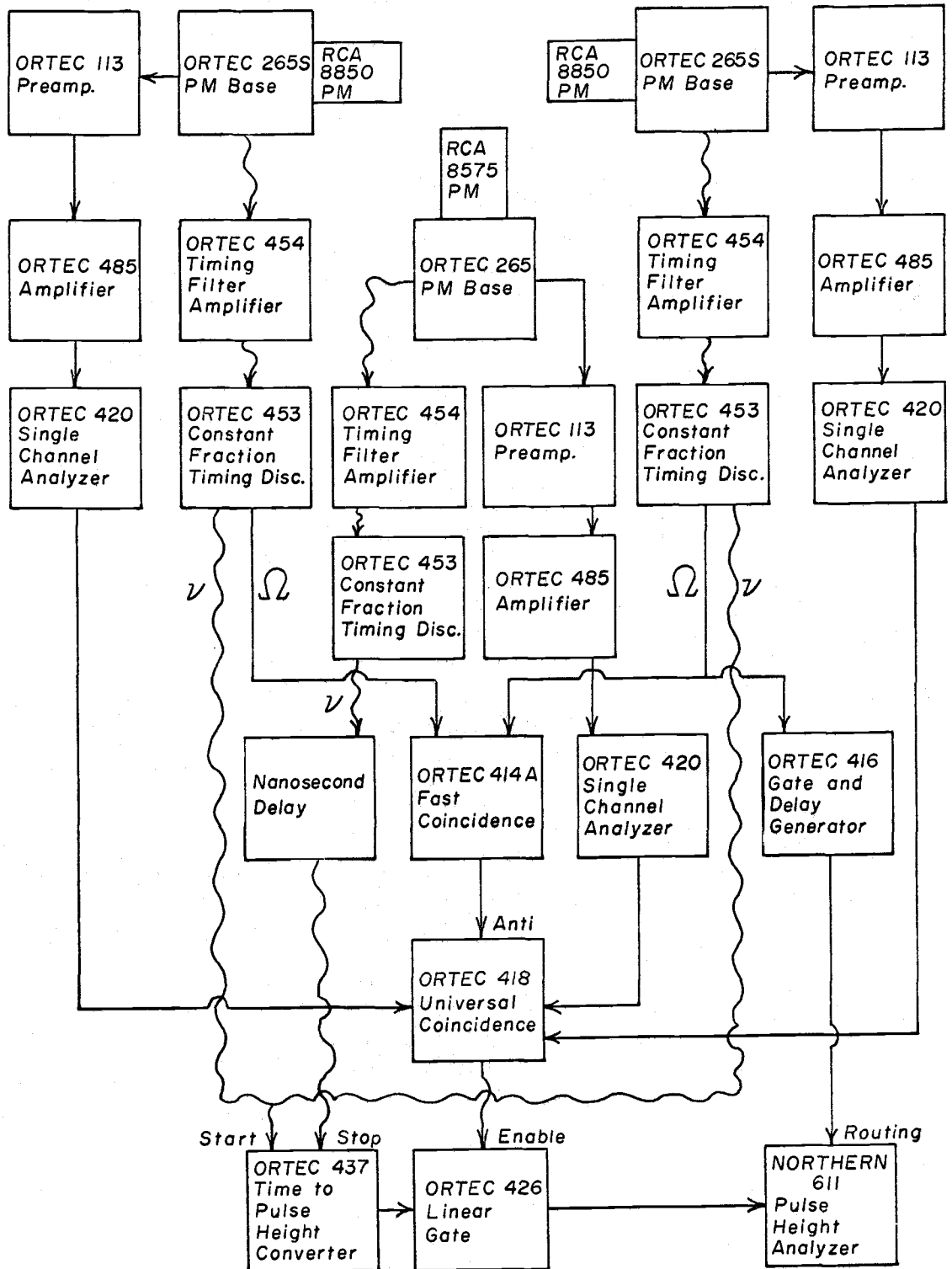


Figure 11. Block diagram of the instrument.

pulse is analyzed by the single channel analyzer (SCA), and an output from the 420 SCA results only when the input has the amplitude associated with a lamp flash. Noise pulses will not cause an output from the trigger SCA. The SCA pulse goes into input A of the 418 coincidence.

The linear signal from a side channel photomultiplier originates at the eleventh dynode of the 8850 and is processed by the preamplifier and amplifier. The SCA is set so that output pulses are generated only when the input is within the pulse height region for single photons. The output is connected to an input of the 418 coincidence. If the coincidence requirements are set at "2", and the pulse from the side channel SCA occurs within the coincidence resolving time of the pulse from the trigger channel SCA, an output occurs. This signal opens the 426 linear gate, allowing the output of the TPHC to reach the pulse height analyzer.

The additional modules, the 414A coincidence, and the 416 gate and delay generator, are used when both side channels operate simultaneously.

Two decay curves or two scatter curves may be collected simultaneously by routing events resulting from a signal in one of the side channels to the second half of memory of the PHA and collecting events from the other side channel in the first half of the PHA. A pulse applied to the rear panel connector of the PHA must completely bracket the incoming TPHC pulse in order to route it.

In addition when events occur in both side channels for a given

lamp flash, they must be rejected. These operations are performed in the following manner.

The 416 gate and delay generator accepts a pulse from the timing discriminator of one of the side channels and broadens and delays it to bracket the incoming pulse from the TPHC. The 414A fast coincidence module determines the coincidence of pulses from the two side channel timing discriminators. A coincidence within a set resolving time generates an output which is then used as an anticoincidence input for the 418 coincidence. The presence of this input inhibits any output pulse from the 418 and the gate does not open. Therefore no data gets to the PHA.

A. Module Interconnections

Figure 11 is a detailed block diagram showing module interconnections, terminations etc. Note the following:

1. Two types of cable are used. Timing pulses employ 53.5 ohm, RG 55 U, double shielded coaxial cable. This cable is represented by the wavy lines. Other signals use 93 ohm, RG 71 B/U, double shielded cable shown by straight lines.
2. Feedthrough terminators (50 ohm) are used to reduce reflections at the inputs and outputs of 454 amplifiers.
3. Cap terminations (50 ohm) are used at:
 - a. Lower bridging inputs of 453 tuning discriminators,
 - b. Shaping delay inputs and outputs on the 453's, when no shaping delay is used (i.e. leading edge timing).

4. Some modules have more than one type of output, e.g., the 420 SCA's, the 453 timing discriminators, the 437 TPHC, and the 416 gate and delay generator.

- a. Use the slow positive logic from the 420's (\sqcap).
- b. Use the 1 ohm output of the TPHC.
- c. Use the positive delayed gate output of the 416.
- d. On the block diagram the symbol γ represents the fast negative logic and \sqcup the slow positive logic for the 453's.

5. The orange BNC connector of the PHA rear panel patch plug is used for the output of the 416.

6. Any slow positive logic may be connected to a frequency meter for count rate monitoring.

B. Module Settings

1. 113 preamplifier; input cap. = 0.
2. 485 amplifier; "positive", "bipolar". Gain settings depending on channel and photomultiplier voltage. Present settings:
 - a. Channel A -- 16 x 10.
 - b. Channel B -- 32 x 10.
 - c. Channel C -- 8 x 10.
3. 420 SCA; "diff", "bipolar", delay .05 μ sec. "E" and " Δ E" settings depend on PM voltage and amplifier gain. They are set according to instructions in the section on "Turning the Single Photon Window" below. Present settings (5-25-71) are:
 - a. Channel A -- "E" = 2.00, " Δ E" = 10.00

b. Channel B -- "E" = 2.11, " ΔE " = 2.42

c. Channel C -- "E" = 1.78, " ΔE " = 0.94

4. 454 timing filter amplifier; time constant "int" and "diff" = out, "neg". Gain settings depend on photomultiplier voltage and discussed under section "Tuning the Timing Discriminators". Present settings:

a. Channel A -- 1 x 2 (minimum gain).

b. Channel B -- 10 x 2.

c. Channel C -- 5 x 2.

5. 453 constant fraction timing discriminators; Channel A - "external reset", Channels B & C - "delayed reset". All other settings are discussed in the section of "Tuning the Timing Discriminators" below. Present settings:

a. Channel A -- LLD = 6.00, f = 0.3 (CF trigger)

b. Channel B -- LLD = 3.20, f = 0.3 (CF trigger)

c. Channel C -- LLD = 5.58, f = 0.0 (LE trigger)

CF = constant fraction, LE = leading edge

6. 437 TPHC; gating mode; "anticoincidence". Range, amplitude and multiplier settings vary for each choice of time resolution and will be discussed later.

7. 418 universal coincidence; resolving time set at 0.6 μ sec for fast decays ($\tau < 50 \mu$ sec). Coincidence requirements = 2. Input controls for single curve operation A and B or C at "coincidence". For simultaneous operation A, B, C at "coincidence", D at "anticoincidence".

8. 426 linear gate; "norm".

9. 414A fast coincidence; resolving time, maximum = 110 ns.
input controls A & B in.

10. 416 gate and delay generator; delay range = 1.0 - 11,
delay = 3.30 μ sec, width = max, amplitude set at 12 o'clock.

C. Single Curve Operation --

The changes here produce a more simple block diagram. See Figure 12. Simply disconnect the 414A and 416 and use only one input to start the TPHC. Switch the input control of the 418 for the channel not used to "out". Switch the anticoincidence input of the 418 to "out".

D. Timing --

The relative time of output pulses from the various modules is important for correct operation. This may be checked by use of a scattering sample giving a good collection rate (2000 to 4000 Hz with a 15,000 Hz excitation rate). Figure 13 shows the position and shapes of pulses from various sources for collection of a scatter curve. The vertical input unit of the oscilloscope is a Tektronix 3A72 which has a .5 μ sec rise time. This distorts the pulses, but relative time is preserved. With a fast (less than .1 μ sec rise time) oscilloscope the trigger discriminator, SCA, and coincidence output pulses would be rectangular 0.5 μ sec wide, 5 volts in amplitude.

The SCA outputs have variable delays to 1.0 μ sec, selectable by a front panel, ten-turn potentiometer. The settings used are 40 and

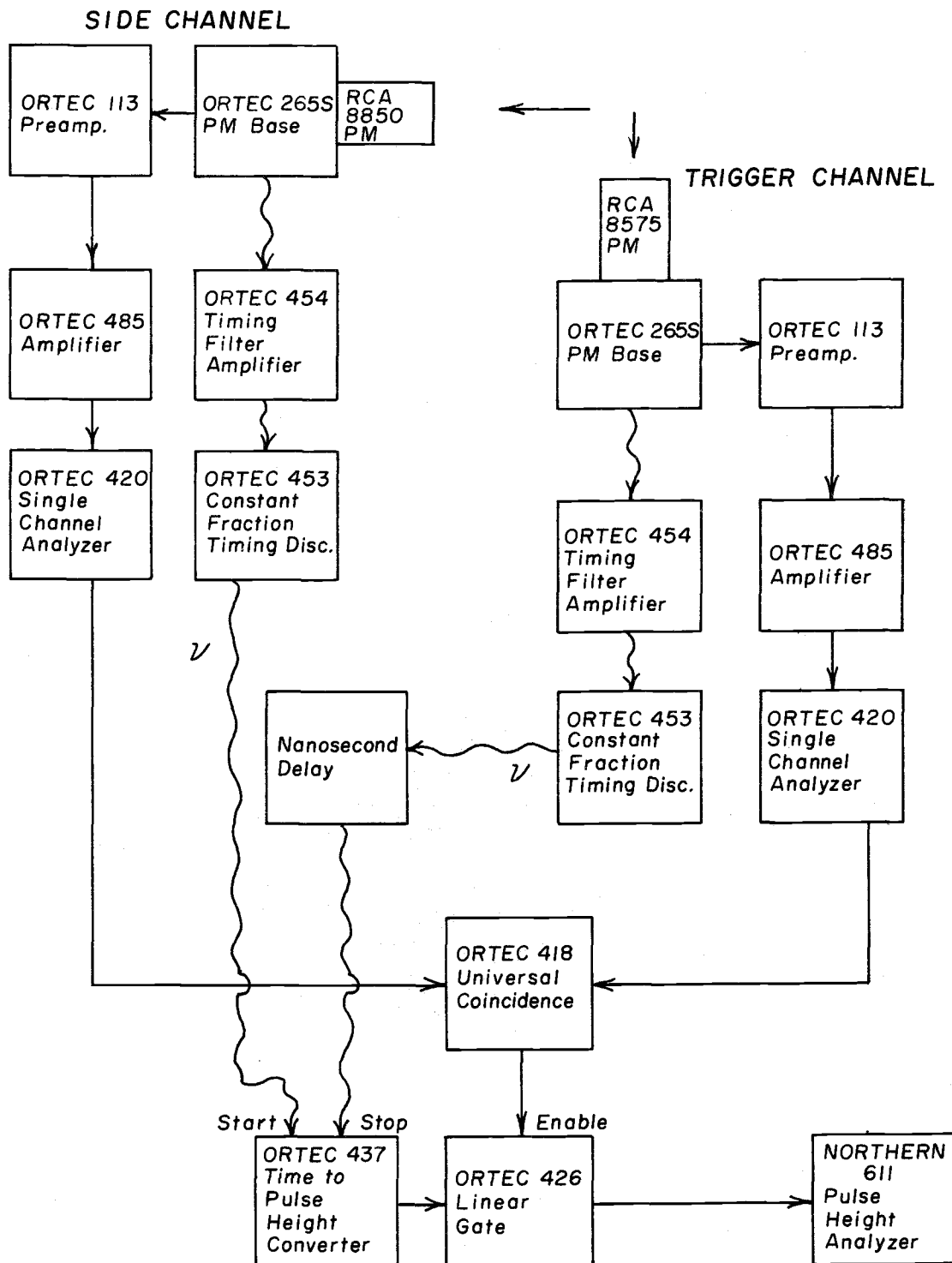


Figure 12. Block diagram of the instrument - single beam.

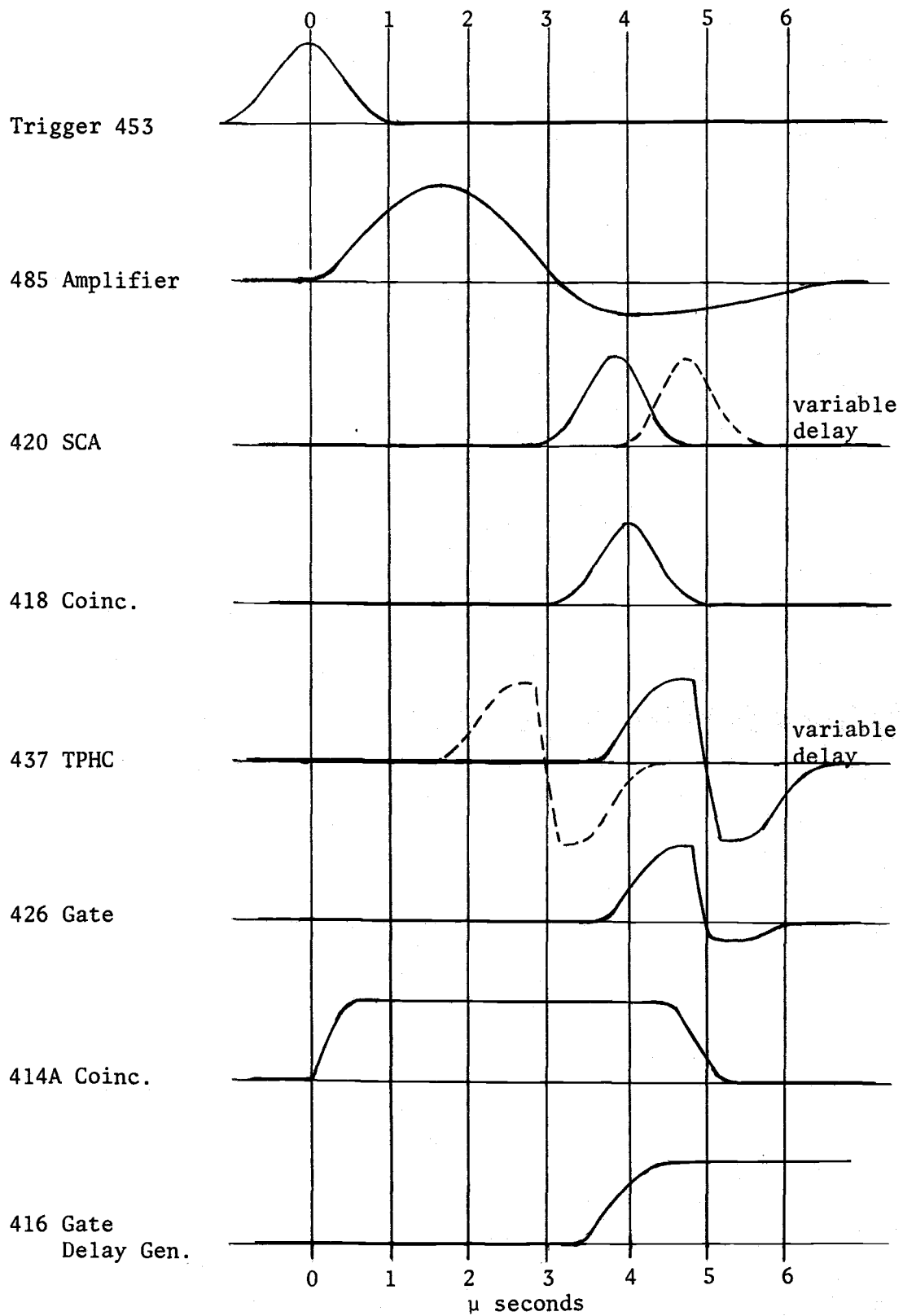


Figure 13. Timing diagram.

70 nsec delays respectively. The TPHC also has a variable output delay as indicated on the timing diagram. The maximum delay available on the module when it comes from the factory was not sufficient, so R102 (on the schematic of the Ortec 437 manual) was changed from 2K to 5K. With this change the front panel screwdriver adjust must be turned to maximum delay (full clockwise) for correct timing.

Also in regard to timing, one should insure that the resolving time of input A on the 418 coincidence module is greater than the range setting on the 437 TPHC, if events late in the time range are to be recorded. This setting is left at 0.6 μ sec unless long lifetime decays are being collected using, for example, the 2 μ sec range on the TPHC. In this case the resolving time potentiometer of the 418 should be turned to 2 μ sec.

The output of the 414A has been lengthened by changing C-10 on the schematic from 470 to 3900 pf. This was necessary to insure that the pulse would extend long enough to disable the output of the 418 coincidence. At present the coincidence resolving time of the 414A is limited to 110 μ sec, and therefore simultaneous operation can be used only for short ($\tau < 15$ ns) time decays.

V. Special Tuning Procedures

A tuning check on the single photon window should be made every time the photomultiplier voltage is changed or every two months. The timing discriminators should be tuned at the same time.

A. Single Photon Window --

The procedure for setting the single photon window will be outlined in detail.

1. A Ludox scattering sample is used and the excitation filter removed to insure multiple photon events.
2. Start the lamp and rotate the trigger tube polarizer and adjust the shutter so that the trigger amplifier signal is ~ 3 volts.
3. Record the side tube voltage, amplifier and SCA settings.
4. Put a BNC tee on the input of the side channel SCA. Attach the amplifier output to one side of the tee and connect the other side to the input of the Canberra linear delay to delay the amplifier signal by three μ sec. Connect the output of the delay module to the input of the Ortec 426 gate. Note carefully the input and output BNCs on the delay module, as Canberra uses a different configuration from Ortec.
5. The trigger and side channel SCA's are connected to the Ortec 418 and the input controls for these are switched to "coincidence". All others remain in the "out" position. Connect the 418 output to the enable input of the Ortec 426 gate.
6. Connect the output of the gate to the 0-10 v input of the PHA and set the ADC zero level of the PHA to 0.10. Below is a block diagram of the completed setup:

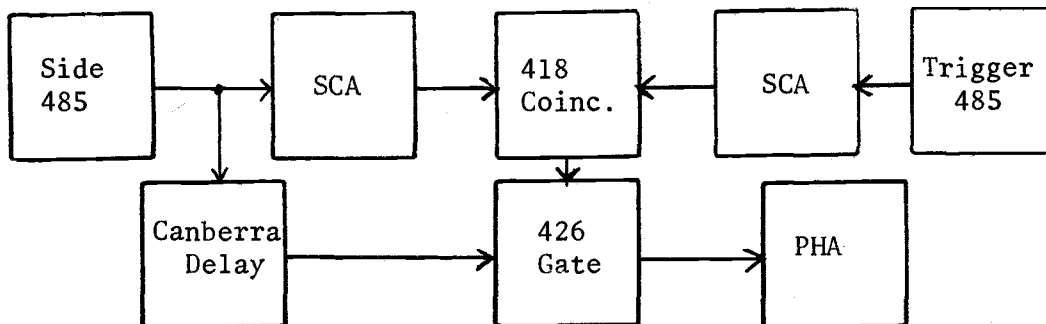
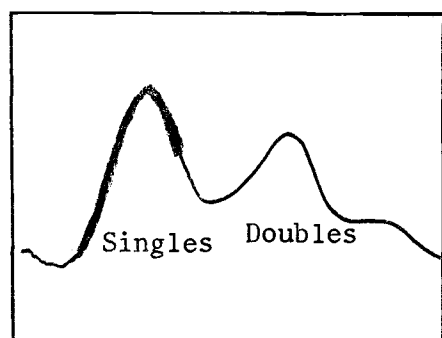


Figure 14. Block diagram for setting the single photon window

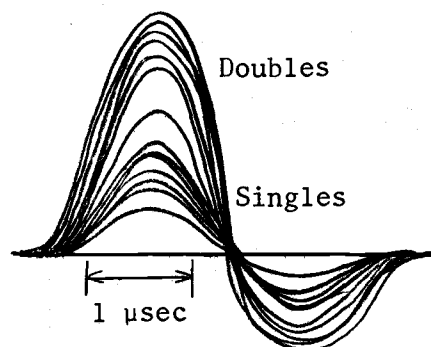
7. Monitor the side channel amplifier with the oscilloscope to insure that a wide range of signals are present. Trigger the scope with the trigger tube timing discriminator as usual.

8. Switch the coincidence requirements on the 418 to one, clear the memory of the PHA, and collect the incoming signals in memory group 1/1.

9. A pulse height spectrum should collect with the following shape (depending on the number of single, double, etc. photon events).



CRT Readout



485 Scope Trace

Figure 15. PHA readout and 485 scope trace at low photon flux.

10. By switching the 418 coincidence requirements to two, only the region of single photon pulse heights (enhanced above) should still be seen collecting in the PHA.

11. One can then adjust the "E" and " ΔE " settings of the side channel SCA to change the region collected. The lower level setting is placed at the beginning of the sharp rise of the single photoelectron peak. The upper level setting, on a curve having roughly the same number of singles and doubles, has usually been half way between the peak of the singles and the valley between the singles and doubles. This is at present somewhat arbitrary and further work might better define these settings.

B. Setting the Timing Discriminators --

Two timing modes have been used in RALF. All the work done through May 20, 1971 has been done with the trigger channel (A) in the constant fraction of pulse height timing mode and channels B and C in the leading edge mode. As the trigger channel triggers on large bursts of photons and the amplitude of the burst may change somewhat during the course of an experiment, the constant fraction of pulse height trigger (CFPHT) mode is important to retain an accurate time reference. The side tubes, however, view only single photon events, and, while these exhibit a range of amplitudes, the variation is random and affects only the time resolution. It may be desirable to change the side channels to the CFPHT mode, and the procedure for doing so is given below.

Tuning or resetting any of the timing discriminators must be done with close attention to the instructions in the Ortec manuals for the 454 timing filter amplifier and the 453 constant fraction timing discriminator. The steps will be referenced here with some detail added.

Leading Edge Timing --

1. With the lamp flashing and a scattering sample in place, trigger the real time oscilloscope on the positive logic output of the 453 timing discriminator of the tube in question. View the 485 amplifier on the scope and open the shutter to the tube until there are a wide range of traces including single and double photon events.

2. Turn off the scope and insert the sampling plug-ins. Trigger on the fast negative output of the 453 and connect a sampling head through the RG8 delay cable to the bottom bridging input of the 453.

3. Adjust the gain of the 454 amplifier so the signals of interest are less than 1 volt (absolute value).

4. Perform the steps of section 4.3 in the Ortec 453 manual, page 4-5.

5. To set the lower level discriminator of the 453 in reference to the bottom of the window of the SCA:

- a. Connect the positive logic output of the 453 to the input of the 416 gate and delay generator.

- b. Connect the positive delayed gate output of the 416 to

input E of the 418 coincidence.

c. Tee the input of the single channel analyzer, sending the amplifier signal through the Canberra linear delay and to the Ortec 426 gate as in Section V,A above.

d. Set 418 input controls at E and B or C (depending on which side tube is being adjusted) to "coincidence". Connect output to enable the gate.

e. Set the delay range on the 416 to 3.2 μ sec, the width to the 9 o'clock position, and the amplitude to the 12 o'clock position.

f. Connect the gate output to the PHA 0-10 v input.

g. With the 453 lower level discriminator at 0.50 and the 418 coincidence requirements at two, the selected single photon region should collect in the PHA.

h. Switch to coincidence requirements "one" and observe a much wider range of pulse heights collecting.

i. Increase the lower level discriminator of the 453 until it matches the bottom of the SCA window.

The effect of varying this level has not been studied.

C. Constant Fraction Triggering (Side Channels) --

1. Read pages 4-1 and 4-2 of the Ortec 453 manual.
2. Perform steps V,B, 1-3 above.
3. Use a 2 foot length of RG 55 U coaxial cable for the external shaping delay.

4. Set the triggering fraction 0.3.
5. Perform steps 5-12 of Section 4.1.3 on page 4-3 of the Ortec 453 manual.
6. The lower level discriminator can be set as in B,5 a-i above.

D. Constant Fraction Triggering (Trigger Channel) --

1. Start the flash lamp and open the shutter to the trigger photomultiplier so that the 485 amplifier pulse is 3 volts when viewed on the oscilloscope, when the amplification is 160 and the photomultiplier voltage is 1600.

2. Use a 2 foot external shaping delay and triggering fraction = 0.3 on the 453.

3. View the bridging input of trigger 453 with sampling scope triggered on fast negative output of 453. With minimum amplification the 454, the pulse should be -0.8 v in amplitude.

4. Complete steps 5-12 of Section f.1.3 on page 4-3 of the Ortec 453 manual.

5. The lower level discriminator of the 453 can be set at 6.00 though any setting above 2.00 and below 7.00 is non-critical.

VI. The Pulse Height Analyzer

The PHA is a 1024 channel system in which any half or quarter of memory can be used. The maximum count in a given channel is 999,999. Two halves may be used simultaneously if the appropriate pulse is

applied to a rear panel connector.

There is a single channel analyzer output for determining the input count rate.

There are three types of readout. A cathode ray tube (CRT) readout shows collection while an experiment is in progress and can be expanded or stopped and displayed. A pen readout driving an recorder, and a teletype-paper tape readout can be initiated after collecting a curve.

I will now describe in more detail the settings and operation of the unit. The functions of the various controls are defined in the Northern Scientific manual.

A. Invariant Settings

1. The toggle switches left to right should read: "ADD", "PHA", "CLOCK", all digital zero offset switches -- "OFF", "ANTICOINC".
2. Program -- "MANUAL"
3. ADC Input -- "HIGH LEVEL"
4. SCA/ACD -- "LLD" = 0.20, "ULD" = 10.00
5. Conversion Gain -- "1024"

B. CRT Controls

1. The six controls below the CRT are self explanatory and have no effect on the data collection.
2. The Display Scale switch controls the vertical axis of the

CRT readout and has no effect on collection. It also controls the vertical axis of the pen readout.

3. The Memory Group switch selects the section of memory which is displayed on the CRT. This switch also determines where the incoming data collects and should not be changed while collecting data.

4. The Read Mode CRT, CRT x 2, and CRT x 4 positions control what portion of the 1024 channels occupies full scale on the CRT tube readout. The Read Mode control maybe switched between these positions without affecting the collection.

5. In combination, the Read Mode and Memory Group switches can be used to overlap quarters or halves of memory. For example, with Read Mode at CRT x 2 and Memory Group at 1/1, the two halves of memory are superimposed on the CRT. With Read Mode at CRT x 4 and Memory Group at 2/2, the third and fourth quarters of memory are superimposed. A few minutes experimentation with these switches should clarify their operation.

C. The Multiplier and Time Base controls are used for presetting a collection time. If one sets the Multiplier at 5 and the Time Base at 10^4 seconds the PHA will collect for 50,000 seconds and switch to stop mode. If a preset collection time is not required, switch the Time Base to " ∞ ".

D. Erasure is done by placing the Read Mode switch at CRT and Selecting the Memory Group to be erased. Press the Start-Readout button.

Press the Erase button.

The Zero Level setting will be discussed later under "Useful Settings".

E. Collecting Data --

1. With the lamp flashing, a scattering sample in place, shutters open, the NIM modules (and PHA Zero Level) set, connect the 426 gate output to the 0-10 v input of the PHA.

2. Set the Read Mode to CRT x 2 and the Memory Group to 1/2 (for a single curve).

3. Press the Start-Readout button and the Erase button to clear the memory.

4. Check the 426 gate output on an oscilloscope to insure that events are present.

5. Adjust the CRT screen controls to bring the baseline to a convenient position on the screen.

6. Press the Stop button then the Start-Measure button. Collection should start at once.

7. If simultaneous collection is desired, set the Read Mode at CRT and the Memory Group to External.

F. Read Out -- CRT

1. Press the Stop button.

2. Press the Start-Readout and switch to the appropriate CRT

setting of Read Mode Switch.

G. Read Out -- Pen

1. Attach the recorder inputs to rear panel pen outputs of the PHA.
2. Push the Stop Button.
3. Switch the Read Mode to "Pen".
4. Turn on the recorder and set x and y axes range and zero.
 - a. With the recorder on, the pen up, and the PHA in stop mode, switch to various Memory Group positions. This should allow range and zero settings for the x axis.
 - b. Under the same conditions the y range and zero can be set by knowing the amplitude of the curve at the beginning of a given quarter of memory (check this in CRT Read Mode). Switch Memory Group to that quarter of memory and press the Start-Readout button. The pen will go to the appropriate amplitude and the y range setting with this amplitude as a reference can be accomplished. Press the Stop button and reset the zero of the y axis.
 - c. Recall that the Display Scale serves the same function for the pen readout as it does for the CRT.
5. Select the appropriate Memory Group, put the recorder pen down, and Press the Start-Readout button of the PHA. Readout is at the rate of one channel per second.

H. Teletype Readout

1. Turn teletype 103 to "On Line" and "Analyzer". Turn on the paper tape punch and put 6" of sprocket holes (HERE IS key) on the tape.
2. Press the Stop button of the PHA.
3. Select the Memory Group for readout.
4. Switch Read Mode to "TYPE".
5. Press the Start-Readout button.
6. After the data is out (one channel per second output rate), the PHA automatically switches to Stop mode. Switch the Read Mode to CRT.
7. Put 6" of sprocket holes on tape, tear it off and roll it up.
8. Turn the teletype off.

VII. Setting the Time Range

The TPHC range and amplitude, the delay, and the PHA zero level are used to control the time per channel in the PHA and the position occupied by the decay or scatter curve in the PHA memory. For nano-second-per-channel settings less than 0.4 the decay curves are generally collected time inverted. The trigger channel timing pulse is delayed and sent to the "stop" input of the TPHC, while the side channel pulse provides the "start". For settings greater than 0.4 ns/ch the trigger channel provides the start and the side channel provides the stop.

A. Useful Settings

These settings were determined for collection into 512 channels of PHA memory. The delayed signal goes through the entire quadruple delay box, and the delay noted is only that switch selected, not that for the connecting cables or the intrinsic delay. See the manual on the SAC model 032 Quadruple Nanosecond Delay for the intrinsic delays.

The following settings were made with side tube B used at -2200 volts with constant fraction triggering in that channel. These settings place the excitation profile at such a position, that at least 30 channels of background are monitored before the flash.

TPHC

| <u>ns/ch</u> | <u>range</u> (μ /sec) | <u>amplitude</u> (clock setting-volts) | <u>delay</u> (nsec) | <u>PHA</u> <u>zero level</u> |
|-------------------|-------------------------------|---|------------------------|---------------------------------|
| .064* | .05 x 1 | 11:00 - 4.4 | 18 | 10.00 |
| .097 | .1 x 1 | 3:00 - 8.6 | 32 | 8.00 |
| .192 | .2 x 1 | 3:00 - 8.6 | 74 | 5.00 |
| .246 | .2 x 1 | 12:00 - 6.5 | 104 | 5.00 |
| .330 | .2 x 1 | 10:00 - 5.1 | 152 | 5.00 |
| .392 | .4 x 1 | 2:40 - 8.4 | 176 | 5.00 |
| ----- | | | | |
| not time inverted | | | | |
| .68 | .8 x 1 | 5:00 - 10.0 | 64 | 3.50 |
| .98 | .8 x 1 | 12:00 - 6.5 | 64 | 2.00 |
| 1.95 | .2 x 10 | 2:00 - 7.9 | 224 | 3.00 |
| 3.90 | .4 x 10 | 2:00 - 7.9 | 224 | 1.50 |

*See D below.

B. Obtaining the Settings

1. Set up to collect a scatter curve in the usual manner.
2. Select settings from the above chart for a ns/ch setting close to the one wanted.
3. To increase the ns/ch, decrease the TPHC amplitude setting and increase the delay, so that the scatter curve collects in the same relative position of memory.
4. Put the fluorescent sample in and insure that collection occurs in all 512 channels. For a time inverted curve, too low a TPHC amplitude setting will cause the far right channels of PHA memory to be empty. Too low a setting on the PHA zero level will leave the left channels empty.
5. Some experimentation is necessary to develop a feel for the settings. If changes from the listed settings are desired, some time should be spent to insure that the collected scatter and decay occupy memory positions such that adequate background channels and a good decay tail are present.

C. Determining the Nanoseconds per Channel

1. With the flash lamp triggering the trigger PM and all settings as desired, disconnect the cable from the fast negative output of the side channel 453 timing discriminator and connect it to the remaining fast negative output of the trigger channel 453 timing discriminator.
2. Clear the memory of the PHA and collect for a few seconds the incoming TPHC pulses and press the Stop button.

3. Change the delay box by switching some delay out (the amount will depend on the ns/ch setting and about 100-300 channels worth is sufficient).

4. Collect again the incoming TPHC pulses for a few seconds.

Stop.

5. Press Start-Readout and expand the horizontal CRT scale so the number of channels between the two collection peaks can be counted.

6. An additional check should be made by switching out a different delay. Each delay switch has an error of ± 1 nsec so it is best to minimize the number of switch positions used.

D. Using 1024 Channels

The full 1024 channels of PHA memory can be used to obtain better time resolution or to collect very short lifetime decays where the lamp curve may not fit into 512 channels with the desired ns/ch resolution. This is the case with the 0.064 ns/ch setting in A above. Good settings with high time resolution for 1024 channel curves are difficult to get and require much checking to insure background channels are present. Two such settings are listed here.

| <u>ns/ch</u> | <u>range</u> | <u>amplitude</u> | <u>delay</u> | <u>zero level</u> |
|--------------|--------------|------------------|--------------|-------------------|
| .045 | .05 x 1 | 3:10 - 8.8 v | 28 ns | 10.00 |
| .085 | .1 x 1 | 5:00 - 10.0 v | 70 ns | 10.00 |

The full range of the high level input is 8.00 v so TPHC amplitudes above 2:00 - 7.9 v must be used. Other settings may be obtained as

in Section B.

VIII. Step by Step Operation

This section gives a step by step procedure for collecting a scatter decay curve and for transferring the data to paper tape. Many of the instructions below will refer to sections in the main body of this manual giving detailed instructions. The whole manual should be read, however, prior to running the instrument, so that the operations listed will be understood.

The instructions here refer to collection of a time inverted curve with decay time less than 30 nsec. They are intended for collection of 512 channels of scatter and 512 channels of fluorescence, and not simultaneous collection of two curves.

Simultaneous collection and long lifetime decays require a few steps to be changed, and these changes will be noted after the following list of instructions.

1. If sample temperature control is desired, set the Lauda temperature control, insure that the connections to the "Sample Temperature" fittings are tight, and switch the bath heater and compressor on. Open the flow valve to full on. See Section II,A, 4-6.

2. Because the photomultiplier tubes are always left with the high voltage on, the lights should be dimmed before lifting the lid of the sample chamber.

3. Select the polarizer settings and filters to be used and set the polarizer and insert the excitation filter as in Section II,A,

1-2.

4. Insure that the module interconnections are as shown in the block diagram, Figure 12, and according to the instructions IV,A, 1-6.

5. Check the module settings and set them according to IV,B, 1-8. The settings for the side channel not used may be ignored.

6. Decide on an appropriate nanoseconds-per-channel setting, and set the TPHC, delay box, and the zero level of the PHA to the settings given on the chart of Section VII. A reasonable setting is 1-2 ns/ch for a 100 ns decay time, scaled linearly for the expected decay.

7. Start the flash lamp according to I,A, 1-9.

8. For setting the appropriate trigger tube intensity refer to II,A, 3.

9. Monitor the side channel 485 amplifier with the oscilloscope, triggering on the slow logic of the trigger tube 453 timing discriminator. Open the shutter and insure that events are occurring in that channel. If, with the shutter completely open (do not turn the set screw so far that the lid begins to lift off the sample chamber), many double photon events are present (see Figure 15), insert a slit in the cuvette holder between the scattering sample and the side channel photomultiplier or partially close the shutter.

10. Monitor the count rate at the output of the 418 coincidence and at the single channel analyzer output of the PHA. These rates should be about the same.

11. Set the PHA switches as in VI,A, 1-5.

12. Collect an excitation curve by following the instructions VI,E, 1-6.

13. Press the PHA Stop button, then the Start Readout button, after the scatter curve reaches 5000 to 10000 counts at the peak.

14. Check the scatter curve to insure that there are 50-80 channels to the right of the sharp rise of the lamp flash. This assures a good background range. If this is not the case refer to Section VII,B.

15. Remove the scatter cuvette and emission slit and insert the emission filter.

16. Change the PHA Memory Group to 2/2 and collect some fluorescence data and view the curve on the CRT readout.

17. The half width of the fluorescence curve should occupy about 75-150 channels. If it appears that the ns/ch setting is too high or too low, choose another and repeat steps 12-17.

18. Erase the data from both halves of memory of the PHA. Consult VI,D.

19. Reinsert the scatter sample and slit, remove the emission filter, replace the lid, and set the trigger tube shutter set screw so the trigger tube 485 amplifier has an output of three volts.

20. Collect a scatter curve until the peak count is half the desired peak count of the decay curve. Follow instructions VI,E, 2-6.

21. Replace the scatter sample with the fluorescence sample. Remove the slit and insert the emission filter.

22. Replace the sample lid and set the trigger amplifier output to three volts as in 19 above.

23. Collect the fluorescence decay curve in Memory Group 2/2 of the PHA.

24. Repeat step 19 and add scatter counts to the curve already present in Memory Group 1/2 to achieve a peak count approximately the same as for the fluorescence decay curve.

25. Switch to Memory Group 1/1 and read out on paper tape as instructed in VI,H, 1-7.

26. Determine the ns/ch as in VII,C, 1-6.

The changes for simultaneous collection of two curves are:

- A. Do 1-3.
- B. At 4 substitute Figure 11 for Figure 12.
- C. At 5 follow instructions IV,B, 1-10. Set both side channels.
- D. Do 6-8.
- E. Do 9 for both side channels.
- F. Do 10-13.
- G. At 14 it may be necessary to introduce some delay at the fast negative timing output of channel B or C to have both occur at about the same position in memory.
- H. Do 15; at 16 use Memory Group "Ext" instead of 2/2.
- I. Do 17.
- J. 18-20 except at 20 collect the scatter to the full desired peak count. Do 25 and clear the memory.
- K. Do 21-23, again use Memory Group "Ext".
- L. Do 25-26.
- M. Repeat J.

One usually collects scatter curves before and after the fluorescence decay. These may be added mathematically or each used for the analysis.

When using ns/ch settings greater than 0.4 the only changes are those which come about because the curve is not time inverted. The trigger tube starts the TPHC and the signal from a side channel (often delayed) stops it. Thus at instruction 4 the block diagram will differ at the inputs of the TPHC. At instruction 14 there should be 50 to 80 channels to the left of the excitation curve.

The entire memory of the PHA (1024 channels) may be used for collection. Use, of course, the directions for single curve collection except Memory Group 1/1 must be used at all times. The settings for ns/ch must be modified as indicated in Section VII,D.